Colloid Science of Sand Remediation: A Study Motivated by the Non-Aqueous Extraction of Bitumen from Oil Sands

by

Shima Afshar

A thesis submitted in partial fulfillment of the requirements for the degree of

Doctor of Philosophy

in

Chemical Engineering

Department of Chemical and Materials Engineering
University of Alberta

Abstract

The current water-based method of bitumen extraction requires withdrawal of fresh water from the Athabasca River — a practice which leads to the continual buildup of tailings ponds and other environmental concerns. As Alberta's bitumen production is expected to more than double by 2020, there is now a real need to explore the possibility of an alternative *non-aqueous* (or solvent-based) extraction technology. The main challenge that any non-aqueous extraction method faces is the recovery of residual oil from oil-laden sand grains. In this research, we propose a possible solution of washing the sand grains with aqueous surfactant solutions. From an interfacial science perspective, for a surfactant to give good residual oil recovery, it must create low oil-water interfacial tensions (IFTs) and desirable wetting characteristics. For this part of the investigation, the challenge was to accurately determine low IFTs and contact angles on the microscale (characteristic of the pore sizes); novel micropipette techniques were developed for this purpose. Of the different surfactants we had examined, natural surfactants extracted from bitumen, which appeared to be essentially sodium naphthenates, yielded the lowest IFT (down to 0.6 mN/m) and exhibited the most desirable (i.e. hydrophilic) wetting properties. On the macroscopic scale, the overall washing efficiencies of sodium naphthenates were also quantified. The efficiencies showed very different behaviors when the system was agitated under low or high shear rate. It is proposed that this discrepancy was due to the formation of thermodynamically stable microemulsions (a third phase) in the presence of surfactants.

Preface

All of the research conducted for this thesis was an original work by Shima Afshar; the investigations in Sections 5.2 and 5.3 were conducted collaboratively with Leyli Mirmontazeri, PhD candidate at the University of Alberta.

Section 5.2 of this thesis is published in *Fuel* 116 (2014) 395-398; it is coauthored by S. Afshar, L. Mirmontazeri and A. Yeung. Section 5.3 of this thesis is published in *Fuel* 128 (2014) 1-6; it is coauthored by L. Mirmontazeri, S. Afshar and A. Yeung. The first and second authors had equal contributions in both these papers; Dr Yeung was the supervisor.

Acknowledgements

First and Foremost I would like to express my wholehearted gratitude to Allah, the Almighty, for enlightening my path and guiding me through each and every success I have or may reach.

I would like to express my sincere gratitude to my supervisor, Prof. Anthony Yeung, for his inspiring guidance, encouragement and support in the past years while I pursued my Ph.D. degree at the University of Alberta. In the thousands of hours he devoted to my education and research, he showed me how to think like a researcher and educator as well as formulate, test, express, and defend my ideas in a clear and concise manner. His ardor and earnestness for studies are respected and will never be forgotten.

This research was conducted under the auspices of the COSI (Centre for Oil Sands Innovation) program at the University of Alberta. I would like to thank Dr. Xiaoli Tan and Ni Yang for their valuable advice and assistance and my colleague, Leyli Mirmontazeri for a collaborative work of soil remediation.

I am forever indebted to my parents for all their endless patience, encouragement and love for my entire life. They raised me with a love of science and supported me in all my pursuits. I am also grateful to my dear brother, Farhang who has always loved and supported me.

I owe my deepest gratitude to my beloved spouse, Ali. Without his encouragement, support and love, this dissertation would have never been completed. I would also like to express my gratitude to the love and support from my parents-in-law.

Table of Contents

1. Introduction 1

2. What are microemulsions? 17

2.1. Macroscale: three common classes of microemulsions 18

2.2. Microscale: many forms of microstructure 19

2.3. Curvature elastic properties of surfactant monolayers 24

2.3.1. Importance of K and C_0 — and how they are manipulated 25

3. Interfacial Tension and Contact Angle Measurements 29

3.1. Theory behind the methods of measuring surface tension 31

3.2. Commercially Available Methods 35

3.2.1. Wilhelmy Plate and du Nouy Ring Methods 37

3.2.2. Measurement of Capillary Pressure (Maximum Bubble Pressure) .. 38

3.2.3. Capillary Rise and Drop Weight or Volume Methods 40

3.2.4. Analysis of Gravity-Distorted Drops 42

3.2.5. Measurement of Ultra-low Interfacial Tension 45

3.2.5.1. Spinning Drop Method 45

3.2.5.2. Capillary Wave Spectroscopy 46

3.2.5.3. Micropipette Technique 47

4. Novel Micropipette Technique for Ultralow Interfacial tension and Contact Angle Measurements 49

4.1. Ultralow Interfacial Tension Measurement with Developed Micropipette Technique 50

4.2. Novel Wettability (Contact Angle) Measurement 54

5. Experimental, Results and Discussion 57

5.1. Considerations When Measuring Ultralow Interfacial Tensions..... 57

5.1.1. Materials 58

5.1.2. Experimental 58

5.2. Potential Use of Naphthenic Acids in Soil Remediation: Examination of Pore-Scale Interfacial Properties..... 65

5.2.1. Materials 67

5.2.2. Experimental 68

5.3. Evaluation of Naphthenic Acids as a Soil Remediation Agent: A Physicochemical Perspective 80

5.3.1. Materials 82

5.3.2. Experimental 83

6. Summary and Recommendations..... 98

7. References..... 103

List of Tables

Chapter 3

Table 3-1: Commercially Available Instruments..... 35

Chapter 4

Table 4-1: Interfacial Tension with deionized water 52
Table 4-2: IFT between n-butanol/water (with different SDS concentrations) 53

Chapter 5

Table 5-1: Interfacial tensions of AOT-hexadecane-brine system 58
Table 5-2: Advancing and receding contact angles matched the decrease in IFT values by adding sodium naphthenates to the system..... 78

List of Figures

Chapter 1

Figure 1- 1: Alberta's Oil Sands Areas (OSAs) [2] 1
Figure 1- 2: Oil Sands Mining and Bitumen Extraction [1] 5
Figure 1- 3: Cyclic Steam Stimulation Process (CSS) [1] 8
Figure 1- 4: Steam Assisted Gravity Drainage Process (SAGD) [1] 9
Figure 1- 5: Schematic of the first-stage separation of coarse solids from solvent-diluted oil sands. My Ph.D. research is motivated by problems which arise in the rejects streams. 12

Chapter 2

Figure 2- 1: The three common forms of microemulsions: (a) Winsor I, (b) Winsor II, and (c) Winsor III. The middle phase of Winsor III can be bicontinuous. 18
Figure 2- 2: A bicontinuous cubic phase with a zero mean curvature [23]. 20
Figure 2- 3: Middle phase microstructure for the AOT + aqueous NaCl + *n*-alkane system. The alkane carbon number is: (a) N<10, (b) N=10, (c) N=12 [26]. 22
Figure 2- 4: An oil-water interface saturated with surfactants. The interface will in general show elastic resistance to changes in curvature. 24

Chapter 3

Figure 3-1: Scheme of contact angles. Liquid (a) wets the solid better than liquid (b). 31
Figure 3-2: Surface tension forces acting on the contact line in mechanical equilibrium [33-36]. 32
Figure 3-3: Curved surfaces that have principal radii of curvature: (a) the same sign, and (b) the opposite sign [33-36]. 33
Figure 3-4: (a) Characteristic dimensions in pendant drop: d_e and d_s, and the coordinates used in the Young–Laplace equation (b) Characteristic dimensions in sessile drop: R & h [33-36]. 34
Figure 3-5: Interfacial tension measurements techniques [37]. 37

Figure 3-6: Schematic of the Wilhelmy plate method and du Nouy ring method [37, 38]. 38
Figure 3-7: Maximum Bubble Pressure Method. (A) The shape of bubble at the stages of bubble growth. (B) Relationship between the pressure inside and radius of the bubble [39, 40]. 39
Figure 3-8: illustration of the Capillary Rise & Drop Volume or Weight Methods [41-44]..... 41
Figure 3-9: Dynamic interfacial tension between bitumen and water at 60°C using the Wilhelmy plate, time intervals started at t=0 and ends at t=90 min [49]. 44
Figure 3-10: Schematic of spinning drop technique [61, 62]. 46
Figure 3-11: Micropipette technique. (a) Based on Δp required to suck a microdroplet into the micropipette [67]. (b) Based on force-drop deformation relation [59]. 48

Chapter 4

Figure 4-1: Schematic of the micropipette/manometer setup for determining IFT between the liquid in the pipette (connected to the reservoir) and a second liquid that the pipette tip is immersed in. Raising the reservoir will lead eventually to expulsion of the first liquid from the pipette tip; the change in reservoir elevation Δh is a direct measure of the IFT. As the pipette tip is ~10 μm in diameter, the process must be monitored under an optical microscope. 52
Figure 4-2: Developed Micropipette Technique and Spinning Drop converge at saturated SDS concentrations..... 54
Figure 4-3: A simple technique of measuring pore-scale contact angles. As shown, a three phase contact line is formed inside the pipette (inner pipette diameter is typically 10–30 μm). By moving the interface forward and backward, receding and advancing contact angles can be determined..... 56

Chapter 5

Figure 5-1: Inadvertent formation of microemulsion phases…….……57
Figure 5-2: Relationship between brine salinity and IFTs measured using the spinning drop and micropipette techniques. The oil phase was *n*-hexadecane with 5 wt% AOT, and the brine was an NaCl solution. Results from both methods suggest saturation was reached when the NaCl concentration was roughly 2.5 wt% or higher; the two saturation IFTs, however, differed significantly…….….59
Figure 5-3: Upon contacting the oil phase (*n*-hexadecane with 5 wt% AOT) with the brine (water with 3.5 wt% NaCl), a third phase — a bicontinuous (BC) liquid — appeared spontaneously. (a) The so-called Winsor III mixture in a test tube, with the oil phase at the top, the aqueous phase in the middle, and the BC phase at the bottom (this BC phase was more dense than the brine); (b) the BC phase was seen to spontaneously engulf an oil droplet that was held at the pipette tip; the oil droplet was roughly 60 μm in diameter. The surrounding liquid was brine……. 61
Figure 5-4: Microscope images and sketches of the situations during IFT measurement. (a) The oil droplet in a spinning drop tensiometer was engulfed by a thin layer of the bicontinuous (BC) phase; the diameter of the cylinder was roughly 0.7 mm. Note that the layer of BC liquid around the oil drop is almost imperceptible in the photograph. (b) Arrangement of various phases in a micropipette experiment……63
Figure 5-5: The binding energy positions of oxygen and carbon peaks. (a) XPS oxygen peak at 531.243 (eV) from carboxyls. (b) XPS carbon peak at 288.2 (eV) from carboxyls……..71
Figure 5-6: SFT adsorption isotherms of Athabasca natural surfactants and Kodak SNs. (a) Area per molecule a_0 (Å^2) = 55.71 Å^2 from Limiting Slope = -7.34, occupied by natural surfactants and surface tension values at critical micelle concentrations (CMC). (b) Area per molecule a_0 (Å^2) = 48.60 Å^2 from Limiting Slope = -8.41 and SFT value at CMC of Kodak SNs…….. 72

Figure 5-7: Interfacial tension as a function of the sodium naphthenates concentration *C* in the aqueous phase (the so-called adsorption isotherm): (a) Oil phase is pure toluene; (b) oil phase is toluene + 10 wt% bitumen. Based on the Gibbs adsorption relation [80], A_0 (area occupied by a surfactant molecule at saturation) can be calculated from the slope of the semi-log plot……75

Figure 5-8: Variations of the advancing and receding contact angles as the sodium naphthenates concentration *C* in the aqueous phase was changed. (a) With *C* plotted on a logarithmic scale, strong contact angle hysteresis is clearly seen at low surfactant concentrations. (b) The same data is plotted on linear scales. It is seen that when *C* is above 10 mg/mL, contact angle hysteresis was decreased significantly, and the surface appeared much more hydrophilic……77

Figure 5-9: Sodium naphthenates not only lowers the IFT values but also decreases the contact angles through aqueous phase……..79

Figure 5-10: A schematic of the washing protocol. Surface-modified sand was first "contaminated" with diluted bitumen, then washed with an aqueous surfactant solution that is equal in mass to the contaminant. The amount of hydrocarbon in the drained liquid is used as a measure of the washing performance……84

Figure 5-11: Washing efficiency as a function of sodium naphthenates concentration at low shear rate. The surfactant's critical micelle concentration (CMC) was around 10 g/L. A dashed line is included to show the functional trend; it is not based on any theoretical calculation……...87

Figure 5-12: Washing efficiency as a function of surfactant concentration at high shear rate. The dashed line only illustrates the trend and is not a theoretical curve……..88

Figure 5-13: Results of mixing equals amounts of the oil phase (10 wt% diluted bitumen) and the aqueous phase (SN solution at 50 g/L) under (a) low shear, and (b) high shear. Note that the white liquid in (b) was

actually quite homogeneous; what appears as “lumps” was due to streaks of black oil that were stuck to the inner wall of the vial…….89
Figure 5-14: A micropipette filled with diluted bitumen was immersed in an aqueous solution of sodium naphthenates. After several minutes, a third liquid, which was immiscible with oil and water, appeared spontaneously at the oil-water interface…… 92
Figure 5-15: A hypothetical (but typical) ternary phase diagram of a surfactant-oil-water system. By removing the diluted bitumen (the oil), the system undergoes a major shift in phase space as shown — moving from a 3-phase (3Φ) region to a single-phase (1Φ) region of swollen micelles in water…….…… 95

1. Introduction

Canada's oil sands, located in northern Alberta, are one of the largest proven oil reserves in the world. An estimated initial volume in-place of approximately 1.8 trillion barrels of crude bitumen catapulted Canada into second position for total oil reserves behind only Saudi Arabia[1] [1].

Alberta's massive crude bitumen resources are contained in sand (clastic) and carbonate formations as shown in Figure 1-1 in three Oil Sands Areas (OSAs)[2] [2].

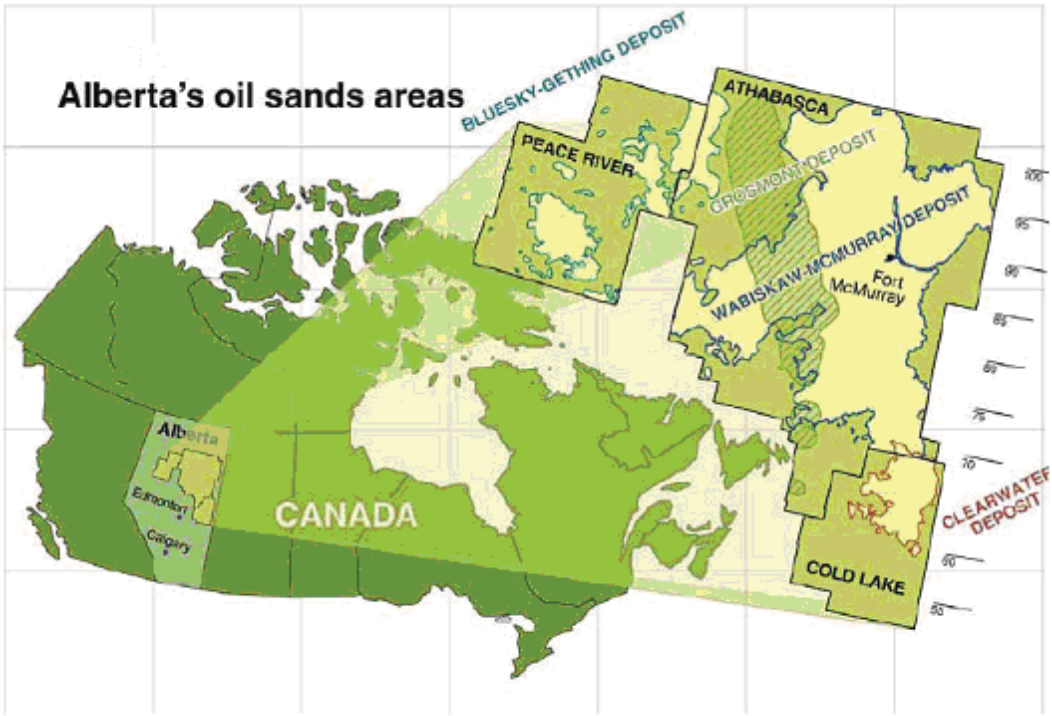

Figure 1- 1: Alberta's Oil Sands Areas (OSAs) **[2]**

[1] Dunbar RB. Canada's Oil Sands — A World-Scale Hydrocarbon Resource. Strategy West Inc; 2011 September

[2] Alberta Energy Resources Conservation Board; Alberta's Energy Reserves 2010 and Supply/Demand Outlook 2011-2020; ERCB ST98-2011; June 2011

[3] Source: Alberta Statutes and Regulations; Oil Sands Conservation Act, Section 1(1) (c)

The bitumen in the three main oil sands deposits: the Athabasca Wabiskaw-McMurray, the Cold Lake Clearwater and Peace River Bluesky-Gething, are found in sand (clastic) formations. To date, most of the production activities have occurred in these three major areas. Four of the fifteen oil sands deposits within the OSAs are in carbonate formations. Township markers that are about 50 kilometres apart are shown as an indication of scale on the right-hand edge of Figure 1-1. Together, the OSAs occupy a vast area of about 142,000 km^2 (54,000 square miles). Therefore, most industry activities to date are centered in Alberta.

Oil sands in general are sands and other mineral materials mixed with extra heavy, non conventional crude oil (crude bitumen). Approximately 80 to 85 percent of oil sands (by mass) are sands, clays and other mineral matters. Five to ten weight percent of the ore is water, and anywhere from 1 to 18 wt% is crude bitumen.

Crude bitumen is a viscous crude oil which is in a near solid state at room temperature. In the industry, crude bitumen is most commonly described as "a naturally occurring viscous mixture, mainly of hydrocarbons heavier than pentane, that may contain sulphur compounds and that, in its naturally occurring viscous state, will not flow to a well"[3].

The Alberta Energy Resources Conservation Board (ERCB), in year 2010, reported that 7 per cent of the volume-in-place crude bitumen in Alberta is contained at depths of less than 65 m (215 feet) from the top of the oil sands zone. The bitumen in these shallow deposits, which are all located in the Athabasca area, is recovered through surface mining and bitumen extraction technologies.

[3] Source: Alberta Statutes and Regulations; Oil Sands Conservation Act, Section 1(1) (c)

The remaining 93 per cent of the bitumen, which is distributed in all three oil sands areas, is found in deeper deposits and the so-called in situ recovery techniques must be used for its extraction [2].

According to the estimation of ERCB, only a fraction of the volume-in-place crude bitumen — about 10 per cent — is technically and economically recoverable. This recoverable bitumen is considered as the reserves of Alberta's oil sands, which amounts to about 176.8 billion barrels. Up to the end of year 2010, only 4 per cent (7.6 billion barrels) of the recoverable bitumen had been produced; this leaves a reserve of 169 billion barrels that are recoverable using proven technology; only a small fraction of these reserves are associated with active development projects.

The history of bitumen and synthetic crude oil production has begun in 1967. The oil sands industry commenced its commercial operation with the start-up of the Great Canadian Oil Sands[4] (GCOS) projects in mining, extraction and upgrading. Imperial Oil's Cold Lake project, in 1985, was the first commercial in situ project. Since these early projects, large scale crude bitumen productions had occurred. In 2010, 53% of Canada's total oil production was from the oil sands industry.

Before delivery of bitumen to downstream upgraders or refineries, the crude bitumen must first be separated from the sands, other mineral materials and formation water[5]. This separation process, known as extraction, occurs in two different ways, depending on whether the deposits are shallow or deep.

[4] GCOS is the predecessor to Suncor Energy's mining, extraction and upgrading operations.
[5] Formation water, or interstitial water, is simply water found in the pore spaces of an oil sand ore.

For shallow deposits, the oil sands are recovered through surface mining before delivery to an extraction plant, where the hydrocarbon is separated from the sands, water and other materials. For deeper deposits, the bitumen is separated from the sands through in situ (or "in place") recovery technologies; in situ techniques are somewhat similar to enhanced oil recovery for conventional wells.

I. Surface mining and bitumen extraction

Oil sands mining operations have evolved over time. Bucketwheel excavators, which discharged their oil sand loads onto conveyer belts for transport to the extraction plants, have been 'retired.' Instead, large mining trucks and power shovels are now used because of their energy efficiency and versatility. Today's trucks are capable of hauling up to 380 tonnes of material and are loaded by hydraulic power and electric shovels with capacities up to 44 cubic meters. The oil sands are transported by the trucks to facilities where the ore is crushed and then 'hydrotransported' to the extraction plant where bitumen is separated from the sand by a flotation process. Hydrotransport, in the present context, involves first mixing mined oil sands with warm water and chemicals (sodium hydroxide for pH adjustment) to form a slurry; the slurry is then pumped (i.e. hydrotransported) through long pipelines to the flotation vessels.

Variations of the original hot water process, which was developed in the 1920s by Dr. Karl Clark of the Alberta Research Council, are currently used at extraction plants where bitumen is separated from the sands, other minerals

and connate water[6]. Syncrude Canada's 'low energy extraction' (LEE) process operates with 55ºC water. Compared to the original process, which required 80ºC water in the flotation vessel, the LEE process consumes only one-third of the energy.

An undesirable by-product of the oil sands extraction process is the tailings, which is an aqueous suspension of sand and fine clay particles. In addition, the tailings stream also contains residual bitumen (oil trapped between the sand grains) and chemicals that were either introduced by the operators or indigenous to the ore (e.g. sodium naphthenates from the crude oil). In regard to treating the tailings water, the coarse sand grains (silica particles with average size of 0.5 mm) present little challenge as they settle rapidly. The fine clays, however, settle very slowly or not at all; they are also known to form gel-like structures in the tailings pond and can seriously hinder the recycling of tailings water. An overall schematic view of oil sands mining and bitumen extraction is shown in Figure 1-2.

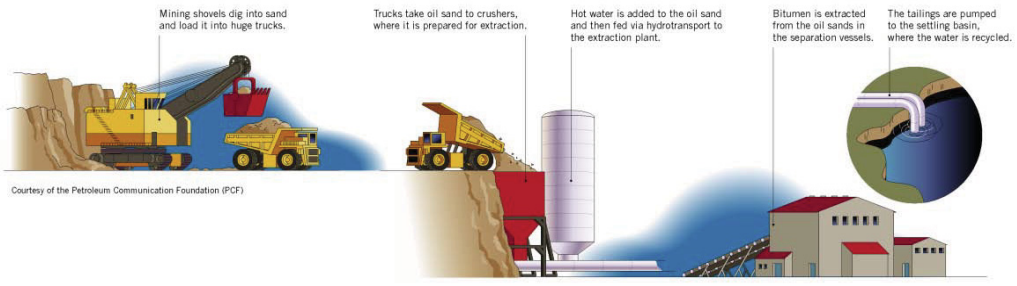

Figure 1- 2: Oil Sands Mining and Bitumen Extraction [1]

[6] Water trapped in the pores of a rock during formation of the rock. The chemistry of connate water can change in composition throughout the history of the rock. Connate water can have salinities as high as those of seawater.

II. In situ bitumen recovery

Due to its very high viscosity (roughly 10^6 times that of water at room temperature), bitumen will not flow under normal reservoir temperature and pressure conditions. In order to extract bitumen from deep deposits, the bitumen viscosity needs to be reduced in situ. This process can be done either by increasing the reservoir temperature or injecting solvents. As such, in situ techniques of bitumen extraction can be steam-based (injecting high temperature steam), solvent-based (injecting organic solvent), or mixed (co-injection of steam and solvents). Other more 'radical' techniques, such as in situ (i.e. underground) combustion or electric heating, have also been proposed.

- **Primary In Situ Recovery**

Primary recovery or "cold production" is used to recover bitumen while no external energy is applied to the reservoir. The oil in these reservoirs is less viscous, although it is still classified as crude bitumen.

Cold heavy oil production with sand (or "CHOPS") is a primary recovery in which sands will be produced along with the bitumen, especially early in a well's life. This is because a system of fluid flow paths, or "wormholes," is formed in the reservoir and results in higher production rates, lower operating costs, and improved economics. Recovery factors vary between 3 to 10 percent using CHOPS.

Horizontal well technology is another technique used in primary recovery. Bitumen is produced via very long single-leg and multi-leg, or multilateral producing wells drilled in the reservoirs.

- **Secondary In Situ Recovery**

Secondary recovery technique, water and polymer flooding, has been showing success in the Brintnell region of the Athabasca Oil Sands Area.

- **Steam-Based Thermal In Situ Recovery**

Thermal energy is applied to heat the bitumen, lower the viscosity and increase its mobility to pump bitumen to the surface through wells using reservoir pressure, gas lift or downhole pumps.

Either cyclic steam stimulation (CSS) or steam assisted gravity drainage (SAGD) are used as the most common thermal techniques by injecting steam into the reservoir.

CSS is a discontinuous cyclic process in three steps. Steam is injected into the reservoir at high temperature and pressure at the first step. As the steam condenses, the latent heat from the steam heats the bitumen and reduces its viscosity; this step is called the soak cycle. At the final (or production) cycle, heated bitumen and condensed steam are transported to the surface. In surface facilities bitumen, water and produced gas are separated. Bitumen is diluted with diluent to be sent to upgraders or heavy-oil refineries via pipelines. Water is treated and recycled and natural gas is used as fuel. CSS is best suited in reservoirs with limited

vertical permeability such as in the Cold Lake and Peace River Oil Sands areas. A sketch of the CSS process is shown in Figure 1-3.

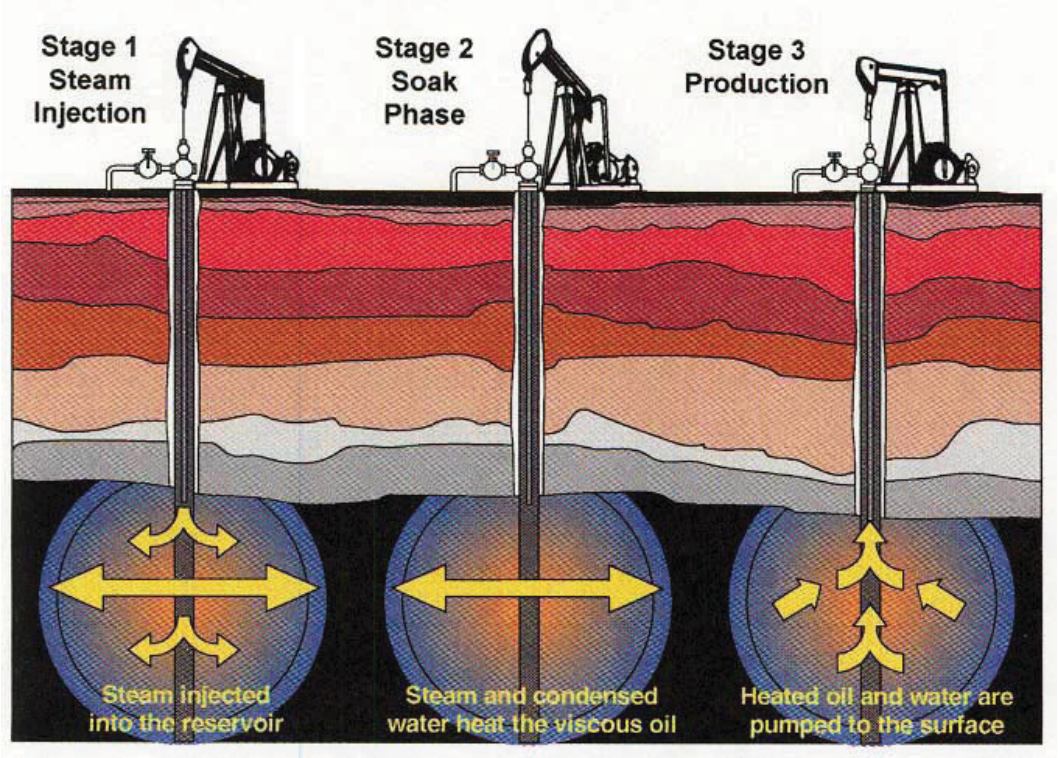

Figure 1- 3: Cyclic Steam Stimulation Process (CSS) [1]

SAGD is a continuous heating and production process that was developed during the late 1970s and early 1980s. Horizontal well pairs (with one directly above the other and separated by several metres) are drilled near the base of the oil sands zone, to up to 1000 m in length. Steam is injected into the upper horizontal well which is about 5 m above the lower horizontal well. The steam heats the bitumen, lowers its viscosity and causes it to drain by gravity into the lower zone of the reservoir. Bitumen and condensed steam are then drawn into the lower (production) well. SAGD is being successfully used in thick reservoirs

with high vertical permeability, such as in Athabasca Oil Sands area. A drawing of the SAGD process is shown in Figure 1-4.

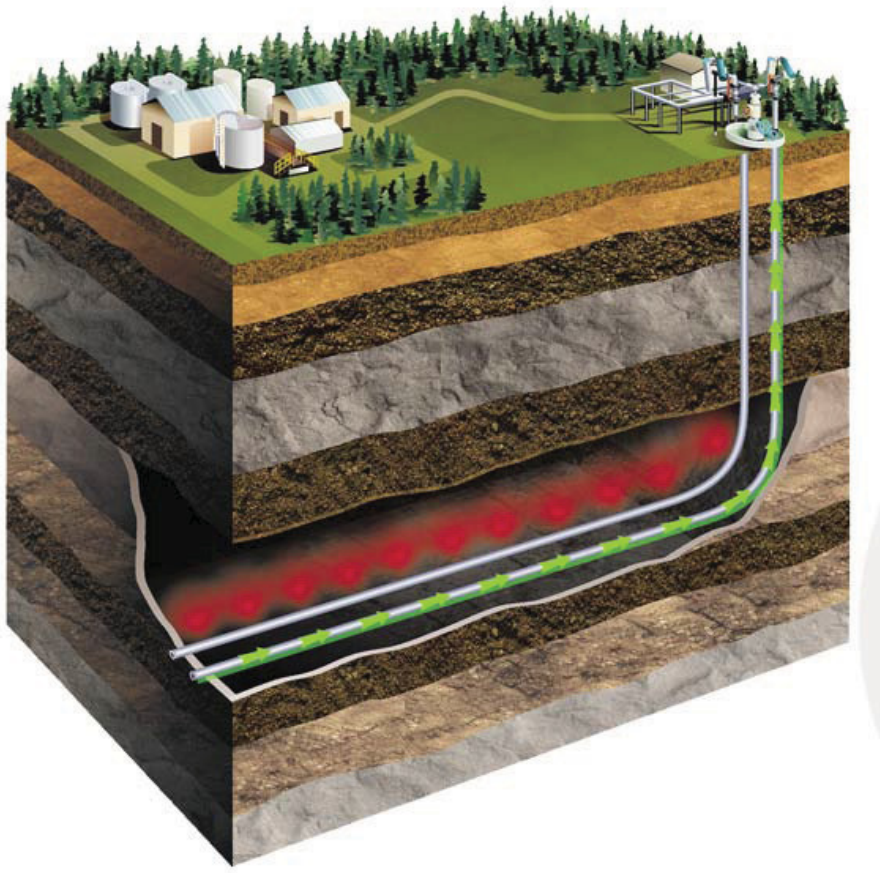

Figure 1- 4: Steam Assisted Gravity Drainage Process (SAGD) [1]

- **Other In Situ Recovery Technologies**

Steam-based thermal techniques consume high energy and water. Therefore the industry is trying to conduct modified and new in situ technologies to reduce both energy and water consumptions:

- Solvent-based processes, for example VAPEX (Vapour Extraction), in which a vaporized hydrocarbon solvent is

injected into the reservoir and the bitumen is produced via horizontal well-pairs.

- In situ combustion process, for example THAI (Toe to Heel Air Injection), which uses vertical air injection and horizontal well production.
- Hybrid processes in which both steam and hydrocarbon solvents are injected.
- Electrical heating (a far less common technique).

After mining/extraction and in situ operations, bitumen is diluted with a light low-viscosity hydrocarbon (diluent) to be shipped by pipeline to downstream refineries, or upgraded to a higher value synthetic crude oil or other petroleum products. Bitumen is converted from a viscous oil, deficient in hydrogen and with high levels of undesirable elements (sulphur, nitrogen, oxygen and heavy metals), to a "synthetic" or "upgraded" crude oil that has similar characteristics to conventional light sweet crude oil that has a very low sulphur content (0.1 to 0.2 percent). After upgrading, the synthetic crude oil is shipped through pipelines to refineries for conversion into various petroleum products (gasoline, diesel, jet fuel, fuel oils, etc.).

III. Proposed new technology: Solvent-based bitumen recovery

Along with the clear economic benefits, there are also serious environmental issues associated with the continuing growth of the oil sands industry: At present, much of the bitumen is extracted from the ore via a *water-based* process. This process requires substantial withdrawal of fresh water from the nearby rivers,

such as Athabasca River — a practice which is the direct cause of many environmental problems, such as those involving forest irrigation, fish habitats, and tailings ponds [3]:

- The current rate of water consumption is having negative impact on the Athabasca River, which supplies fresh water to the city of Fort McMurray, its neighbouring communities, and Lake Athabasca extended deltas. There is already reported damage to the habitat of fish species. Approved oil sands projects are allowed to draw 349 million m^3 of water per year from the Athabasca River; this amount of water is about the water usage of a city twice the size of Edmonton [3].
- Greenhouse gas emissions and depletion of natural gas resources are the issues raised from enormous energy consumptions to heat the process water.
- Tailings ponds result in environmental issues such as contamination of surface water and surrounding soils.

With planned increases in oil production in the coming decades (by up to five times the current level), these environmental issues will only become worse if the oil sands industry continued with its current practices. Indeed, because of these environmental problems, the future of the Canadian oil sands industry can become uncertain. Revolutionary changes in bitumen extraction techniques are therefore urgently needed. As the above-mentioned problems all stem from excessive water usage, there is a possibility that they can all be resolved at their roots if an alternative *non-aqueous* (or *solvent-based*) extraction method could be developed.

As shown in Figure 1-5, the basic principles of the non-aqueous technology are deceptively simple:

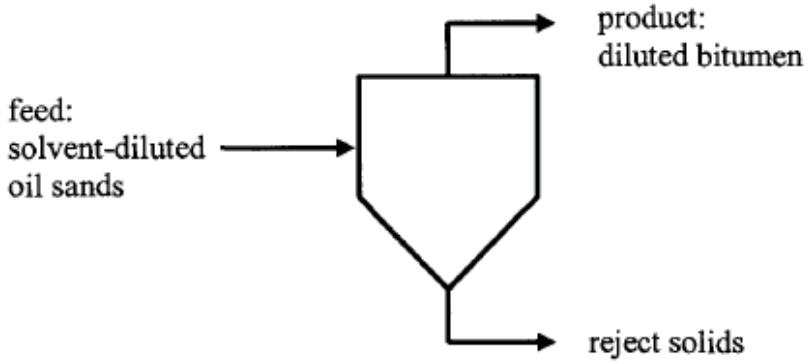

Figure 1- 5: Schematic of the first-stage separation of coarse solids from solvent-diluted oil sands. My Ph.D. research is motivated by problems which arise in the rejects streams.

The scenario begins with mined oil sand being first diluted in an organic solvent. This feed stream is then put through an initial stage of separation where large sand grains are removed as tailings, and the product, in the form of solvent-diluted bitumen, is sent downstream for further upgrading. Note that despite the shape of the above "vessel," the actual process need not be gravity settling. The removal of large solids from the feed stream can be accomplished using, for example, centrifuges, screens or liquid cyclones [4]. Such techniques are employed routinely in the industry, and the process in Figure 1-5 can be viewed as a tractable "engineering problem."

In the past decades, different non-aqueous bitumen extraction had been proposed. Solvent extraction-spherical agglomeration (SESA) process is an example. In this process, the solid particles coagulate with the addition of little amounts of water and implementation of mechanical agitation [5-9]. Water

droplets act as binders which trap hydrophilic solids and easily removable solid-water agglomerations are formed. Unfortunately, these proposed methods had not progressed beyond pilot testing.

The real challenges to non-aqueous extraction arise in the two outgoing streams in Figure 1-5:

- To avoid problems of fouling and general contamination, fine solids must be removed from the product (upper outgoing) stream before the diluted bitumen can be sent to downstream upgrading facilities.
- To avoid solvent loss, the residual oil attached to the reject sand grains (in the reject stream) must be recovered prior to disposal of the solids.

These challenges, as mentioned above, are the two major obstacles to any non-aqueous extraction process [5, 6, 7, 8-17].

To develop a viable non-aqueous extraction technology, it is necessary to acquire first an understanding of its underlying mechanisms. For this, research efforts are aimed at the basic science which governs the non-aqueous bitumen extraction process — particularly in regard to the above-mentioned obstacles to commercial implementation.

This PhD research is motivated by the second challenge that was mentioned above, namely, the need to recover residual oil from oil-soaked sand grains. Conventional methods of recovering this residual oil, such as evaporation and mechanical displacement, can be effective only to a point; after application of such methods, it is estimated that there will still be about 1% (by weight) of

residual oil left between the interstices of the sand grains. In this research, we propose to remove the remaining oil by washing the sand grains with water and surfactants. (The amount of water consumption for such a process is negligible in comparison to the current water-based process.) To minimize the use of water, *it is important to find a recipe which uses the least amount water to emulsify the maximum amount of diluted bitumen*.

This took my research into the realm of *microemulsions*. The theme of my thesis involves the use of microemulsions as "pseudo solvents" for dissolving the residual oil (i.e. diluted bitumen) trapped between the reject sand grains. Such an approach is inspired by the successful use of microemulsions in enhanced oil recovery operations [18, 19].

The research proceeded in two parallel directions:

- A systematic search for an optimal recipe for cleaning the oil-bearing sand grains, and
- Development of novel micromechanical (micropipette) techniques to investigate the fundamental interfacial characteristics of microemulsion systems.

By correlating the findings from these two lines of research, I will attempt to answer the important questions of *what* microemulsion system works, and also *why* it works.

To achieve near 100% recovery of residual oil from the oil-laden sand grains, it is essential to focus on the particular composition of surfactant solution, as well

as the washing process itself. This research focused heavily on the interfacial science that underlies the non-aqueous bitumen extraction.

Trapped oil between the reject sand grains is in general held back by capillary forces. Therefore, to achieve a good recovery of residual oil, it is important to not only look for lower interfacial tensions (IFTs) and desirable wetting characteristics, but the naturally available surfactants.

Based on low IFTs, small contact angles and availability, natural surfactants extracted from the Athabasca oil sands were found effective in this application. So firstly, the water-soluble surfactants were extracted from bitumen. Then the characteristics of the natural surfactants, the sodium naphthenates (SNs), were compared with commercially available SNs. These surfactants are natural constituents in many petroleum sources, including bitumen in the oil sands of Northern Alberta, Canada [20]. SNs can also be produced in abundance in refineries as the mixture of naphthenic acids is derived from straight-run distillates of petroleum, mostly from kerosene and diesel fractions [21]. The major advantage of using natural surfactants (SNs) during the so-called washing process is to keep the environmental risks of adding other chemicals to a minimum.

In Chapter 2 of this thesis, a literature review will be given on the basics of microemulsions. This will help to understand the science of how different types of microemulsions or liquid crystalline structures are formed.

The available viable techniques of measuring IFTs and contact angles are described in Chapter 3. This part of the thesis describes how these techniques can suffer from several disadvantages in the presence of surfactants.

Chapter 4 introduces the novel micropipette techniques for both IFT and contact angle measurements. These techniques were developed in this Ph.D. research to quantify ultralow IFTs and to measure the in situ oil/water/solid three phase contact angle.

The experimental results and discussion on the underlying mechanisms (on both the micro- and macro- scales) of residual oil recovery are provided in Chapter 5. Finally, the contributions of this research and suggestions for future work are discussed in Chapter6.

2. What are Microemulsions?

Microemulsions (μE's) are emulsions which consist of at least three components: two immiscible liquids (oil and water) and a surfactant; a "cosurfactant" (often a medium chain alcohol) may also be needed to further reduce the oil-water interfacial tension (IFT). These types of emulsions have three characteristics which distinguish them from ordinary emulsions: transparency, fluidity (i.e. low viscosity) and long-term stability. Microemulsions occur when properly-chosen surfactants drive the oil-water IFTs to ultra-low values (10^{-4} mN/m or lower); in some cases, the IFT may even be zero. In such situations, the highly flexible oil-water interface will allow oil and water to intermingle on the submicron (or "nano") scale, giving rise to very complex and non-spherical structures that range from 1 to 100 nm in size. Microemulsions are transparent because their nano-scale structures are too small to scatter optical light (which has wavelengths of typically a fraction of a micrometer); they are fluid because the ultralow IFTs allow for random intermingling of the two immiscible phases. Furthermore, the complex nano-scale morphologies in microemulsions often give rise to entropic effects which dominate over the enthalpic part of the free energy and result in thermodynamically stable systems.

Microemulsions can take on a variety of nano-scale structures. Some examples are oil-in-water dispersion, water-in-oil dispersion, and the so-called bicontinuous mixture. These structures are controlled by physicochemical parameters such as temperature, water/oil ratio, and salinity of the aqueous phase. It is believed that the physicochemical parameters can influence the mechanical

properties of the oil-water interface, which in turn determines the emulsion's nano-structure [22]; this will be further discussed in §2.3.1.

2.1. Macroscale: three common classes of microemulsions

Three types of microemulsions are seen to occur frequently (see Figure 2-1). They were first reported by Winsor [23] and are now known by his name; these are

- Winsor I: an oil-in-water dispersion, in the form of swollen micelles, which is in equilibrium with excess oil. It is commonly formed at low salt concentrations.
- Winsor II: a water-in-oil dispersion, in the form of swollen reverse micelles, which is in equilibrium with excess water. It is commonly formed at high salt concentrations.
- Winsor III: a middle phase, believed to be a bicontinuous mixture, which is in equilibrium with both excess oil and excess water. It is commonly formed at intermediate salinities.

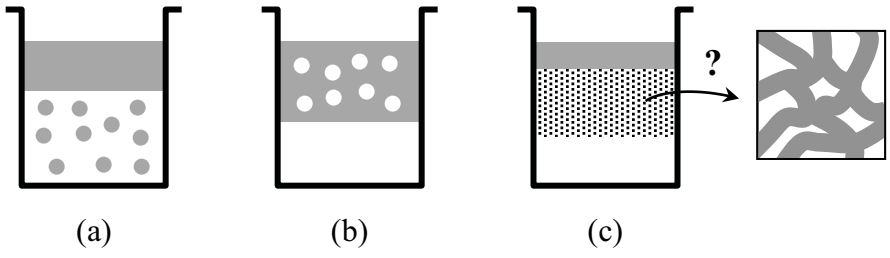

Figure 2- 1: The three common forms of microemulsions: (a) Winsor I, (b) Winsor II, and (c) Winsor III. The middle phase of Winsor III can be bicontinuous.

It should be noted that the above classifications do not include all possible microemulsion types. For example, at high surfactant contents, a less common single-phase microemulsion appears; it is sometimes called the "Winsor IV" microemulsion.

2.2. Microscale: many forms of microstructure

On the colloidal (i.e. nanometre) scale, microemulsions can exhibit many different structures. These microstructures are controlled by physicochemical parameters such as temperature, water/oil ratio, salinity of the aqueous phase, and, in the case where the oil phase is an alkane, the chain length of the hydrocarbon molecules. Optical microscopy is often not useful for characterizing microstructures because the important details occur on the nanometre scale (wavelength of visible light is approximately 0.5 μm). Some examples of the techniques that are used for microstructure characterization include: freeze fracture electron microscopy, x-ray diffraction, and neutron scattering.

Figure 2-1 illustrates the commonly-accepted view regarding the microstructures of the bottom phase of Winsor I μE, and of the top phase of Winsor II μE. These structures are, respectively, swollen micelles and swollen reverse micelles. In the first case (Fig. 2-1a), liquid oil is "solubilized" in water as it is carried inside the spherical micelles. The opposite occurs in the second case (Fig. 2-1b): liquid water is "solubilized" in oil by residing inside the reverse micelles. In contrast to these simple pictures, the situation is much more complicated when we deal with the middle phase of Winsor III microemulsions (Fig. 2-1c). Judging from its location in the vessel, it is clear that the middle layer

has a density that is intermediate between those of pure oil and pure water—it must therefore be a mixture of oil and water. Under normal conditions, oil and water will mix as macroemulsions, i.e. with one liquid dispersed as micron-sized spherical droplets in the other (this is always the case when the oil-water interfacial tension is reasonably large, e.g. > 1 mN/m). However, as the middle layer in a Winsor III system is seen to be immiscible with both excess oil and excess water, it cannot simply be an oil-in-water or water-in-oil emulsion. This has led many researchers to speculate that the middle phase is a complex *bicontinuous* mixture, consisting of networks of water and oil strands interpenetrating on the colloidal (i.e. nanometre) scale. An unrealistic bicontinuous structure is shown in Figure 2-2, where a surface of regularly ordered pattern (more precisely, a bicontinuous cubic pattern) subdivides space into two continuous regions of equal volumes [23].

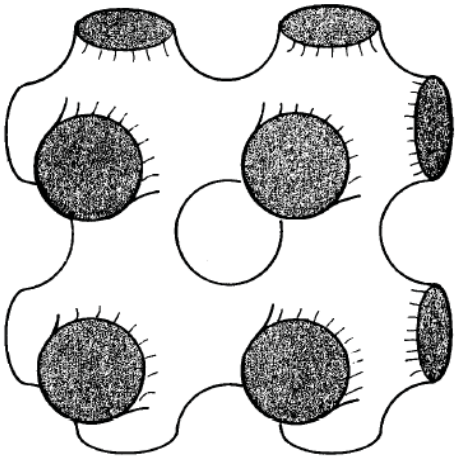

Figure 2- 2: A bicontinuous cubic phase with a zero mean curvature [23].

The dividing surface can either be (a) a surfactant monolayer, with oil and water on opposite sides, or (b) a surfactant bilayer, perhaps slightly swollen with oil, with water on either side of the surface. In reality, the notion of a surfactant sheet (monolayer or bilayer) forming a bicontinuous cubic pattern is not realistic, as Brownian undulations can easily disrupt and randomize the cubic pattern (i.e. the structure in Fig. 2-2 is the so-called "zero-Kelvin" shape). On the other hand, thermally randomized bicontinuous structures are entirely realistic and occur frequently in Nature. When the dividing surface is a surfactant monolayer, the mixture is called a *bicontinuous microemulsion*; when the dividing surface is an oil-swollen bilayer, the mixture is often called an L_3 phase [23-25]. Two features are worth noting about these random structures: (1) For the bicontinuous μE or L_3 phase to occur, the oil-water IFT must be ultralow (typically 10^{-4} mN/m or less); (2) while bicontinuous μE's have water-to-oil (w/o) ratios of order unity, L_3 phases are characterized by very large w/o ratios.

In addition to random bicontinuous mixtures, the middle layer in Winsor III systems can also adopt other microstructures. Two of the most common structures share a similar trait in that they are characterized by stacks of parallel sheets. When the sheets are surfactant monolayers separating alternating layers of oil and water, the structure is called the *lamellar phase*; when the sheets are oil-swollen bilayers with water on both sides, the resulting mixture is called the L_α phase. As in the previous case, lamellar phases are known to have w/o ratios of order unity, while L_α phases have $w/o >> 1$ [23-25]. Unlike the bicontinuous structures, the lamellar and L_α phases are not completely random: they both

exhibit a periodic (or crystalline) pattern in the direction normal to the surfactant layers. For this reason, these sheet-like structures belong to a general class of materials called *liquid crystals*. Because they are partially crystalline, liquid crystals are in general much more resistant to flow compared to mixtures with completely randomized microstructures.

Kellay et al. [26] had produced experimentally the above microstructures for an AOT + aqueous NaCl + *n*-alkane system. (AOT, or Aerosol OT, is a common anionic surfactant.)

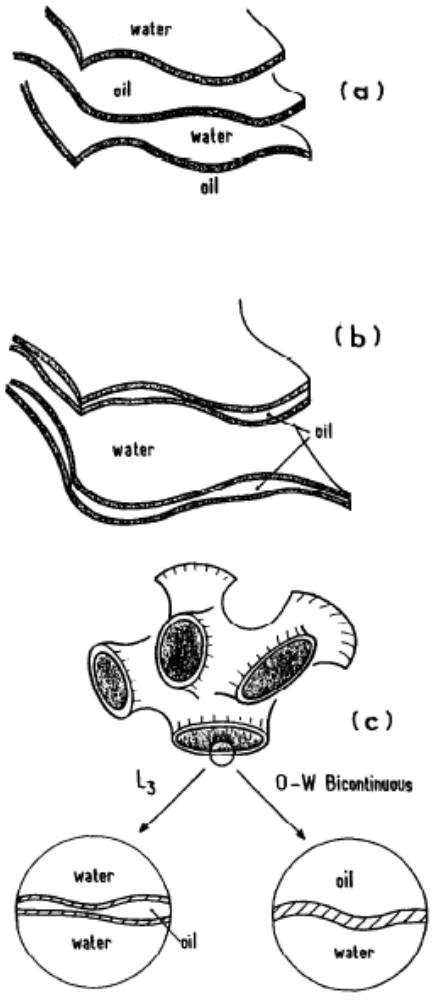

Figure 2- 3: Middle phase microstructure for the AOT + aqueous NaCl + *n*-alkane system. The alkane carbon number is: (a) N<10, (b) N=10, (c) N=12 [26].

As seen in Figure 2-3, by varying the chain length of the oil phase, Kellay et al. [26] were able to produce the various microstructures as discussed above. In particular, shorter chain alkanes produced lamellar third phases which contained a significant amount of oil. For example, with octane as the oil phase, a lamellar structure consisting of films of water and oil separated by surfactant monolayers of thickness ~10 Å was produced (Fig. 2-3a). Using decane as the oil led to an L_α phase comprising of surfactant bilayers slightly swollen by oil, and with water existing between the bilayers (Fig. 2-3b). For mixtures with dodecane as oil, the salinity of the aqueous phase determined whether the third phase was of a bicontinuous isotropic or L_3 structure (Fig. 2-3c). As expected, the L_3 structure retained virtually no oil, while the bicontinuous phase contained comparable amounts of water and dodecane.

As our goal is to solubilise oil with the least amount of water, the lamellar and bicontinuous structures (Fig. 2-3a and the right side of Fig. 2-3c), both with $w/o \sim 1$, appear to fulfil such a need. However, since the lamellar phase (Fig. 2-3a) is a liquid crystal, its transport will be problematic. For this reason, it is concluded that the bicontinuous phase (right side of Fig. 2-3c) will be the ideal form of microemulsion for solubilizing the residual oil trapped between the waste sand grains.

To understand how different types of microemulsions or liquid crystalline structures are formed, it is essential to first examine the physics (in particular, the mechanical properties) of surfactant layers. This will be discussed below.

2.3. Curvature elastic properties of surfactant monolayers

Figure 2-4 shows an oil-water interface that is saturated with surfactants. Due to the interplay of the various intermolecular forces, the interface will, in general, *not* prefer to be in a planar state (much like an old photograph which has been exposed to humidity). In the absence of external forces, the interface will adopt a curved shape that is characterized by a *spontaneous curvature* C_0 (units of m^{-1}); this will be the interface's minimum energy configuration.

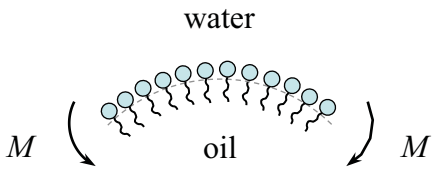

Figure 2- 4: An oil-water interface saturated with surfactants. The interface will in general show elastic resistance to changes in curvature.

From this minimum energy configuration, any curvature change imposed on the interface will be resisted by an elastic bending moment M. To first order, we have the relation

$$M = K(\bar{C} - C_0) \tag{2.1}$$

where M is the bending moment, $\bar{C}$ is the mean curvature of the interface (i.e. the sum of the two principal curvatures), and K, the proportionality constant, is called the *bending elasticity* of the surfactant monolayer. The curvature elastic properties of a surfactant monolayer is therefore characterized by two parameters: K and C_0. As sign convention, C_0 is defined as positive if the interface is bent

toward the oil side (favouring oil-in-water emulsions), and negative if the opposite occurs. The bending elasticity K is positive definite.

Although an extremely small effect, curvature elasticity can be important — even dominant — when the IFT becomes vanishingly small. For a surfactant monolayer, the interfacial free energy F is given by the following expression due to Helfrich [27, 28]:

$$F = \frac{K}{2} \int (\bar{C} - C_0)^2 \, \mathrm{d}S + \gamma S \,. \tag{2.2}$$

In the above expression, S is the interfacial area and $\overline{C} - C_0$ is the local excess curvature which is integrated over the entire surface. As will be explained next, the two physical parameters in equation 2.2, K and C_0, are critical to the phase behaviours of microemulsions.

2.3.1. Importance of K and C_0 — and how they are manipulated

For reasonably large interfacial tensions ($\gamma > 1$ mN/m), the curvature elastic properties, K and C_0, are completely negligible. Indeed, equation 2.2 suggests that curvature effects (the first term on the RHS) can be ignored when

$$K\left(\overline{C} - C_0\right)^2 / \gamma << 1,$$

or equivalently, when $r_c >> \sqrt{K/\gamma}$, where r_c is the radius of curvature of the surfactant sheet. Putting in typical values for K and γ (10^{-21} J or $1\,k_B T$ for K, and 1 mN/m for γ), it is seen that the radius of curvature of an interface must be nm's or smaller before bending effects are appreciable; this is not likely to happen as the thickness of the surfactant layer is itself nm's in thickness. However, if the

IFT is lowered by orders of magnitude (through addition of surfactants and cosurfactants) bending effects will play an increasingly important role. Since microemulsion systems are characterized by ultralow IFTs, it is not surprising that their microstructures are controlled by K and C_0. The following is a discussion on how K and C_0 control a microemulsion's nano-scale structure.

As the interfacial tension attains ultralow values (10^{-4} mN/m or less), K and C_0 will be the two parameters which control the nanoscale morphology of microemulsion (or liquid crystal) systems. We first focus on the spontaneous curvature C_0. It is easy to see that an interface which bends spontaneously toward the oil phase will favour formation of oil-in-water emulsions. In accordance to the sign convention, it can be stated that a positive C_0 favours Winsor type I systems. Conversely, a negative C_0 will favour Winsor type II systems. What is most interesting is that Winsor III microemulsions, the type that is most valuable to our application, are associated to zero (or very small) spontaneous curvatures [29]. In the absence of Brownian undulations, surfactant layers with $C_0 = 0$ will likely form a periodic, bicontinuous array such as the one shown in Figure 2-2 [30]. If one now "switches on" Brownian motions, a randomized bicontinuous microemulsion will result if the thermal energy is strong enough to disrupt the periodic array [31]. Whether a bicontinuous μE will form is determined by the bending elasticity K of the interface. De Gennes and Taupin [32] proposed the following very simple idea: a random bicontinuous μE (Fig. 2-3c) can be formed if the surfactant layer is "floppy." If, on the other hand, the

adsorbed layers were "stiff," it would easier to stack the layers on top of one another and form a lamellar or L_α structure (Fig. 2-3a or 2-3b). To determine whether a surfactant layer is floppy or stiff, de Gennes and Taupin [32] introduced a parameter known as the persistence length ξ_K. This can be thought of as the lateral distance along the interfacial surface over which the surfactant layer is considered stiff. (Very roughly, a surfactant layer of dimensions $\xi_K \times \xi_K$ will behave as a stiff sheet, whereas a layer with area $10\xi_K \times 10\xi_K$ or larger will appear floppy.) An expression for the persistence length will reflect the competition between thermal and bending energies; it is given by [32]

$$\xi_K = a \exp(2\pi K / k_B T) \tag{2.3}$$

where $k_B T$ is the thermal energy and a is the "molecular cutoff" (i.e. the size of a surfactant molecule). The persistence length ξ_K is often compared to the average distance λ between the water and oil domains in a mixture. As a very rough guide, when $\xi_K > \lambda$, a lamellar or L_α liquid crystal will result (Fig. 2-3a or 2-3b); this is analogous to the stacking of a deck of stiff cards. When $\xi_K < \lambda$, the surfactant layers can be strongly folded and wrinkled, and this will lead to bicontinuous or L_3 microemulsions (Fig. 2-3c). De Gennes and Taupin [32] also emphasized the strong (exponential) dependence of ξ_K on the bending rigidity K (see eqn. 2.3). Using typical values, they demonstrated that it was very easy to "soften" a monolayer through addition of a suitable cosurfactant; the value of K could typically be decreased by a factor of five. Because of the exponential dependence, this led to a dramatic reduction in the persistence length ξ_K — from

1 μm (corresponding to lamellar liquid crystals) to 10 nm (corresponding to bicontinuous microemulsions). As such, a gel-like liquid crystal is said to be "melted" by addition of a small amount of cosurfactant, which is often a medium chain alcohol. (Note that the above description is somewhat oversimplified as it does not account for colloidal forces between the surfactant sheets. In reality, all surfactant sheets interact through van der Waals attraction. Repulsive forces between the sheets can be electrostatic across a water layer and steric across an oil layer [22]).

The bending elasticity K and spontaneous curvature C_0 are sensitive to many physicochemical factors. It is known, for example, that a microemulsion can be driven from a Winsor I to Winsor III to Winsor II phase by increasing salinity, decreasing temperature, or increasing surfactant concentration [18]. For instance, as can be seen in Figure 2-3, since the structure of the third phases is a function of alkane chain length, it is possible that the elastic properties of surfactant monolayers at the oil-water interface depend on this factor as well. With regard to other factors, higher salinities may decrease the double layer repulsion between surfactant head groups, thus bending the interface toward the water side; lowering the temperature may decrease the lateral pressure between the hydrocarbon chains, thus curving the interface toward the oil side; etc. All these changes will have profound effects on K and C_0, which will in turn control the microstructure of the oil-water mixture.

3. Interfacial Tension and Contact Angle Measurements

The effect of surface tension is observed every day. The force of surface tension causes a slowly leaking faucet to drip, or a steel needle to float on the surface of water even though its density is much higher than that of water. Under tension, the surface of a liquid is thought of as having a "skin." A clean liquid surface, however, is not elastic like a rubber sheet in which the tension increases as it is stretched; a clean liquid surface can be indefinitely expanded without changing the surface tension.

A skin under tension is the mechanical model of the liquid surface. Any given patch of the surface, everywhere on the surrounded surface, experiences an outward force tangent to the surface. The perpendicular force to the perimeter, per unit length of the surface, is defined as the *surface tension*, γ. Due to imbalanced intermolecular attractive forces, molecules at the interface have a higher potential energy than molecules in the bulk. The difference in potential energy results in an excess free energy per unit area of the surface which is numerically equivalent to the surface tension. Imagine a flat patch of fluid interface of rectangular shape with dimensions of W in width and L in length. An amount of $\gamma W \Delta L$ is needed at the boundary to expand the length to $L+\Delta L$. In other words, the work done to expand the area is $\Delta A \gamma$, as $W \Delta L$ is the change in area. This work corresponds to the increase in surface free energy. Therefore, the surface tension γ is equivalent to the surface free energy per unit area. Surface tensions of room-temperature organic fluids are in the range of 20 mN/m to 40 mN/m, while the value for pure water is 72 mN/m at 25ºC. The *interfacial*

tension is a tension associated with the interface between two immiscible liquids, such as oil and water.

To understand the shapes adopted by liquid surfaces, the *surface energy* is essential. A system at equilibrium is in a state of minimum free energy; since the surface free energy is proportional to the surface area, the surface area is also minimized. For instance, in the absence of gravity, a liquid droplet is spherical in shape, as the sphere has the least surface area for a given volume. A droplet suspended from a needle tip in a gravitational field does not show a spherical shape because its elongation reduces the gravitational potential energy.

The behaviour of surface active agents, or *surfactants*, can become much clearer from the perspective of surface energetics. For a two-component liquid mixture in thermodynamic equilibrium, there is a preference of adsorption of one component at the surface if it causes the surface energy to decrease. Surfactants are the molecular species strongly adsorb at the surface even while they have very low concentration in the bulk liquid. Surfactants are very important in many biological and industrial processes, as well as in oil-water-surfactant systems such as food colloids and tertiary oil recovery.

Surface free energy can be applied also to the interface between a solid and a fluid. Figure 3-1a shows a liquid droplet resting on a solid surface surrounded by a gas (e.g. air). Three different interfaces exist in this system: solid-gas, solid-liquid, and liquid-gas, with each interface having its characteristic surface free energy per unit area. The trade-off in the surface areas of the various interfaces results in the state of minimum free energy for this system. *Contact line* is the

region of contact between the gas, liquid, and solid. The liquid-gas surface makes an angle θ with the solid surface measured through the liquid. This angle is known as *contact angle*. The contact angle is a characteristic of a particular three-phase system which achieves a value that minimizes the free energy of the system. Figure 3-1a shows a system with smaller contact angle than a system in Figure 3-1b. Better wettability occurs at smaller contact angles. For zero contact angle (i.e. $\theta = 0$), the liquid perfectly wets the solid surface.

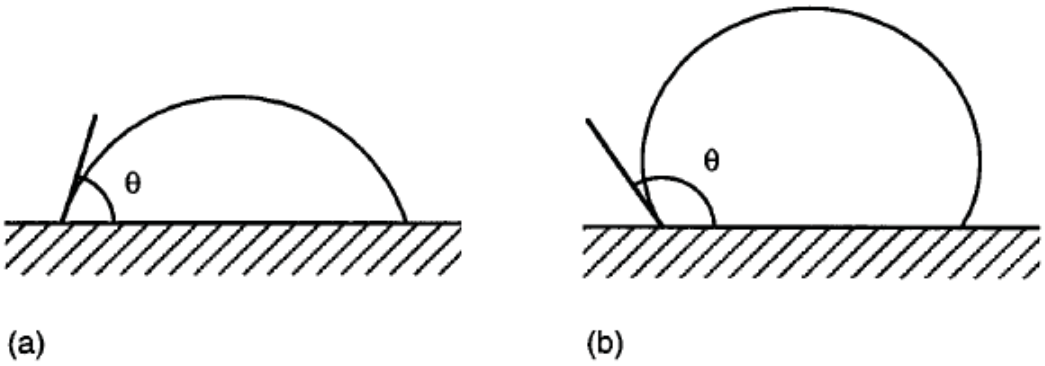

Figure 3-1: Scheme of contact angles. Liquid (a) wets the solid better than liquid (b).

Measurements of surface tension, interfacial tension and contact angle are very important in many fields of science, medicine, engineering and environment. A number of standard methods are available to measure these characteristics.

3.1. Theory behind the methods of measuring surface tension

In a three-phase (solid, liquid, and gas) system, while the system is in static mechanical equilibrium, the contact line is motionless. The net force on the line is zero. Interfacial energies of the solid-gas, solid-liquid, and liquid-gas interfaces, denoted by γ_{SG}, γ_{SL}, and γ_{LG}, raise the forces acting on the contact line.

Figure 3-2 shows *Young's equation* at the condition of zero net force and contact angle θ:

$$\gamma_{SG} = \gamma_{SL} + \gamma_{LG} \cos\theta \tag{3.1}$$

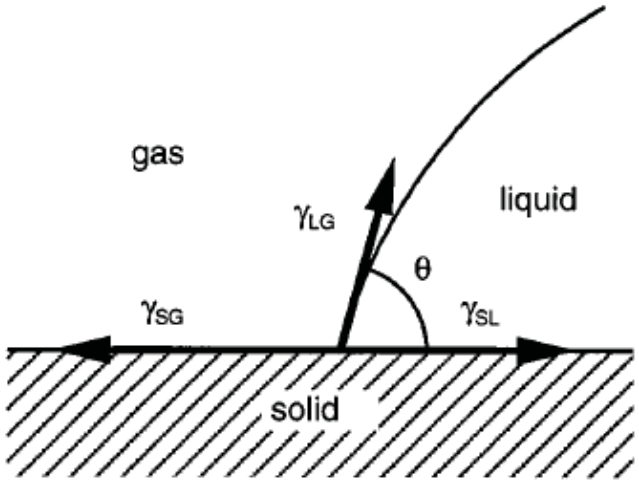

Figure 3-2: Surface tension forces acting on the contact line in mechanical equilibrium [33-36].

Since the contact angle is dependent on the surface energies between the various phases in the system, it is an intrinsic property of the system.

Figure 3-3a illustrates a curved section of surface. Because of the curvature, the surface tension forces, acting on a curved section, pull the surface toward the concave side of the surface. As such, for mechanical equilibrium, the surface tension of the droplet causes an increase in pressure in the droplet. On the other hand, if one had a saddle-shaped section of surface as shown in Figure 3-3b, the surface tension forces oppose each other and reduce or eliminate the required pressure difference across the surface. The mean curvature of a curved surface is defined in terms of the two principal radii of curvature, R_1 and R_2, whose arcs are perpendicular to one another. From basic force balance, it can be shown that the

pressure difference across the curved surface is proportional to the surface tension and to the mean curvature:

$$P_{\mathrm{A}} - P_{\mathrm{B}} = \gamma\left(\frac{1}{R_1} + \frac{1}{R_2}\right) \tag{3.2}$$

where γ is the surface (or interfacial) tension, and the term in brackets is twice the mean curvature. The sign of the radius is positive if the center of curvature lies in phase A and negative if it lies in phase B. Equation 3.2, known as the *Young–Laplace equation*, gives the pressure change across a curved surface (the so-called the *Laplace pressure*). By measuring the Laplace pressure of a surface with known curvature, the surface tension can be determined.

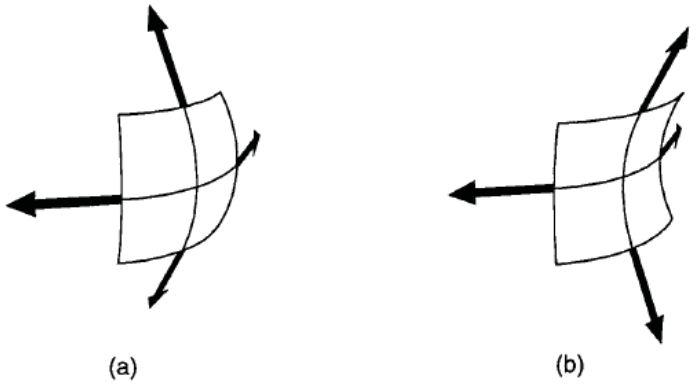

Figure 3-3: Curved surfaces that have principal radii of curvature: (a) the same sign, and (b) the opposite sign [33-36].

Methods of measuring surface tension are usually based on quantifying the static shape of an axisymmetric drop or bubble, or on the mechanical instability of such drops or bubbles. Figure 3-4a shows the shape of a hanging droplet (the pendant drop), and Figure 3-4b shows a captive or sessile drop. In these two techniques, the gravitational field creates a non-spherical droplet as it attaches to a

solid support. The Young–Laplace equation for an axisymmetric surface in a gravitational field can be written as a set of first order differential equations:

$$\begin{aligned} \frac{dx}{ds} &= \cos\phi \\ \frac{dz}{ds} &= \sin\phi \\ \frac{d\phi}{ds} &= \frac{2}{b} + \left(\frac{\Delta\rho g}{\gamma}\right) z - \frac{\sin\phi}{x} \\ x(0) &= z(0) = \phi(0) = 0 \end{aligned} \tag{3.3}$$

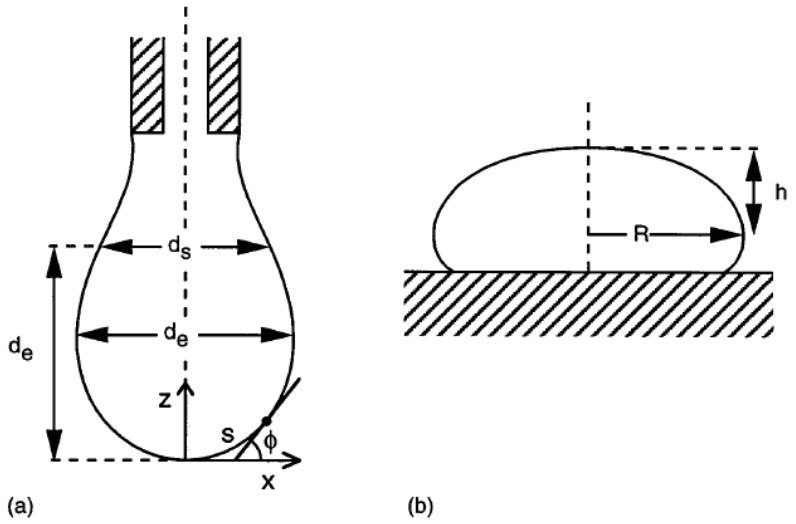

Figure 3-4: (a) Characteristic dimensions in pendant drop: d_e and d_s, and the coordinates used in the Young–Laplace equation (b) Characteristic dimensions in sessile drop: R & h [33-36].

Figure 3-4 shows x and z, respectively the horizontal and vertical coordinates; *s* is the arc-length, Φ is the angle between the surface tangent and horizontal, *b* is the radius of curvature at the apex of the droplet or bubble, Δρ is the density difference between two fluid phases, and g is acceleration of gravity. Useful method of measuring surface tension can be achieved by matching the computed

drop shape to the experimental one. The computed shapes are derived from numerical integration of Equation 3.2. Dividing all lengths in Equation 3.2 by *b*, leads to the equation that only contains one dimensionless parameter, $\beta=\Delta\rho g b^2/\gamma$, which is sometimes called the Bond number or shape factor. The shape of an axisymmetric droplet, bubble or meniscus depends only on this parameter. It can also be written as $2b^2/a^2$, where $a = \sqrt{2\gamma / \Delta\rho g}$ has units of length and is known as the capillary constant.

Surface tension can also be measured by dynamic methods based on capillary waves. Oscillations of the liquid surface result in capillary waves; the surface tension and wavelength are two parameters which the frequency of oscillation is dependent on. Owing to thermal fluctuations, very low amplitude capillary waves are always present at the liquid surfaces. By purposely perturbing the surface, larger amplitude capillary waves can be created.

3.2. Commercially Available Methods of Tensiometry

Several commonly used methods of measuring surface/interfacial tension and contact angle exist. The choice of a method depends on the conditions of the system to be studied, the accuracy required, and the ability to automate the measurements. Table 3-1 shows a list of commercially available instruments:

Table 3-1: Commercially Available Instruments

Method	Instrument type
Capillary rise	Manual
Wilhelmy plate/du Nouy ring	Manual, mechanical balance
Wilhelmy plate/du Nouy ring	Manual, electrobalance

Wilhelmy plate/du Nouy ring	Automatic, electrobalance
Maximum bubble pressure	Automatic
Pendant/sessile drop	Manual
Pendant/sessile drop	Automatic
Drop weight/volume	Automatic
Spinning drop	Manual

This Chapter reviews the methods that are used in surface science laboratories. Many of the industrial operations require measurements of interfacial tension in liquid-fluid systems. In multiphase and multicomponent systems, in order to understand and control the interfacial processes, the importance of dynamic interfacial tensions has been increasingly recognized. When the value of interfacial tension becomes significantly lower than 1mN/m, techniques of measuring ultralow interfacial tensions are needed. Ultralow interfacial tensions are common in liquid-liquid emulsification processes when surfactant solutions are used.

Figure 3-5 classifies common interfacial tension methods into five groups. Group I are the techniques commonly used as direct interfacial tension measurements with a microbalance. Group II represents the techniques which determine the interfacial tensions from direct measurements of capillary pressure. Equilibrium between capillary and gravity forces is used in the techniques of Groups III and IV. The balance between surface tension and variable volume of liquid determines the interfacial tension of Group III, and the distortion of a fixed volume liquid droplet is measured under the influence of gravity is a technique

used for Group IV. Group V introduces the techniques in which the distortion of a fluid droplet is measured under centrifugal forces. This last group is more common in determining ultralow interfacial tensions.

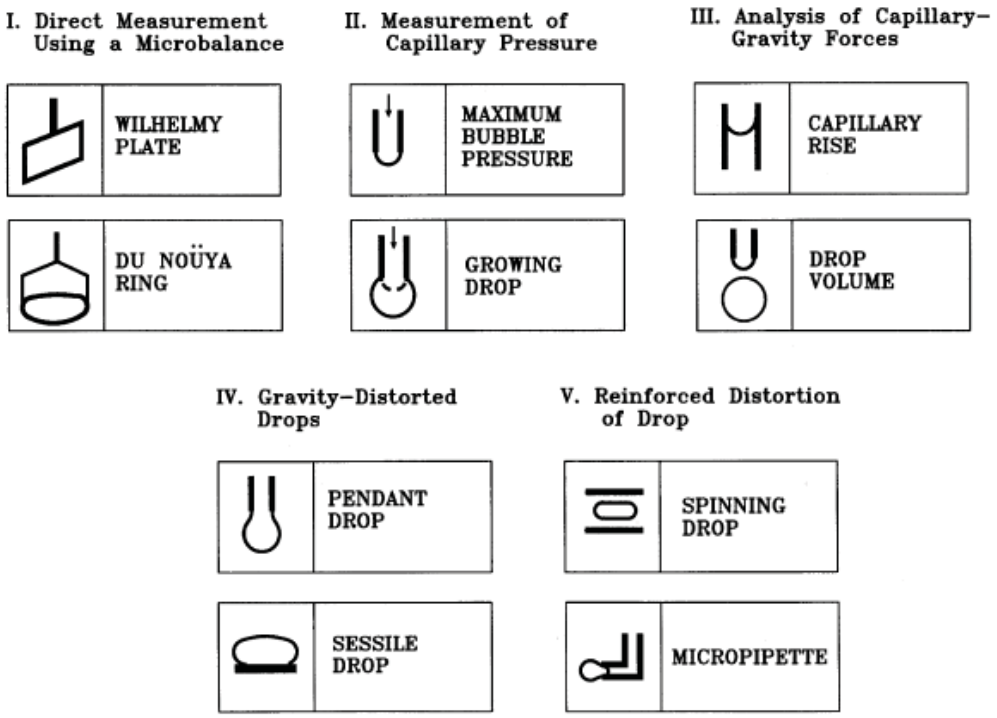

Figure 3-5: Interfacial tension measurements techniques [37].

3.2.1. Wilhelmy Plate and du Nouy Ring Methods

These two standard methods are based on the pull of a liquid surface directly on a solid object. The solid object in the Wilhelmy plate method is a flat, thin plate which wets the test liquid with a contact angle of zero degree. The surface tension force of the liquid causes the plate to be pulled down into the liquid. The above force applied to the plate is gradually increased to level the bottom edge of the plate with the flat surface of the liquid. The surface tension is determined via the force measurement, f:

$$\gamma = \frac{f \cos\theta}{2(l+t)} \tag{3.4}$$

where l is the plate length and t is its thickness. The du Nouy ring method is to contact the liquid surface with the ring and measure the force as the surface is lowered till the maximum force $f_{\max}$ occurs. This maximum force is recorded just before the ring detaches from the surface. The surface tension is computed from the following equation:

$$\gamma = \left(\frac{f_{\max}}{4\pi R}\right) F\left(\frac{R^3}{V}, \frac{R}{r}\right) \tag{3.5}$$

where R and r are, respectively, the radii of the ring and wire, V is the liquid volume raised by the ring, and F is a correction Factor [tabulated in Table 5 of [36]].

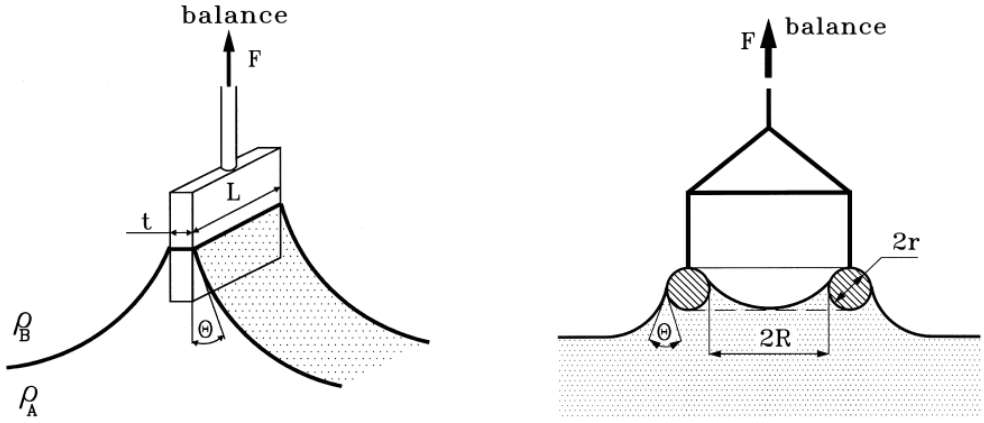

Figure 3-6: Schematic of the Wilhelmy plate method and du Nouy ring method [37, 38].

3.2.2. Measurement of Capillary Pressure (Maximum Bubble Pressure)

The Maximum Bubble Pressure Method (MBPM) determines the surface tension via direct measurement of the pressure in a bubble. As shown in Figure 3-7, a

tube is immersed at the depth t of the test liquid and gas is injected to form a bubble at the tip of the tube. The sum of hydrostatic and Laplace pressures gives the increase in bubble pressure, P_b , over ambient pressure, P_a , arising from the interface:

$$\delta P = P_b - P_a - \Delta\rho g t = \Delta\rho g Z_B + \frac{2\gamma}{b} \tag{3.6}$$

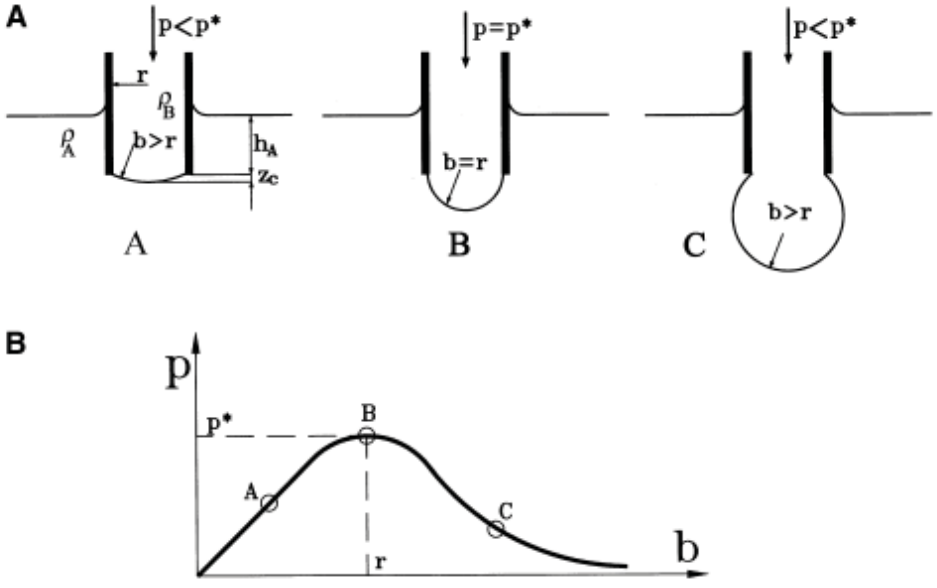

Figure 3-7: Maximum Bubble Pressure Method. (A) The shape of bubble at the stages of bubble growth. (B) Relationship between the pressure inside and radius of the bubble [39, 40].

The new bubble begins to form and while b, the radius of curvature at the bubble apex decreases, Z_B increases and this procedure results in an increase in pressure in the bubble. When δP reaches a maximum, thus the pressure in the bubble reaches a maximum. This in turn is theoretically related to the surface tension. Equation 3.6 can be rewritten in dimensionless form for $\delta P = \delta P_{max}$:

$$\frac{r}{X} = \frac{r}{b} + \frac{r}{a}\frac{Z_B}{b}\left(\frac{\beta}{2}\right)^{1/2} \tag{3.7}$$

where r is the radius of the tube, X is defined as a length $X = 2\gamma/\delta P_{\max}$, a is the capillary constant, and β is the Bond number. Values of X/r are dependent on a given value of r/a within the range $0 < r/a < 1.5$. The relation in equation 3.7 is combined with the numerical solutions of equation 3.3 to calculate the surface tension by an iterative procedure [33]. A knowledge of the fluid densities, tube radius, and depth of immersion of the tube is required for standard MBPM. In studying the dynamic interfacial tensions, the maximum bubble and drop pressure method or its modifications have proved very efficient and useful.

3.2.3. Capillary Rise and Drop Weight or Volume Methods

In the capillary rise method, a glass capillary tube is brought into contact with a liquid surface. If the liquid rises into the tube and wets the glass with a contact angle of less than 90°, the surface tension is directly proportional to the height of rise h. Applying equation 3.2 to the meniscus in the capillary tube leads us the following relationship:

$$\Delta\rho g h = \frac{2\gamma}{b} \tag{3.8}$$

where b is the radius of curvature at the meniscus and $\Delta\rho$ is the difference between the liquid and gas densities. By using a clean glass capillary with a very uniform diameter of less than 1 mm, accurate results can be obtained. This technique is very useful for pure liquids and provides high accuracy results at low cost.

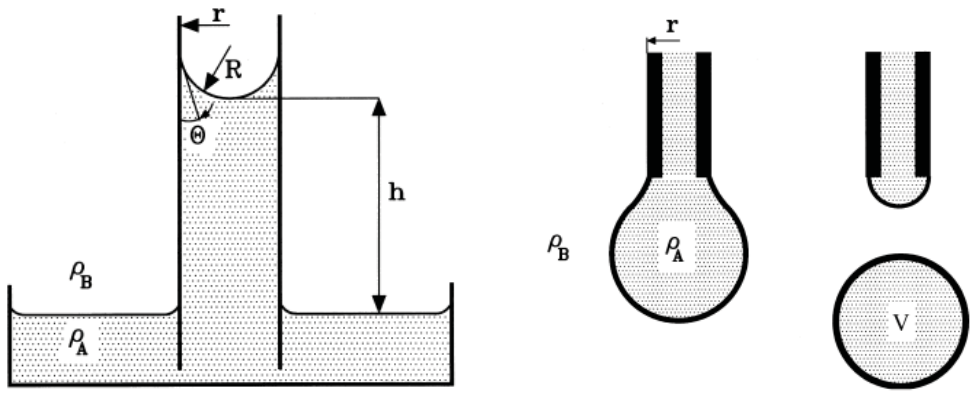

Figure 3-8: illustration of the Capillary Rise & Drop Volume or Weight Methods [41-44].

In the drop volume or weight method, the volume or weight of a falling droplet from a capillary (with radius r) is measured. The weight of the drop has the following relationship with the interfacial tension:

$$W = V\,\Delta\rho g = 2\pi r\gamma\, f\left(\frac{r}{\sqrt[3]{V}}\right) \tag{3.9}$$

where V is the drop volume, r is the capillary radius, and f is the correction factor. Since only a portion of the drop volume detaches from the capillary, f as a function of $r/V^{1/3}$ is required [41, 44]. Although the measurement of interfacial tension with the drop weight or volume method is simple, the results are quite sensitive to vibrations of the apparatus: vibrations can cause premature detachment of the droplet from the end of the capillary before reaching the critical size. Another issue occurs in multicomponent solutions, where the measurements might not reflect the equilibrium saturation at the interface.

3.2.4. Analysis of Gravity-Distorted Drops

In the pendent or sessile drop methods (Figure 3-4), the shape of an axisymmetric droplet depends on the Bond number. The relative importance of gravity to surface tension in determining the shape of the drop is shown via the Bond number. For near-zero Bond numbers, the dominant force is surface tension and the droplet is spherical. For larger Bond numbers, the droplet is significantly deformed by gravity. These two techniques, pendent and sessile drop, capture an image of the droplet and compare its shape and size to theoretical profiles obtained from integration of equation 3.3 for different values of β and b. The β and b values are determined from shape and size comparison, then the surface tension is calculated from:

$$\gamma = \frac{\Delta\rho g b^2}{\beta} \tag{3.10}$$

As shown in Figure 3-4, for pendent drops, the ratio d_s/d_e is correlated with H, a shape factor from which the surface tension is calculated [35, 45]:

$$\gamma = \frac{\Delta\rho g d_e^2}{H} \tag{3.11}$$

For sessile drops, analytical equations are used to directly calculate surface tension from the characteristic dimensions [35]. Methods in which the entire shape of the drop is fitted to the Young-Laplace equation can give more accurate results. Recently the entire process has been automated by using digital imaging and computer image analysis. Analyzing a sequence of images enables us to track changes in interfacial tension of surfaces covered with surfactants, and track the surface area and volume of the droplet or bubble [46-48]. Automated pendent

drop is considered as a common commercial technique to determine ultralow interfacial tensions, as well as its dependence on parameters such as pressure, temperature and time.

Most of the techniques mentioned in this section have been commercialized. The accuracy of most of these techniques for two-phase systems (pure liquid/gas) is about 0.1 mN/m, and they are successfully applied to liquid-liquid systems. In Wilhelmy plate and du Nouy ring methods, the accuracy is reduced due to difficulties in weight calibration of the ring or plate immersed in the less dense liquid. If very viscous liquids are involved, several problems will be encountered regarding handling of the liquid, injection of specific volumes into the apparatus, low-velocity flow of the liquid, and long time required for deformation of the interface. Those techniques are recommended for surface tension measurements of viscous liquids in which samples have enough time to be equilibrated before the measurements. The Wilhelmy plate (not the detachment option) and the sessile drop methods are techniques suitable to examine the surface tension of viscous liquids.

Surface active solutes (introduced intentionally or present as impurities) can significantly affect the value of the interfacial tension. This issue occurs while the results are dependent on a presumed wettability of a solid probe by one of the liquids. Interfacially active solutes can adsorb on both the fluid-fluid and fluid-solid interfaces, changing the wettability of the solid surface, thus influencing the measured results. Although this might not be a problem, the fluid-fluid interfaces should achieve equilibrium before making measurements. And it is only after

solute redistribution from one or both phases (i.e., adsorption). Sometimes it is important to measure the interfacial tension when interfaces are freshly created, and such measurements are known as "dynamic surface tension" measurements.

Changes in interfacial tension occur over intervals of several seconds and continue over several minutes, hours, or days. For example, Figure 3-9 shows the interfacial tensions measured with a Wilhelmy plate between bitumen and water of different pH values [49]. The dynamic character is caused by diffusion of natural surfactants from bitumen to the interface and the aqueous phase, and the reaction of surfactants with dissolved ions in water [50].

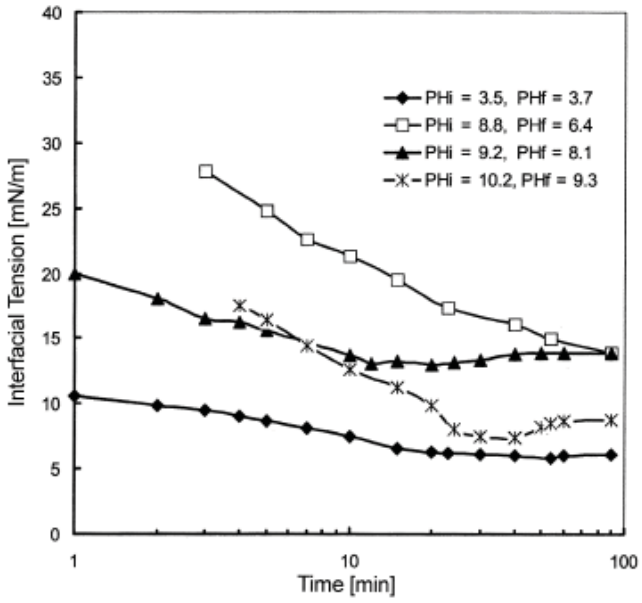

Figure 3-9: Dynamic interfacial tension between bitumen and water at 60°C using the Wilhelmy plate, time intervals started at t=0 and ends at t=90 min [49].

In industrial processes such as froth floatation of particles, detergency, foam or froth generation, short-time/dynamic interfacial tensions and wetting effects become very important to the success of the process [51-53].

3.2.5. Measurement of Ultra-low Interfacial Tension

Surfactants are often used to lower the interfacial tension between immiscible liquids to ultralow values (much less than 1mN/m). This plays an important role in many industrial processes, such as the recovery of petroleum using tertiary oil recovery [54], the cleaning of solid surfaces from dirt, grease and oil, the formulation of stable emulsions, and the in situ remediation of oil-contaminated soil with surfactant solutions. Ultralow interfacial tensions can be measured by alternative methods rather than most classical or dynamic techniques. Some examples are the spinning drop method, capillary wave spectroscopy (an optical method based on surface light scattering) [55, 56], the micropipette technique [57-59], and an additional method proposed by Lucassen [54]. (The last technique is based on the shape analysis of a drop suspended in liquid that has a density gradient; the need for a highly controlled liquid density profile restricts this method to relatively few applications.)

3.2.5.1. Spinning Drop Method

This method is similar to the pendent and sessile drop techniques in that it is based on shape measurement. The deformation of the droplet in a rapidly spinning tube is caused by radial pressure gradient. The more dense liquid fills a horizontal glass tube with sealed ends through a filling port; the tube

is then spun about its axis. When a liquid drop of lower density is injected into the spinning tube, the pressure in the outer liquid increases from the center toward the wall of the cylinder (as a result of the spinning motion). This pressure gradient pushes the droplet to the center and causes it to elongate; the elongation is in turn resisted by the interfacial tension. Interfacial tension is calculated by the measurement of the maximum drop diameter $2r_{\max}$, and length $2h_{\max}$, together with the angular velocity of rotation ω:

$$\gamma = \frac{1}{2}\left(\frac{r_{\max}}{r^{*}_{\max}}\right)^{3} \Delta\rho\, \omega^{2} \qquad 12)$$

where $r^{*}_{\max}$ is correlated to the aspect ratio $r_{\max}/h_{\max}$ [60].

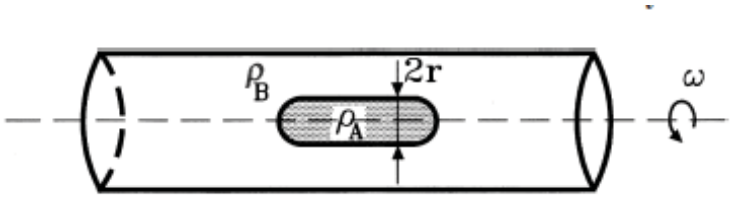

Figure 3-10: Schematic of spinning drop technique [61, 62].

3.2.5.2. Capillary Wave Spectroscopy

Due to thermal excitations, fluid interfaces on the microscopic scale are never perfectly flat. The amplitudes of these surface corrugations are very small (a few Angstroms). To accurately determine surface tension, mechanically generated surface waves with known frequency are used as optical diffraction gratings [63]. Small frequency shifts of light resulting from its interaction with the spontaneous surface modes are measured by capillary wave spectroscopy.

This technique explores a specific mode of surface waves being thermally excited to give information on surface tension and viscosity. The capillary waves will propagate along the interface and interact with the light beam like a moving diffraction grating, while the damping forces due to the viscosity of the fluids are normally weak. The interfacial tension can be obtained directly from the frequency shift of the scattered light by the Doppler effect, which exhibits two Lorentz-shaped peaks symmetrically displaced from the incident frequency [64]. Interfacial tension measurement by capillary wave spectroscopy is different for highly viscous fluids and intermediate viscosities [65]; details of the experimental set up and calculations are described elsewhere [64, 66].

3.2.5.3. Micropipette Technique

This technique is developed for direct measurements of interfacial tensions of micrometer-sized droplets. The droplet is captured at the tip of the micropipette and then sucked into the pipette as shown in Figure 3-11a [59, 67]. By determining the minimum pressure at which the droplet is pulled into the pipette, the interfacial tension is calculated:

$$\Delta p = 2\gamma \left(\frac{1}{R_{\mathrm{p}}} - \frac{1}{R_{\mathrm{o}}} \right) \tag{3.13}$$

where R_{p} is the inner pipette radius and R_{o} is the radius of exterior segment of the droplet.

If the droplet wets or adheres to the pipette surface, a large (and undetermined) pressure difference is required to draw the droplet into the pipette. To overcome this issue, a two-pipette technique can be used. In this

case, as shown in Figure 3-11b, a tensile force is applied between the pipettes to deform the droplet. The tensile force is measured and interfacial tension is calculated from the force-drop deformation relation [59].

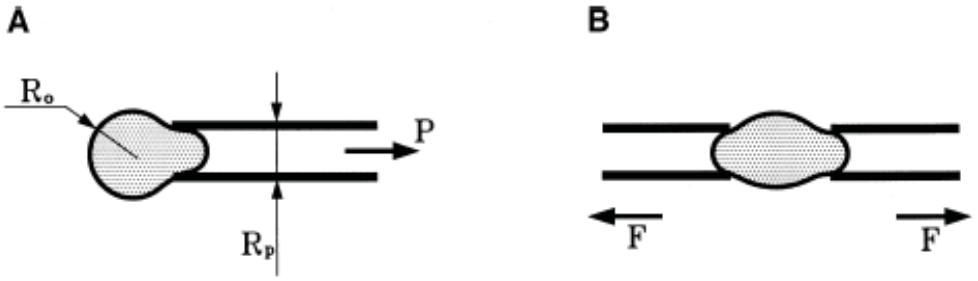

Figure 3-11: Micropipette technique. (a) Based on Δp required to suck a microdroplet into the micropipette [67]. (b) Based on force-drop deformation relation [59].

Most of the common techniques of measuring interfacial tension between two immiscible liquids have been introduced in this chapter. It should be noted that these methods, although numerous, may not span all possible applications. In some situations, interfacial tension measurement can present unique difficulties depending on the components, temperatures and/or pressures of the system, densities of the two liquids, range of interfacial tensions, and the peculiar behaviours of surfactants (see, for example, the next two chapters).

4. Novel Micropipette Technique for Ultralow Interfacial tension and Contact Angle Measurements

Many industrial and biological processes (e.g. in detergency, drug delivery, or enhanced oil recovery) require "ultralow" oil-water interfacial tensions (less than 0.l mN/m) to facilitate blending of the two immiscible liquids [68-70]. To acquire such low tensions, surfactants must often be added. For such systems, it is important to note that the presence of surfactants may introduce unintended complexities to the measurement of oil-water interfacial tensions (IFTs): For ternary oil-water-surfactant systems, a variety of microemulsion phases are often created. These are thermodynamically stable oil-water "blends" that coexist and are immiscible with one another on the macroscopic scale. Immiscibility between the microemulsion phases necessarily results in IFTs between them — in addition to the IFT which exists between the intrinsically immiscible oil and water phases. These different IFTs can, in many situations, lead to confusions in tensiometric studies; [71, 72] this will be further discussed in what follows.

In regard to the measurement of ultralow IFTs, the spinning drop technique appears to be the only viable method that is currently available. [73-76] (The "capillary wave" method, although sensitive, is an indirect approach which involves many assumptions and technical difficulties. [77, 78]) Despite its general acceptance, however, the spinning drop technique can suffer from several disadvantages:

- It is a macroscopic (i.e. mm-scale) technique which requires, at the minimum, millilitres of test samples. This can be a problem when only minute amounts of liquids are available.
- The technique requires a substantial density difference between the liquids, with the dispersed phase necessarily being the one of lower density.
- As mentioned, the inadvertent appearance of additional microemulsion phases may complicate IFT measurements. (This will be demonstrated in section 5.1.)

The purpose of this chapter is twofold: We report a novel micropipette technique, based on the original design of Evans and coworkers for the study of biomembranes, [58, 79] that was developed to quantify ultralow IFTs. I will also give a description of a novel wettability (contact angle) measurement technique using the same micropipette (section 4.2).

4.1. Ultralow Interfacial Tension Measurement with Developed Micropipette Technique

The ultralow IFTs were measured in two ways: by the spinning drop method (Krüss, model SITE 100) and by micropipettes. The former technique is well-established and requires no further description. The micropipette technique proceeded as follows: a hollow glass capillary (1.0 mm OD; 0.7 mm ID), with one of its ends tapered down to ~10 μm ID (while remaining open), was first filled completely with a liquid (say liquid A). The untapered end of the pipette was connected, via a flexible tubing, to a reservoir containing the same liquid. As

such, liquid A occupied entirely the region from the reservoir, through the tubing, to the micron-sized tip of the pipette; care was taken to ensure that no gas bubbles existed anywhere along this assembly. The micropipette was then immersed in another liquid (liquid B) that was immiscible with the liquid inside the pipette (liquid A). Owing to capillary forces (which stemmed from the IFT between liquids A and B), a minimum positive pressure was needed to expel liquid A from the pipette tip. This positive pressure Δp is given by the Young-Laplace equation as $\Delta p = 2\gamma_{AB}/R_p$, where γ_{AB} is the IFT between liquids A and B, and R_p is the inner radius of the pipette tip (typically several microns). In our experiment, Δp was controlled by adjusting the elevation of the reservoir; the relevant hydrostatic relation is $\Delta p = \rho_A g \Delta h$, with ρ_A being the density of liquid A, g the gravitational acceleration, and Δh the change in elevation of the reservoir. Combining the above relations, we have

$$\gamma_{AB} = \frac{\rho_A g R_p}{2} \Delta h \tag{4.1}$$

For ultralow IFTs (say 10^{-3} mN/m), Δh is typically 10 to 100 μm. In practice, this change in elevation can easily be effected by mounting the reservoir onto a micrometer drive. A sketch of the micropipette setup is shown in Figure 4-1.

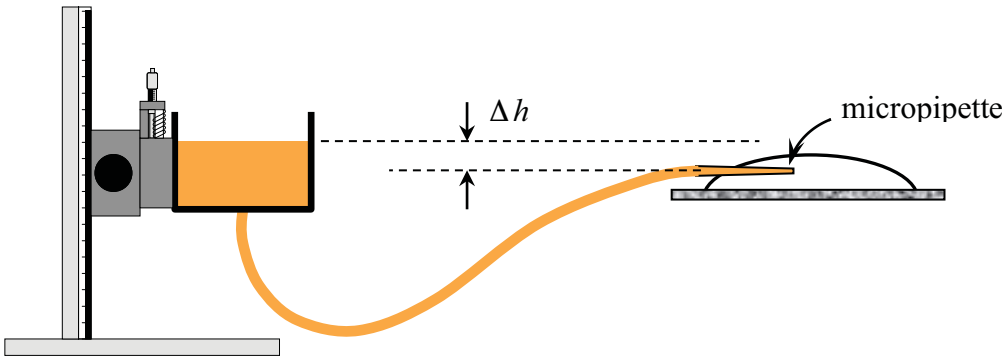

Figure 4-1: Schematic of the micropipette/manometer setup for determining IFT between the liquid in the pipette (connected to the reservoir) and a second liquid that the pipette tip is immersed in. Raising the reservoir will lead eventually to expulsion of the first liquid from the pipette tip; the change in reservoir elevation Δh is a direct measure of the IFT. As the pipette tip is ~10 μm in diameter, the process must be monitored under an optical microscope.

This new method of measuring ultralow IFTs was verified by comparing its results with:

(a) literature values for pure liquids (e.g. IFT between water and *n*-butanol) the results are shown in Table 4-1. All results compared favourably — to within 4% discrepancy or less.

Table 4-1: Interfacial Tension with deionized water

pure liquid	spinning drop technique (mN/m)	micropipette technique (mN/m)	discrepancy
1-Butanol	2.06 ± 0.012	1.98 ± 0.058	3.89%
n-Amyl Alcohol (1-Pentanol)	4.61 ± 0.017	4.44 ± 0.018	3.68%

(b) measurements using the spinning drop technique. Table 4-2 shows the results of IFT measurements between n-butanol and water with different surfactant, sodium dodecyl sulfate (SDS) concentrations. Figure 4-2 is a proof that two techniques converge at higher (saturated) concentration of surfactants regardless

of which technique is used. This phenomenon is known as *partitioning* effect (More explanation is provided in section 5.1.2).

Table 4-2: IFT between n-butanol/water (with different SDS concentrations)

Molarity of SDS Solutions	Mean IFT (mN/m)	
	Micropipette Technique	Spinning Drop
0	1.984	2.0643
0.00063	0.9624	1.5964
0.00125	0.9746	1.5996
0.0025	0.8174	1.4410
0.005	0.6478	1.2197
0.075	0.4918	1.0892
0.01	0.5722	1.2073
0.015	0.3868	0.8364
0.02	0.4462	0.6564
0.022	0.398	0.6233
0.025	0.3776	0.6441
0.028	0.3222	0.6886
0.03	0.3138	0.4996
0.035	0.2862	0.4970
0.04	0.2434	0.4655
0.05	0.2102	0.4247
0.06	0.1502	0.3847
0.07	0.1282	0.3224
0.08	0.09252	0.3548
0.1	0.09902	0.2732
0.16	0.0769	0.1262
0.24	0.05316	0.0830

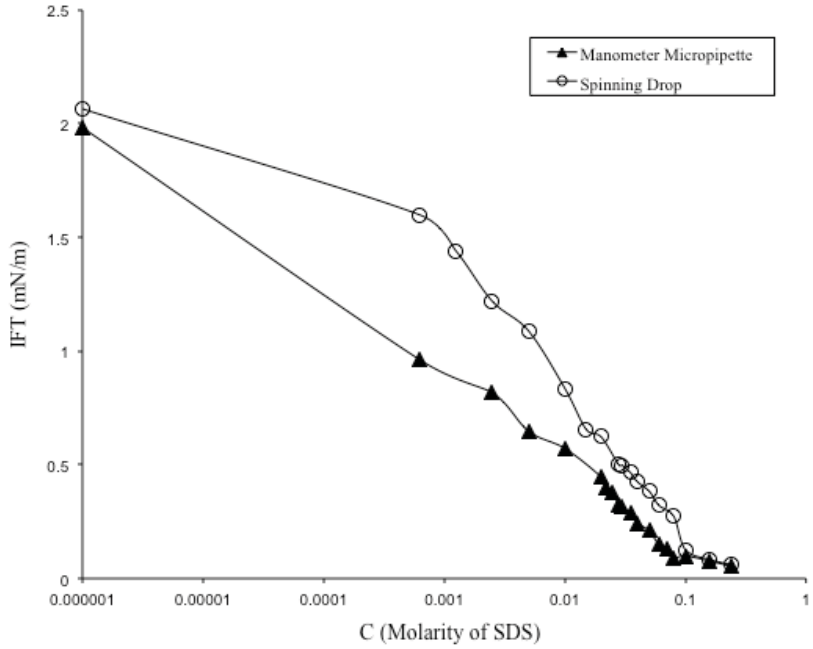

Figure 4-2: Developed Micropipette Technique and Spinning Drop converge at saturated SDS concentrations.

We note here several immediate advantages that the micropipette has over the spinning drop technique: the new method requires much smaller sample volumes (as little as 10 μL); it is not contingent on any density difference between the liquids; and it is immaterial which liquid has the higher density.

4.2. Novel Wettability (Contact Angle) Measurement

Another physical property that is central to the liberation of oil from sand grains is the contact angle θ_c (between the oil-water interfacial surface and the solid substrate). Contact angles are traditionally observed *directly* from drop profiles, or determined *indirectly* through measurement of capillary forces or liquid penetration into porous structures [41, 80, 81]. As indirect methods inevitably involve various assumptions (some less justified than others), it is always

preferable to obtain contact angles through direct means. Methods of directly measuring θ_c, such as with sessile drops, are often carried out on the 'lab scale' (i.e. dimensions of millimetres and centimetres). The pendent drop technique is the common method to measure the contact angle of a heavier liquid phase that seated on a solid surface surrounded by the lighter liquid phase. But in this case, the oil phase would be the phase with lower density and buoyancy forces lead bitumen droplets to float up to the surface of the aqueous phase rather than resting on the glass surface surrounded with the aqueous solution. Therefore the wetting angle cannot be measured with the pendent drop technique. Here, in the spirit of characterizing wettability on the pore (i.e. micro) scale, we introduce a micropipette method which allows direct determination of θ_c within small confines of the order of 10 μm.

The micropipette technique of determining contact angles is shown in Figure 4-3. A glass pipette, with inner diameter of order 10 μm, is filled partially with a liquid that is immiscible with the medium in which the pipette is immersed. (In this case, the liquid inside the pipette was toluene-diluted bitumen, and the surrounding liquid was an aqueous surfactant solution.) To emulate sand grain surfaces (silica with prolonged exposure to crude oil), the surface of the glass pipette — particularly its inner portion — was pre-treated with a toluene/bitumen mixture at 1:1 weight ratio as follows: After immersing the pipette in diluted bitumen overnight, it was flushed with clean toluene (including its inner core), removing all diluted bitumen and leaving only an irreversibly adsorbed layer of crude oil material on the glass surface. The surface-modified pipette was then filled with the oil phase (toluene-diluted bitumen) and immersed in an aqueous

surfactant (naphthenic acids) solution. By drawing some of the aqueous phase into the front end of the pipette, a three-phase contact line was formed at the pipette inner surface (Figure 4-3). Two contact angles — the upper and lower angles from a 2-D microscope image — could be directly measured using an imaging software (e.g. AxioVision from Carl Zeiss). These two pore-scale contact angles, which should in principle be identical, were compared as a self-consistency check. In addition, through control of the pipette pressure, it was also straightforward to move the leading edge of the 'oil tube' toward or away from the pipette orifice, thus creating situations for advancing and receding contact angles (which serves as a useful check for contact angle hysteresis).

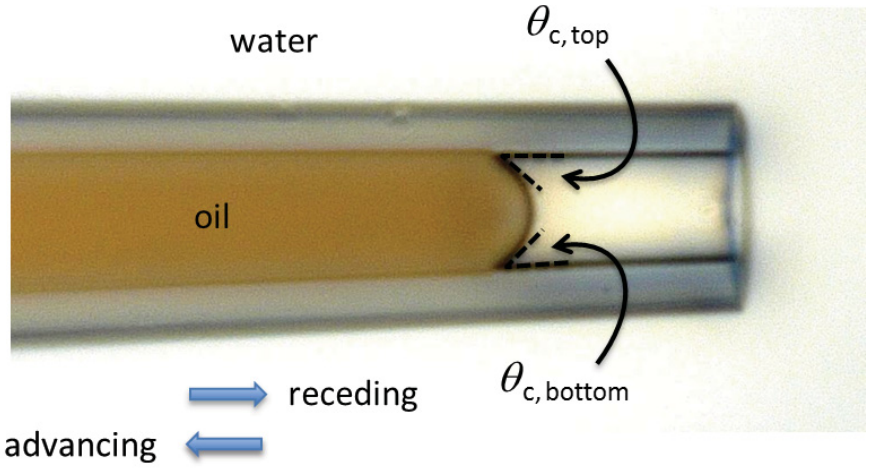

Figure 4-3: A simple technique of measuring pore-scale contact angles. As shown, a three phase contact line is formed inside the pipette (inner pipette diameter is typically 10–30 μm). By moving the interface forward and backward, receding and advancing contact angles can be determined.

5. Experimental, Results and Discussion

5.1. Considerations When Measuring Ultralow Interfacial Tensions

Surfactants are often used to create low to ultralow oil-water interfacial tensions (IFTs). These molecules, however, may also lead to the inadvertent formation of microemulsion phases which can obscure IFT measurements. Figure 5.1 illustrates an animation of a third phase formation depending on the spreading coefficient. This section provides a case study of such an issue. The novel micropipette technique (see Section 4.1), which has many advantages over the more common spinning drop method, is used for determining low IFTs.

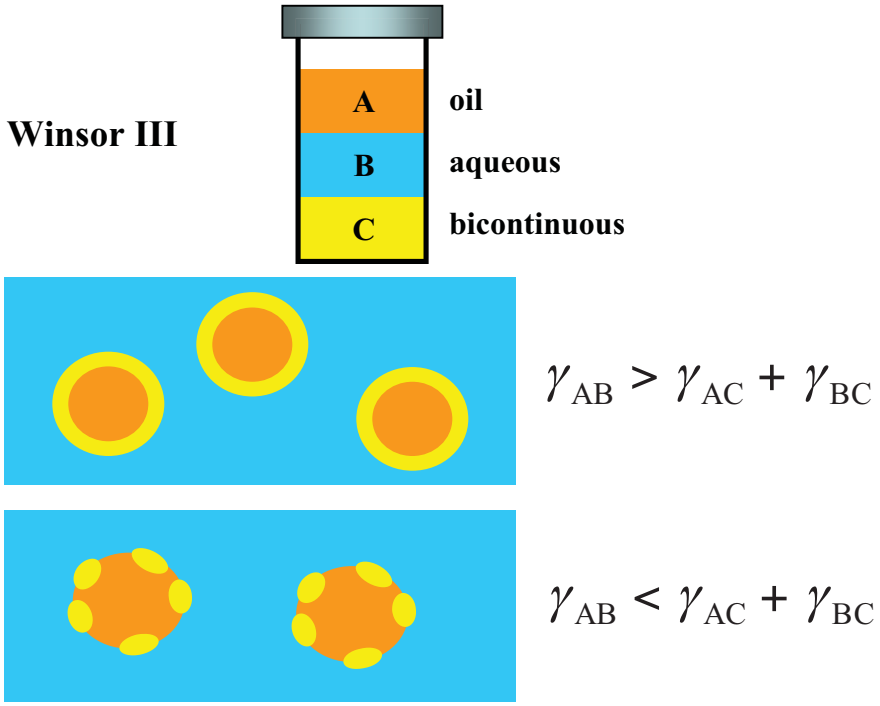

Figure 5-1: Inadvertent formation of microemulsion phases

5.1.1. Materials

For the present case study, the oil phase was *n*-hexadecane with 5 wt% dissolved AOT (Aerosol-OT) as surfactant. The aqueous phase was a brine solution of variable salinity — specifically, distilled water containing NaCl at 0.25 to 4.0 wt%. The AOT (98% purity) was supplied by Sigma Aldrich; *n*-hexadecane (HPLC grade) and sodium chloride were obtained from Fisher Scientific with no further purification.

5.1.2. Experimental

In what follows, both the spinning drop and micropipette techniques will be applied to the above-mentioned AOT-hexadecane-brine system. Specifically, equilibrium IFTs between the oil phase (hexadecane with dissolved AOT) and the aqueous phase (water with dissolved NaCl) will be determined.

Figure 5-2 shows variations in equilibrium IFT as NaCl concentration in the aqueous phase was increased from 0.25 wt% to 4.0 wt%. The raw values of interfacial tensions are listed in Table 5-1. Interfacial tensions measured by the two above-mentioned methods are plotted against brine salinity in Figure 5-2.

Table 5-1: Interfacial tensions of AOT-hexadecane-brine system

Brine salinity (wt%)	Mean IFT (mN/m) Micropipette Technique	Brine salinity (wt%)	Mean IFT (mN/m) Spinning Drop
0.75	0.633	0.25	0.568
1.1	0.648	1	0.558
1.3	0.632	1.2	0.525
1.5	0.430	1.4	0.539
1.7	0.362	1.7	0.519
1.9	0.247	2	0.487
2.5	0.238	2.5	0.427
3	0.259	3	0.422
3.5	0.212	3.5	0.404
4	0.240	4	0.415

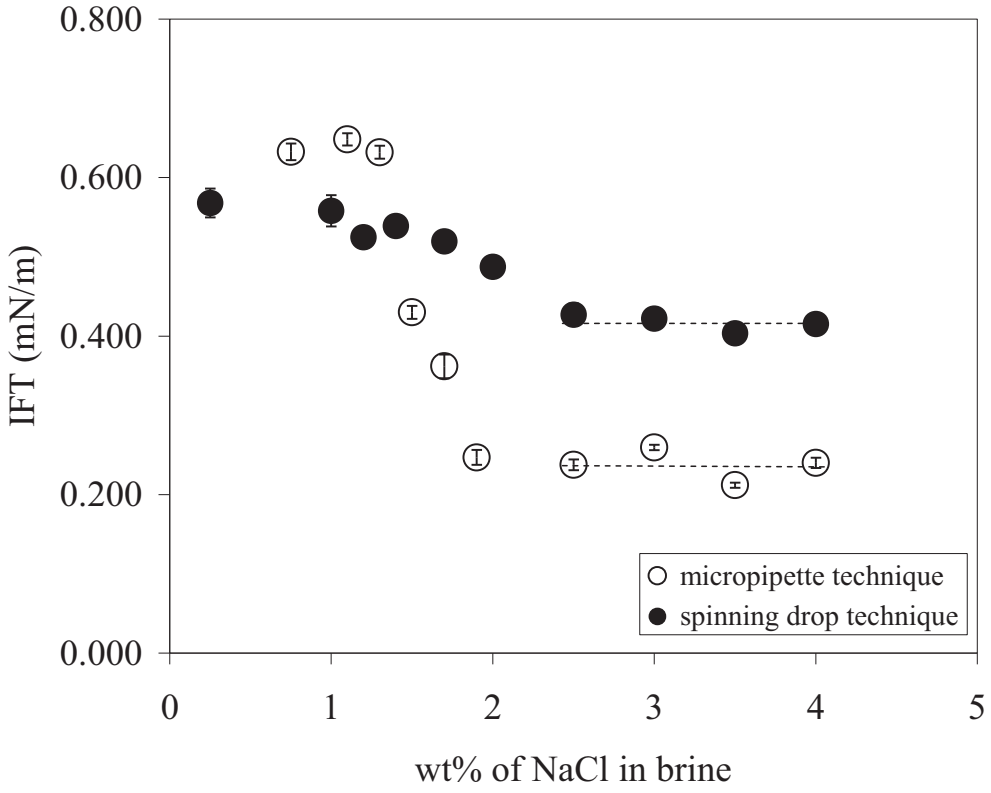

Figure 5-2: Relationship between brine salinity and IFTs measured using the spinning drop and micropipette techniques. The oil phase was *n*-hexadecane with 5 wt% AOT, and the brine was an NaCl solution. Results from both methods suggest saturation was reached when the NaCl concentration was roughly 2.5 wt% or higher; the two saturation IFTs, however, differed significantly.

The two dashed lines in the figure show "plateauing" of IFT values, suggesting that, when the NaCl concentration was ca. 2.5 wt% or higher, the interface was saturated with surfactants. Owing to *partitioning* effects, it is not surprising to see the two techniques detecting different IFTs before the point of saturation [67]. (Partitioning refers to the distribution of surfactants between the two bulk liquids *and* the interface. This distribution depends on the particular experimental setup

and will in turn give rise to different equilibrium IFTs for different measuring techniques; see ref. 67.) However, when in the saturation regime, the packing of surfactants at the interface is "intrinsic" in that the surface concentration of surfactants is independent of how the excess molecules are partitioned (i.e. distributed) between the oil and aqueous phases; as such, the IFT values detected by the two methods should coincide. The discrepancy between the two saturation IFTs in Figure 5-2, which may first appear inexplicable, can be rationalized as follows.

"Winsor III" microemulsions (i.e. coexistence of aqueous, oil, and "bicontinuous" phases) are known to appear in AOT-hexadecane-brine systems [82]. Such microemulsion phases can be clearly seen in Figure 5-3 — on both the centimetre and micron scales. In this case, the oil phase was *n*-hexadecane with 5 wt% dissolved AOT, and the aqueous phase was a 3.5 wt% NaCl solution (i.e. well within the saturation regime in Fig. 5-2). On the bench scale, if a mixture of the aqueous and oil phases (e.g. of roughly equal volumes) were mixed and allowed to equilibrate, a Winsor III system would appear; this is shown in Figure 5-3a. Here, the bottom liquid was a surfactant-rich, bicontinuous (BC) oil-water mixture which was immiscible with both the oil and aqueous phases on the macroscopic scale. (This system is somewhat anomalous in that the BC phase is actually more dense than the brine.) Figure 5-3b shows the same three phases on a much smaller scale: A micropipette, with inside diameter of ~20 μm, was first filled with the oil phase. It was then immersed into the brine, and a small amount of the hydrocarbon was expelled into the aqueous surrounding, forming an oil

droplet at the pipette tip. Within seconds, a third liquid — the bicontinuous (BC) phase — appeared. As seen, the surface energies between the three liquids were such that the BC phase would spontaneously engulf the oil droplet in the aqueous surrounding.

(a)

(b)

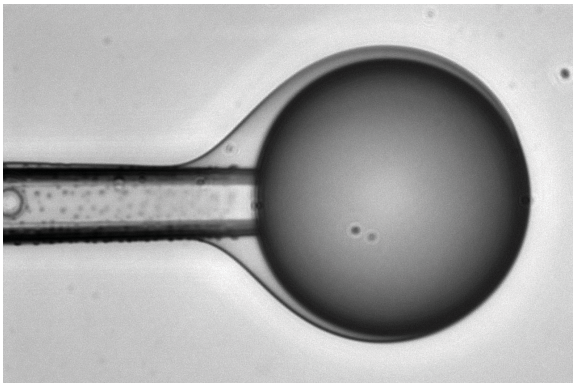

Figure 5-3: Upon contacting the oil phase (*n*-hexadecane with 5 wt% AOT) with the brine (water with 3.5 wt% NaCl), a third phase — a bicontinuous (BC) liquid — appeared spontaneously. (a) The so-called Winsor III mixture in a test tube, with the oil phase at the top, the aqueous phase in the middle, and the BC phase at the bottom (this BC phase was more dense than the brine); (b) the BC phase was seen to spontaneously engulf an oil droplet that was held at the pipette tip; the oil droplet was roughly 60 μm in diameter. The surrounding liquid was brine.

When surfactants are used to drive the oil-water IFT to low values, it is often of interest to know the value of the IFT. Such measurements, unfortunately, are not always straightforward (or even possible): the surfactant molecules can lead to inadvertent — and often unnoticed — formation of additional phase(s) which complicate tensiometric studies. This is demonstrated in the present case study: We first attempted to measure the oil-water IFT using the spinning drop technique. On close examination of the image in Figure 5-4a, a layer of the third phase (the BC liquid) was visible around the dispersed oil drop. As such, the IFT registered by the spinning drop device would be the sum of *two* interfacial tensions. Denoting the oil phase as "o", the aqueous phase as "w", and the bicontinuous phase as "BC", the IFT given by the spinning drop technique would be $\gamma_{\mathrm{o-BC}} + \gamma_{\mathrm{BC-w}}$, where γ is the general symbol here for interfacial tensions. Based on the data in Figure 5-2, we have

$$\gamma_{\mathrm{o-BC}} + \gamma_{\mathrm{BC-w}} = 0.42 \text{ mN/m} \tag{5.1}$$

Figure 5-4b reveals why the micropipette-measured IFT was different from the spinning drop result (i.e. difference between the two dashed lines in Fig. 5-2).

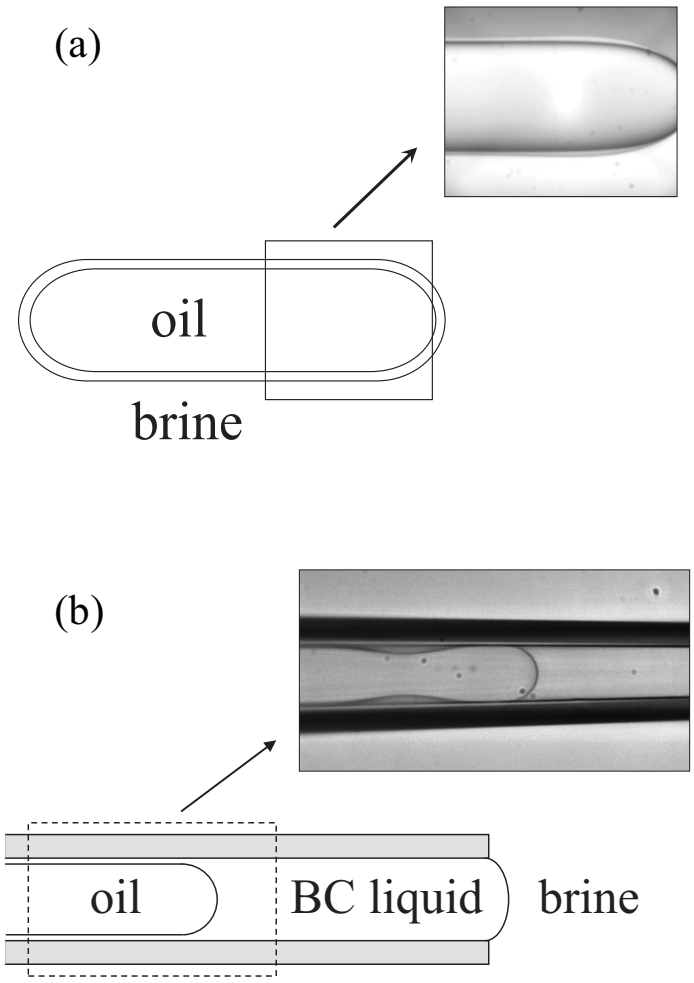

Figure 5-4: Microscope images and sketches of the situations during IFT measurement. (a) The oil droplet in a spinning drop tensiometer was engulfed by a thin layer of the bicontinuous (BC) phase; the diameter of the cylinder was roughly 0.7 mm. Note that the layer of BC liquid around the oil drop is almost imperceptible in the photograph. (b) Arrangement of various phases in a micropipette experiment.

When the oil-filled pipette was immersed into the brine solution, a bicontinuous liquid was formed spontaneously at the oil-brine interface. This BC liquid would grow and penetrate deep into the interior of the pipette, eventually engulfing the front portion of the oil phase (Fig. 5-4b). The pressure drop across the oil-BC interface, even if substantial (due to a non-zero $\gamma_{\mathrm{o-BC}}$), would remain unchanged during the measuring of $\gamma_{\mathrm{BC-w}}$ (the BC-brine interfacial tension).

This is because the measurement process involves displacement of only a very minute amount of fluid within the pipette interior. (To be exact, the displaced fluid volume is that of a hemisphere of radius R_p.) Such a small perturbation will not lead to any appreciable change in the oil-BC interfacial shape; as such, the Laplace pressure across the oil-BC interface would remain unchanged. As IFT measurement by micropipette depends only on *differences* in pipette pressure (see eqn 4.1), the existence of a *stationary* oil-BC meniscus inside the pipette would not affect the results. As such, one can be confident that the micropipette method will provide an accurate measure of the BC-brine interfacial tension. Based on the data in Fig 5-2, we have

$$\gamma_{\mathrm{BC-w}} = 0.24 \text{ mN/m} \tag{5.2}$$

Combining eqns (5.1) and (5.2), the oil-BC interfacial tension is thus

$$\gamma_{\mathrm{o-BC}} = 0.18 \text{ mN/m} \tag{5.3}$$

Finally, we note that our original intent was to determine $\gamma_{\mathrm{o-w}}$, the oil-brine interfacial tension. This information, unfortunately, could not be obtained even if results from both the spinning drop and micropipette techniques were combined. We could, however, retrieve partial information by noting that the BC liquid was spreading spontaneously onto the oil-brine interface (Fig. 5-3b). For this spreading to occur, the surface energies must be such that [83]

$$\gamma_{\mathrm{o-w}} \geq \gamma_{\mathrm{o-BC}} + \gamma_{\mathrm{BC-w}}$$

From eqn (5.1), it follows that

$$\gamma_{\mathrm{o-w}} \geq 0.42 \text{ mN/m} \tag{5.4}$$

In summary, the formation of a bicontinuous liquid had prevented measurement of the oil-water interfacial tension. However, through careful interpretation of results from the two tensiometric techniques, we were able to determine IFTs between the third phase and the two original liquids (eqns 5.2 and 5.3), and it was possible to put a lower bound on the oil-water IFT (relation 5.4). The micropipette technique, which was introduced in this study, can be combined with other more traditional methods of tensiometry to extract important information on heterogeneous systems involving ultralow interfacial tensions.

5.2. Potential Use of Naphthenic Acids in Soil Remediation: Examination of Pore-Scale Interfacial Properties

Although the water-based extraction of bitumen is a well-proven technology, recent concerns with excessive water usage [1, 3] have motivated the industry to explore alternative *solvent-based* methods (see discussion in Chapter 1). Similar to dry cleaning, solvent-based bitumen extraction involves mixing mined oil sands with an organic solvent, giving rise to solvent-diluted bitumen as the product (which is transported downstream for further processing), and a substantial amount of leftover sand grains that are laden with residual oil. For solvent-based extraction technology to be viable, the reject sand grains must be 'remediated' (i.e. rendered free of residual oil) and returned to the environment for land reclamation. Indeed, successful remediation of waste sand grains is the leading challenge of any solvent-based extraction technology.

Within a pile of reject sand, the residual oil is trapped between the solid particles in small void spaces (dimensions of typically 10–100 μm). Common methods of oil removal, such as mechanical displacement or drying, are unlikely to be effective. (The Laplace pressure on small length scales can create strong resistance to mechanical displacement of the oil. Also, the sand particles can act as heat absorbers which render a drying process impractical.) An alternative method, one which we explore in our research program, is to wash the oil-laden sand grains with water and surfactants. Specifically, we identify *naphthenic acids* as a potential surfactant due to its water solubility, strong surface activity, and ready availability as a crude oil by-product. (Naphthenic acids are natural constituents in many petroleum sources, including the oil sands of northern Alberta [84]. They are derived from straight-run distillates of crude oil at various fractions [85].) We envision a washing process in which moderate amounts of aqueous surfactant solutions are used to remediate/wash the contaminated sand grains. Unlike applications in chemical enhanced oil recovery, relatively vigorous hydrodynamic shearing is possible in the washing process. To readily dislodge residual oil from the sand grains, the surfactant (naphthenic acids) must perform two functions: it must significantly reduce the capillary forces which retain the oil ganglia in the void spaces, and enhance 'dewetting' of hydrocarbon from the sand grain (silica) surfaces. In the terminology of colloid science, the surfactant should have the ability to lower the oil-water interfacial tension (IFT) and, at the same time, reduce the contact angle between the oil-water interface and the solid substrate (angle measured through the aqueous phase). The present study is

guided by the following two notions: (a) Before 'field testing' naphthenic acids as a remediation agent, its role, from a colloid science perspective (in terms of IFT and contact angle), should first be delineated; (b) the interfacial properties should be studied on the 'pore scale' (i.e. dimensions characteristic of the void spaces between sand particles, of order 10–100 μm), as such properties can be specific to the length scale in question [67, 86]. The focus of this section is thus to examine the pore-scale interfacial properties of naphthenic acids as a surfactant and remediation agent.

5.2.1. Materials

The aqueous phase was formed by dissolving naphthenic acids, at different concentrations, into deionized distilled water. Naphthenic acids is a collective name (used here as a singular noun) for an unspecific mixture of several cycloalkane (cyclohexane and cyclopentane) carboxylic acids with aliphatic side chains. They occur naturally in a variety of petroleums [20, 21, 85, 87] and are also found in the Athabasca oil sands deposits [88, 89]. It was shown that the properties of naphthenic acid sodium salt (sodium naphthenates), isolated from Athabasca bitumen, are similar to those of Eastman Kodak practical grade sodium naphthenates [84, 90]. Natural surfactants were extracted from 50 wt% toluene diluted bitumen. Bitumen was from the Diluent Recovery Unit (DRU) bottoms of Athabasca oil sands. 1:1 weight ratio sample was prepared with deionized boiling water (pH=10) and 50 wt% toluene diluted bitumen in a Teflon bottle. The bottle was shaken gently at 50 rpm for an hour. Hot water with high pH along with

gently shaking will cause natural surfactants to migrate from the oil phase to the aqueous phase. The two phases were separated in a separatory funnel. The aqueous phase was then concentrated 575 times with a B"U"CHI Rotavapor R-215. Kodak sodium naphthenates, which is a white-yellowish crystalline material, was used without further purification. The aqueous mixtures were put in a sonicator bath for several minutes, resulting in complete dissolution of the surfactants in water.

The oil phase was either (a) pure toluene (HPLC grade from Fisher Scientific), or (b) toluene containing 10 wt% dissolved bitumen (the so-called 'DRU bottoms' bitumen, provided by Syncrude Canada Ltd.). The hydrocarbon in the latter case resembles diluted bitumen in a solvent-based extraction situation, while the former case (with pure toluene) is for comparative purposes.

As alluded to earlier, measurements of IFTs and contact angles are to be conducted on the 'pore scale' (i.e. dimensions of 10–100 μm).

5.2.2. Experimental

Interfacial tensions were measured using a recently introduced micropipette technique [91, 92] that is capable of quantifying common to very low IFTs on the pore scale. Briefly, a micropipette, with an inner radius of order 10 μm, is filled with a liquid (say liquid A). The assembly is then inserted into another liquid (liquid B) that is immiscible with that inside the pipette. Next, the pressure in the pipette is slowly increased via one of two means: (i) using a syringe that is connected directly to the micropipette, and (ii) by raising the elevation of a liquid

reservoir and thus the hydrostatic pressure at the pipette tip. The threshold pressure to expel liquid A from the micropipette, into an environment of liquid B, is a direct measure of the IFT between liquids A and B. The first method of controlling the pipette pressure is suitable for measuring IFTs of order 1 to 10^2 mN/m; the second method is tailored for low IFTs ranging from 10^{-3} to 1 mN/m. There are two notable advantages in using the micropipette technique for determining IFTs: the measurements are made directly on the pore scale, and it does not depend on the density difference between the liquids (i.e. it works equally well for density-matched liquids).

Further details of this micropipette technique for determining interfacial tensions and contact angle measurements can be found in Chapter 4.

Previous studies [84, 90] showed that the properties of sodium naphthenates from Athabasca bitumen are similar to Kodak SNs. Along with the above claim, some preliminary studies were done to substitute Kodak SNs with natural surfactants extracted from Athabasca bitumen:

a) X-ray Photoelectron Spectroscopy (XPS) results of the 575 times concentrated sample (see Materials section) containing natural surfactants are shown in Figure 5-5. The binding energy positions of oxygen and carbon peaks were at 531.243 (eV) and 288.2 (eV), Fig. 5-5 (a) and (b). These two peaks show the carbon–oxygen bond in carboxyl groups. So the natural surfactants in this work extracted from Athabasca bitumen considered to be in the class of sodium naphthenates.

b) Langmuir isotherms of Athabasca natural surfactants and Kodak SNs, Figure 5-6 (a) and (b), showed the same IFT values (~ 30 mN/m) at critical micelle concentrations (CMC).

c) Areas per molecule occupied by Athabasca natural surfactants and Kodak SNs were calculated using the limiting slope of Langmuir isotherms shown in Figure 5-6. The areas per molecules were also very similar.

Therefore Kodak SNs were used as a proper substitute for Athabasca natural surfactants in the rest of studies in this work.

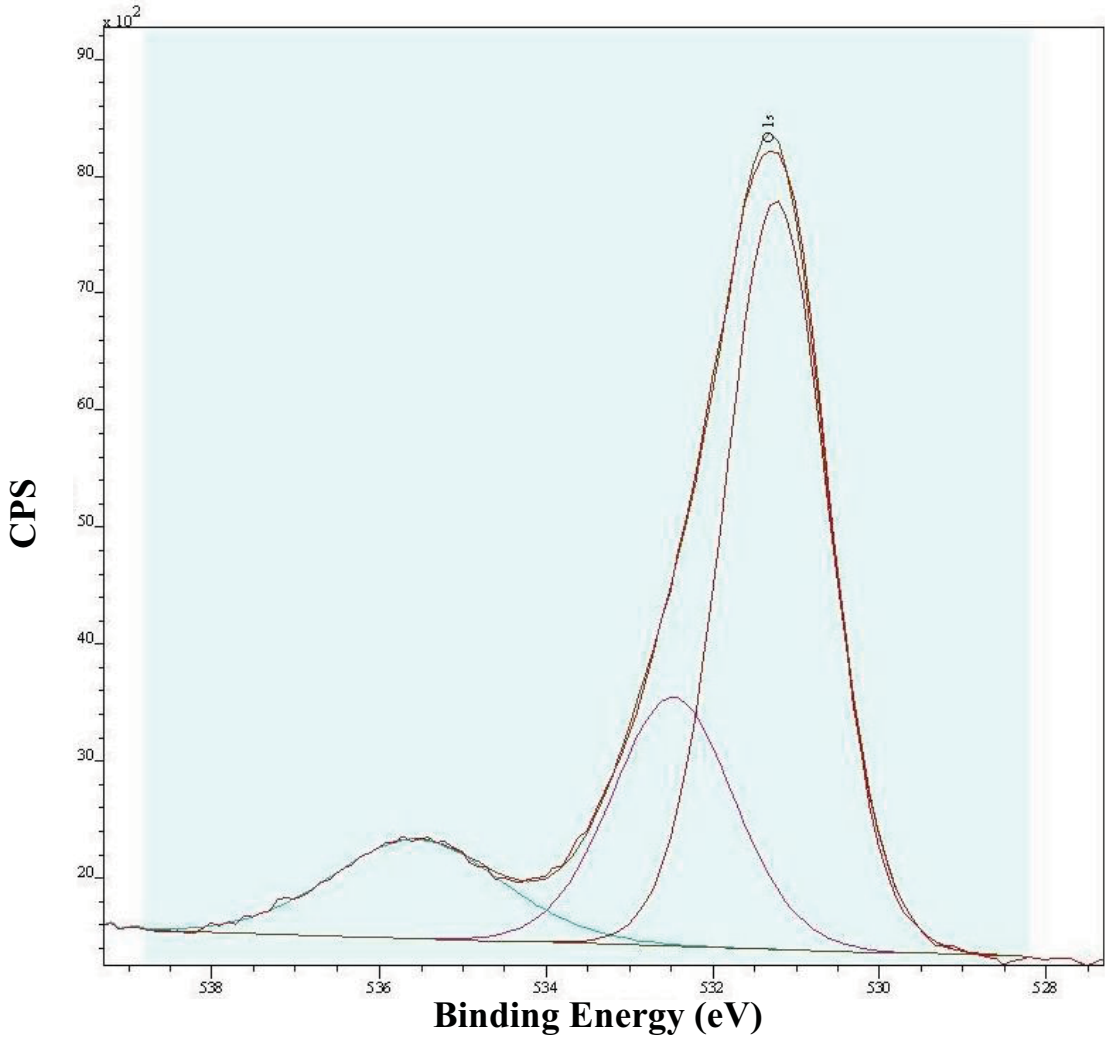

(a)

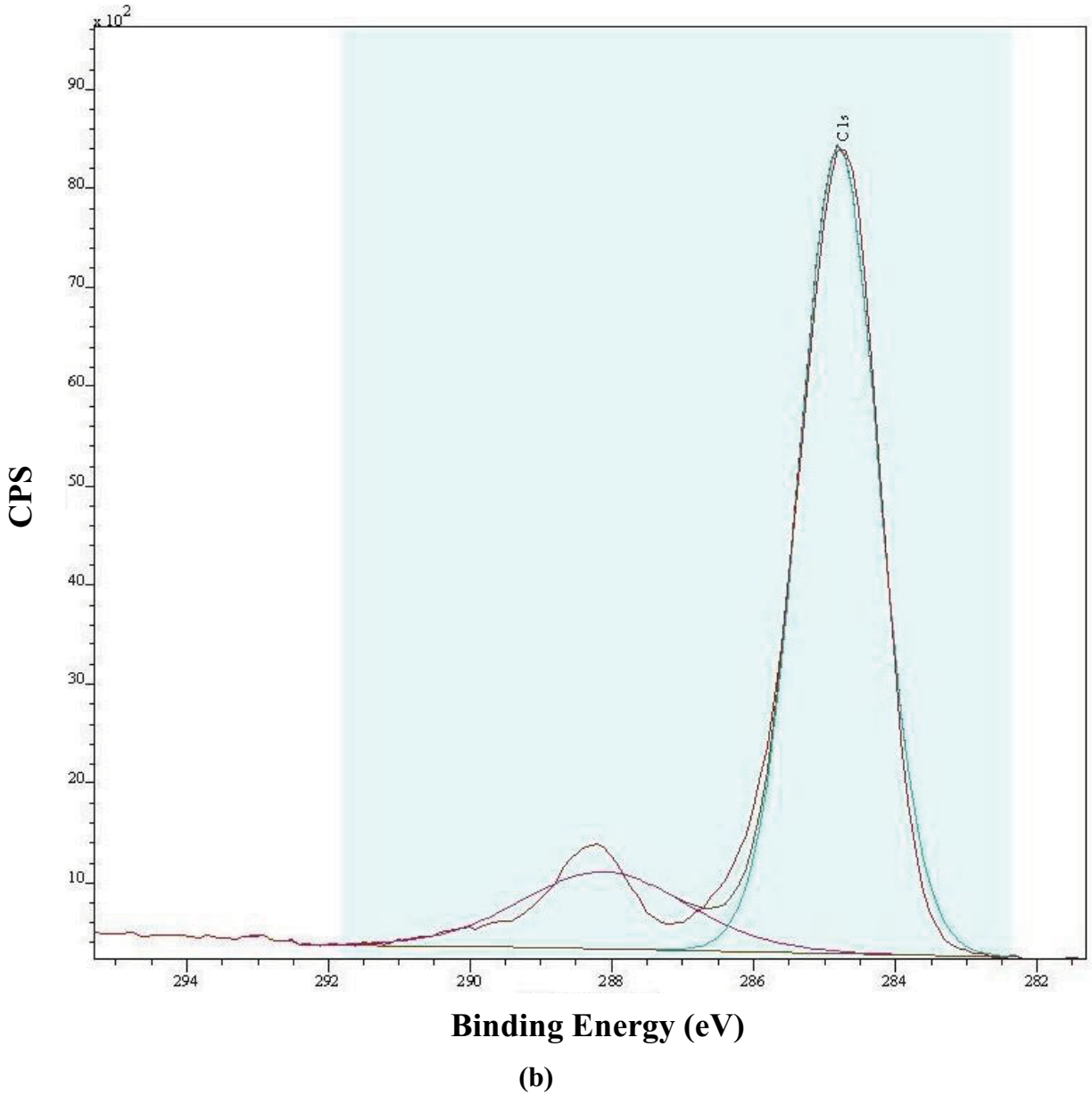

(b)

Figure 5-5: The binding energy positions of oxygen and carbon peaks. (a) XPS oxygen peak at 531.243 eV from carboxyls. (b) XPS carbon peak at 288.2 eV from carboxyls.

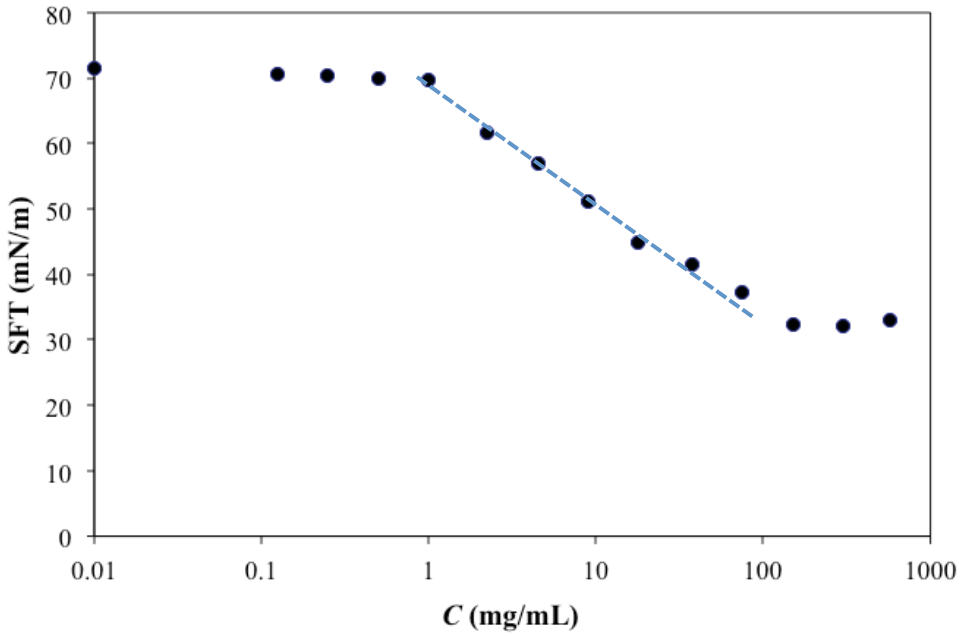

(a)

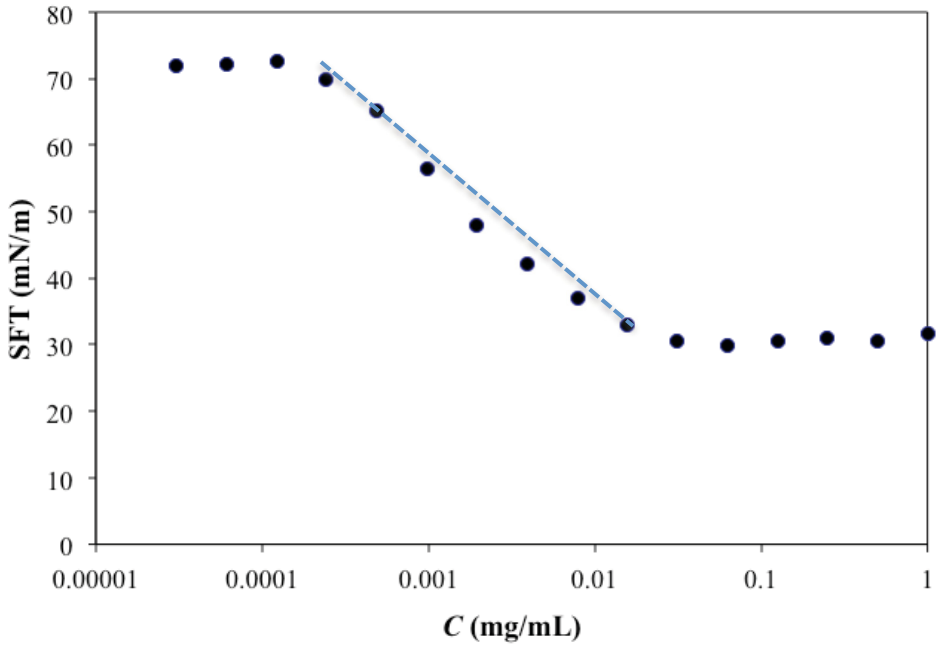

(b)

Figure 5-6: SFT adsorption isotherms of Athabasca natural surfactants and Kodak SNs. (a) Area per molecule a_0(Å^2) = 55.71 Å^2 from Limiting Slope = -7.34, occupied by natural surfactants and surface tension values at critical micelle concentrations (CMC).

(b) Area per molecule a_0(Å^2) = 48.60 Å^2 from Limiting Slope = -8.41 and SFT value at CMC of Kodak SNs.

The goal of our present study is to ascertain whether naphthenic acids (NA) have the desired interfacial properties (on the pore scale) to be a potential remediation agent. The two criteria for such a chemical are the abilities to acquire (a) low oil-water IFTs, and (b) small contact angles (angle θ_c measured through the aqueous phase). It is difficult to define precisely the meaning of 'low' and 'small'; the following is a semi-quantitative attempt: Unlike in enhanced oil recovery, the washing process that we envision allows for reasonably vigorous hydrodynamic shearing. For this reason, it is not necessary to decrease the IFT to 'ultralow' values ($< 10^{-3}$ mN/m). To acquire sufficiently large capillary numbers (ratio of hydrodynamic to capillary forces), we believe the IFT should be decreased from typically 20–30 mN/m (in the absence of surfactants) to values of order 1 mN/m. As for the contact angle, the approximate rule-of-thumb is that surfaces with θ_c larger than 90° are hydrophobic, while those with $\theta_c < 90°$ are hydrophilic. It would be desirable if addition of NA had the effect of rendering the silica surfaces hydrophilic (thus promoting liberation of oil from the solid surface).

Using the micropipette technique, pore-scale IFTs were measured as the surfactant concentration in the aqueous phase was varied. The IFT was between (i) water containing sodium naphthenates at a concentration C (mg/mL), and (ii) an oil phase, which was either pure toluene or toluene-diluted bitumen (at 10 wt% bitumen). Figure 5-7 shows the results for the two hydrocarbons. It is clear from

the figure that the two plots are qualitatively similar — both exhibiting classic features of monolayer adsorption [41, 80]. Quantitatively, the two plots show also similarities in two respects: (a) In both cases, the oil-water interface appeared to reach saturation when surfactant concentration in the bulk liquid was $C \approx 10$ mg/mL; (b) at saturation, the interfacial area occupied by each surfactant molecule, which can be calculated from the negative slope of the IFT vs log C plot [41, 80], was 49 $Å^2$. These features suggest that it was indeed the naphthenic acids that are responsible for the interfacial activity (i.e. occupying the oil-water interface and reducing the IFT). The only difference between the two plots was seen in the limiting IFTs as the surfactant concentration became vanishingly small. This difference, however, was expected: Figure 5-7a shows a limiting IFT of 36 mN/m, which is the interfacial tension between water and pure toluene. The corresponding limiting IFT in Figure 5-7b is 25 mN/m, suggesting that there were natural surfactants in the bitumen that were responsible for lowering the IFT by 11 mN/m. (These natural surfactants in fact may very likely be naphthenic acids as well [88, 89].) It is clear that naphthenic acids indeed could lower the IFT to values of order 1 mN/m, provided the sodium naphthenates concentration exceeded the 'critical micelle' value of ~10 mg/mL. The lowest IFT that we had observed (last three data points in Figure 5-7b) was 0.6 mN/m.

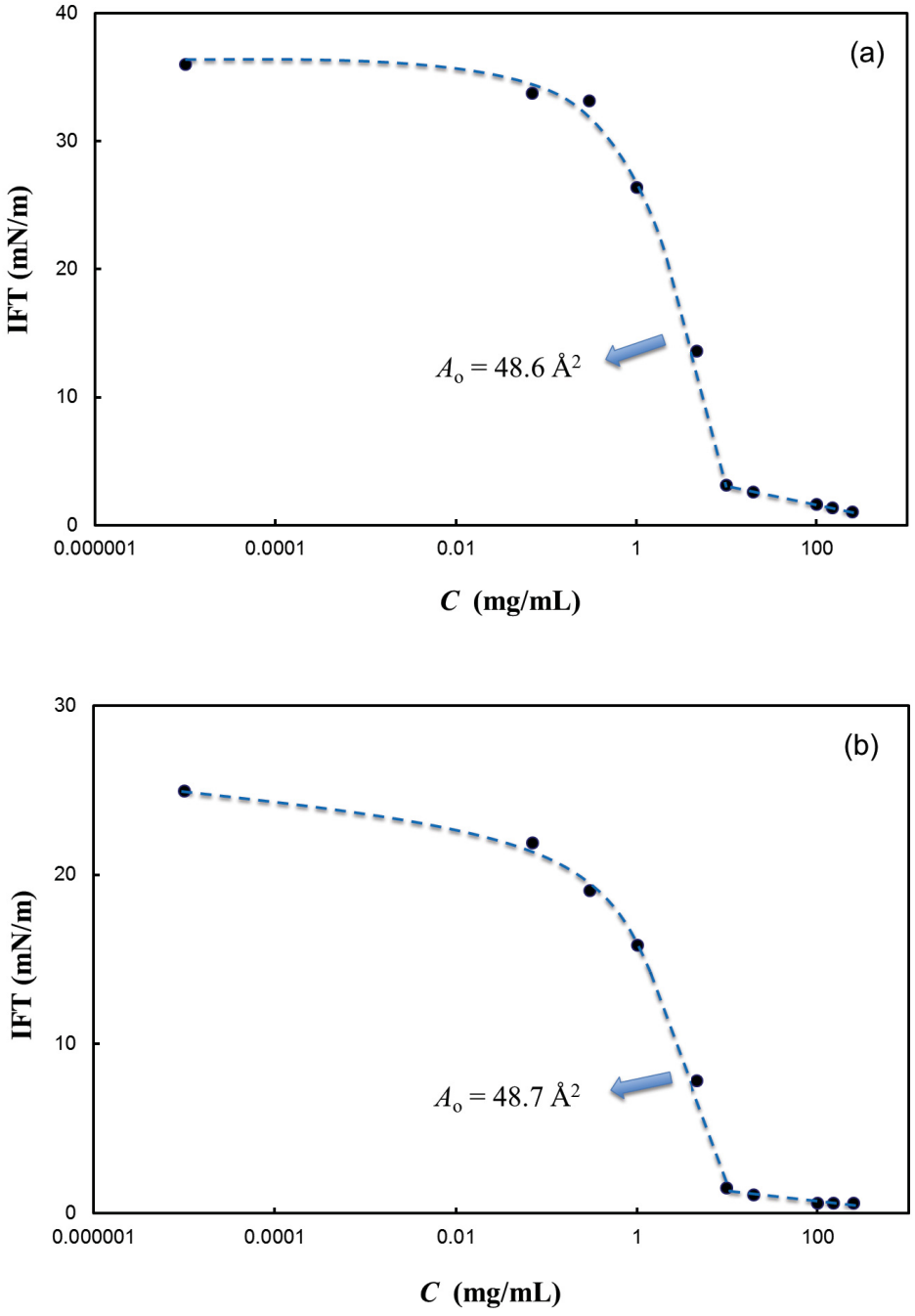

Figure 5-7: Interfacial tension as a function of the sodium naphthenates concentration C in the aqueous phase (the so-called adsorption isotherm): (a) Oil phase is pure toluene; (b) oil phase is toluene + 10 wt% bitumen. Based on the Gibbs adsorption relation [80], A_o (area occupied by a surfactant molecule at saturation) can be calculated from the slope of the semi-log plot.

Next, we consider water wettability of the glass surface upon addition of NA to the water phase. (The smaller the contact angle θ_c, the easier it is for water to wet the solid surface — and hence dislodgement of attached oil ganglia.) Figure 5-8 shows the pore-scale contact angles — both advancing and receding — plotted as functions of the surfactant concentration *C*. (Referring to Figure 4-3, the aqueous surfactant solution was external to the micropipette, while the oil phase, which was toluene with 10 wt% bitumen, was on the inside. For every measurement, there was remarkably no measurable difference between the top and bottom contact angles.) Figure 5-8a, with *C* plotted on a logarithmic scale, shows clearly that there was substantial hysteresis in θ_c at low surfactant concentrations: the difference between advancing and receding contact angles was close to 75°. Indeed, depending on the direction of motion, the surface was either 'hydrophilic' or 'hydrophobic' (with 90° being the rough dividing line). The same data points are re-plotted in Figure 5-8b on a linear scale. Here, it is seen that as the sodium naphthenates concentration *C* increased to 10 mg/mL and beyond, the contact angles hysteresis was much less severe (difference of less than 10° between advancing and receding angles). Moreover, the surfactants had rendered the glass surface much more water wet (θ_c substantially less than 90°). These desirable effects began to appear as the concentration *C* was increased roughly to the value of 10 mg/mL, which coincidentally is also the critical micelle concentrations seen in Figure 5-7. This leads one to speculate that it was the oil-water interfacial tension that controlled the 'dewetting' of hydrocarbon from the

solid substrate, although adsorption of surfactants onto the oil-solid and water-solid interfaces may also play important roles.

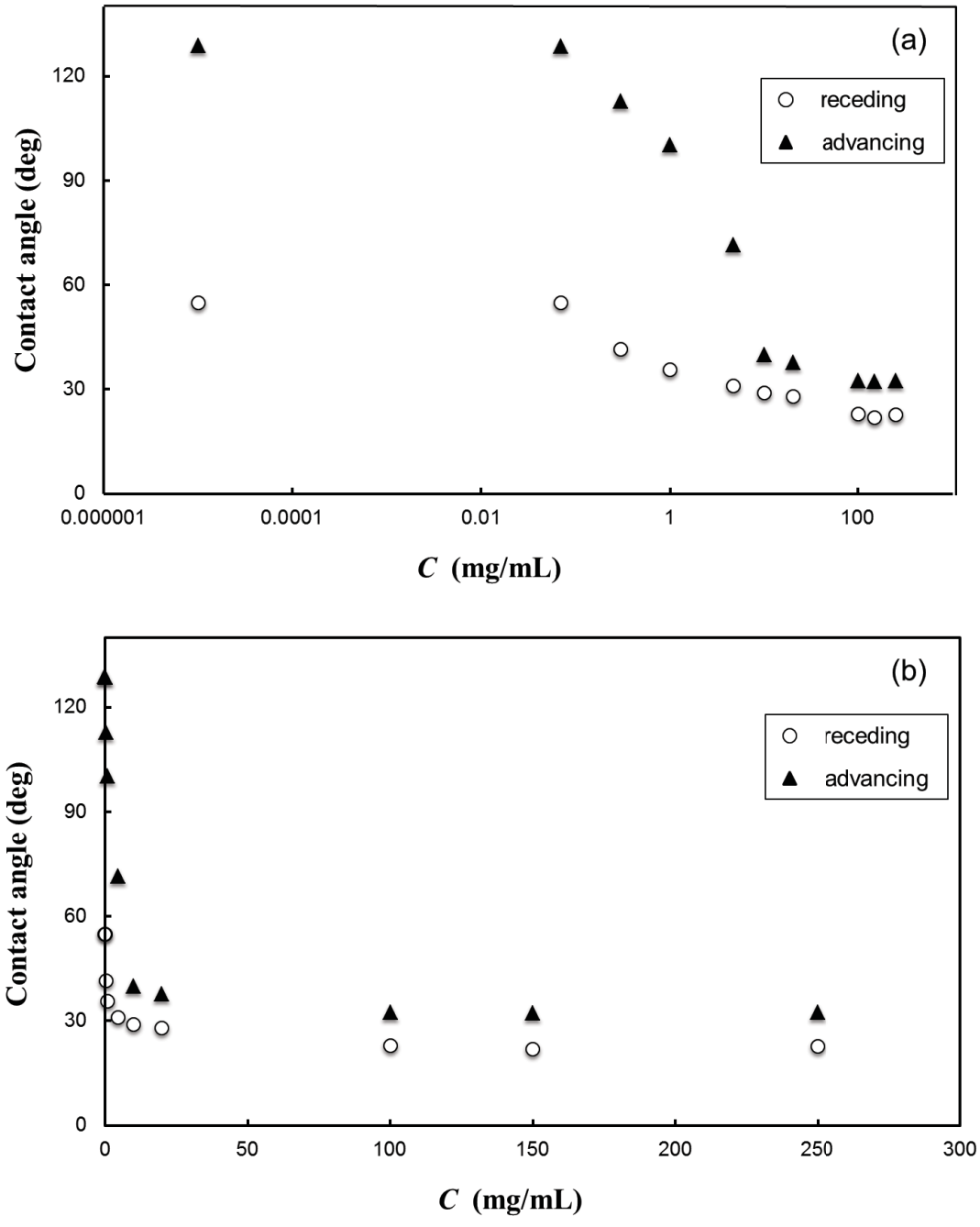

Figure 5-8: Variations of the advancing and receding contact angles as the sodium naphthenates concentration *C* in the aqueous phase was changed. (a) With *C* plotted on a logarithmic scale, strong contact angle hysteresis is clearly seen at low surfactant

concentrations. (b) The same data is plotted on linear scales. It is seen that when *C* is above 10 mg/mL, contact angle hysteresis was decreased significantly, and the surface appeared much more hydrophilic.

Table 5-2 and Figure 5-9 summarize measured IFT values along with contact angles both advancing and receding. Either advancing or receding contact angles were low enough at higher sodium naphthenates concentration comparing the ones at lower surfactant concentrations.

Table 5-2: Advancing and receding contact angles matched the decrease in IFT values by adding sodium naphthenates to the system

Concentration of SN in aqueous solution (mg/mL)	**Contact Angle (deg)**		**IFT values with 10wt% Toluene Diluted Bit (mN/m)**
	Receding	**Advancing**	
0	54.91	128.71	24.93
0.07	54.78	128.42	21.89
0.3	41.47	112.71	19.06
1	35.64	100.09	15.86
4.7	31	71.39	7.85
10	28.88	39.94	1.51
20	27.97	37.60	1.08
100	22.97	32.31	0.61
150	21.92	32.11	0.62
250	22.64	32.31	0.60

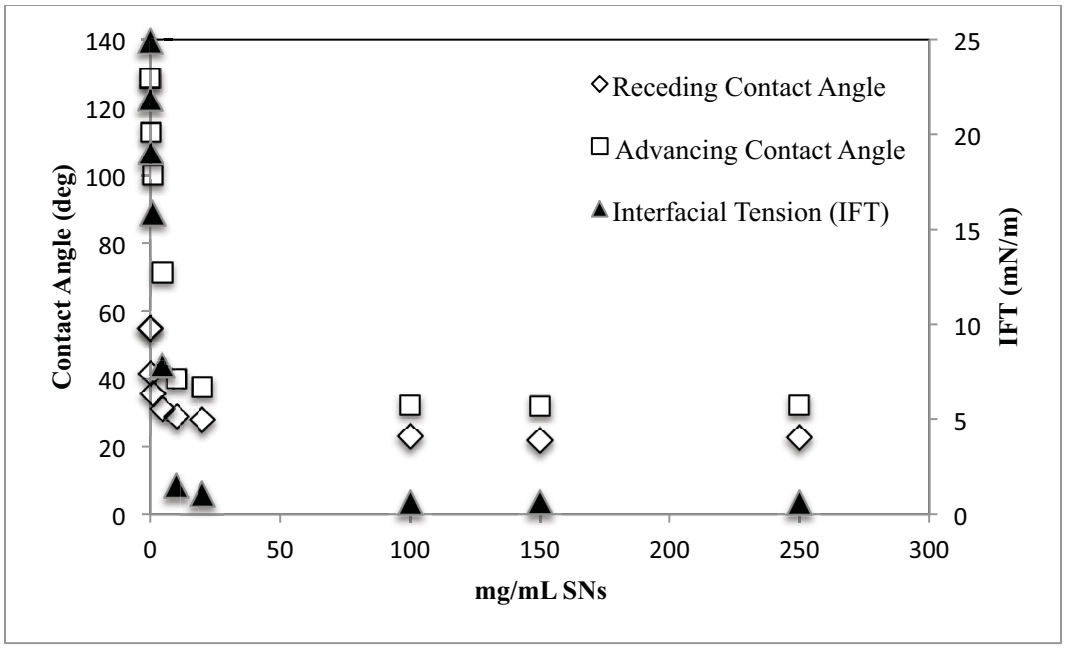

Figure 5-9: Sodium naphthenates not only lowers the IFT values but also decreases the contact angles through aqueous phase.

Adding sodium naphthenates not only lowers the IFT values but also decreases the contact angles through aqueous phase. From both points of view, interfacial tension and wettability, we can say naphthenic acids (NA) is shown to be a very promising agent in the remediation of oil-contaminated sand grains. This conclusion is based on the pore-scale interfacial properties of NA: it has the ability to lower the oil-water interfacial tension to ~1 mN/m, thus reducing the capillary forces which trap the oil ganglia. NA can also modify the wettability of the sand grain surface in a way that liberation of oil from the surface is favoured.

5.3. Evaluation of Naphthenic Acids as a Soil Remediation Agent: A Physicochemical Perspective

As mentioned before, the primary method of extracting bitumen (extra heavy oil) from the Canadian oil sands is a flotation process which produces, as a by-product, contaminated water which must be kept in increasingly large tailings ponds [3, 93]. To address this problem, recent efforts are under way to develop alternative *solvent-based* extraction methods which require little or no water [13, 94]. Briefly, a solvent-based process involves mixing mined oil sand with a light hydrocarbon solvent, creating (i) a product in the form of diluted bitumen, and (ii) a reject stream which consists of the left-over sand grains. An alternative approach, one that we recently began to explore, is to wash the oil-laden sand particles with water-surfactant systems. This is a technique that is often employed in soil remediation [95, 96], and shares many similarities with chemical enhanced oil recovery [97, 98].

Unfortunately, no clear guideline can be found in the literature regarding the choice of surfactants for soil remediation: the 'optimal' surfactant appears to depend on the type of soil and the nature of the contamination; there is also no consensus on the chemical structure of the surfactant (e.g. whether it should be anionic or non-ionic) or the dosage that should be applied (e.g. whether it is above or below the critical micelle concentration) [99, 100]. With little guidance from field-based experience, we turn our focus to the fundamentals of colloid and interface science. There are several conditions that a good washing agent should satisfy: Recognising that the residual oil is held in place by capillary forces, the

first requirement of a washing agent is its ability to significantly lower the oil-water interfacial tension γ. In addition, a small contact angle θ_c between the oil-water interface and the silica surface (angle measured through the aqueous phase) would greatly facilitate detachment of oil ganglia from the sand. Lastly, the surfactant should also be abundant and readily available to the operator.

In an earlier section (section 5.2), we had demonstrated that a particular class of surfactants, called naphthenic acids (NA), fulfils all of the above requirements [101]. Naphthenic acids is a class of anionic surfactants (consisting of cycloalkane carboxylic acids) that is indigenous to the Athabasca bitumen and many other types of crude oils [102-104]; it has an abundance of 1–2wt% in Athabasca bitumen [105]. Our earlier study showed that NA had just the desired pore-scale interfacial properties for a washing process, i.e. it was able to create low γ and small θ_c [101]. Along with its ready availability, it appears naphthenic acids is an ideal candidate as a washing agent.

In this section, we take the next logical step and evaluate the performance of naphthenic acids as an agent for cleaning oil-contaminated sand grains. We will demonstrate that, despite its promising interfacial properties, NA performs rather poorly as a washing agent. As such, we are reporting a negative finding. The main focus of this communication, however, is not on identification of a viable washing agent; rather, it is to reveal, from a fundamental perspective, the underlying mechanisms that led to NA's poor performance. The learning from this study, perhaps as a cautionary note, can be of relevance to many soil remediation and chemical enhanced oil recovery operations.

5.3.1. Materials

Surface treatment of sand

Before experiments, the sand grains were pre-treated under controlled conditions as follows: "Quack sand" (silica grinding sand with average diameter of 0.8 mm) was purchased from Quackenbush Company Inc. (Crystal Lake, Illinois) and used as the solid matrix. The sand was first thoroughly washed in toluene (HPLC grade) and dried under convective air flow. The particles are next surface-treated by dispersing them in 10 wt% diluted bitumen (i.e. 1 part bitumen + 9 parts toluene) to allow extensive exposure of the silica to bituminous materials — just as in the case of the waste sand grains in a solvent-based extraction operation. Bitumen samples (the so-called "DRU bottoms") were obtained from Syncrude Canada Ltd. The sand particles were suspended and stirred in the diluted bitumen solution for two days, then washed multiple times with toluene until all residual diluted bitumen was rinsed away; the particles were again allowed to dry under a fume hood. This pre-treatment step was to render the sand particles hydrophobic: exposure to diluted bitumen would cause irreversible adsorption of bituminous materials onto the silica surface, despite subsequent washing of the particles in toluene [106, 107].

Surfactant solution and its surface tension

Naphthenic acids was the surfactant used in this study. Sodium naphthenates (SN), which is the salt form of naphthenic acids, was supplied by Eastman Kodak (practical grade) as a yellowish crystalline material. The Kodak SN was used

without further purification. Aqueous solutions of sodium naphthenates were prepared at various concentrations by dissolving the SN crystals in deionised and distilled water. To speed up the dissolution process, the mixtures were placed in a sonication bath for 1 to 2 minutes. It is known from an earlier study (Section 5.2) that the critical micelle concentration (CMC) of SN is roughly 10 g/L [101]. The surface tensions of SN solutions were measured by a Krüss K100 device using a Wilhelmy plate.

5.3.2. Experimental

Washing protocol

We devised the following protocol to quantify the overall performance of a washing agent. Here, "overall performance" includes the ability of the surfactant to: liberate oil fragments from the sand grains, emulsify the oil in the aqueous phase, and facilitate transport of the oil/water mixture out of the porous sand matrix. In accordance with the principle of minimal water use (see Introduction), we also stipulated, somewhat arbitrarily, that the amount of water consumption would be equal to the amount of oil that was to be washed.

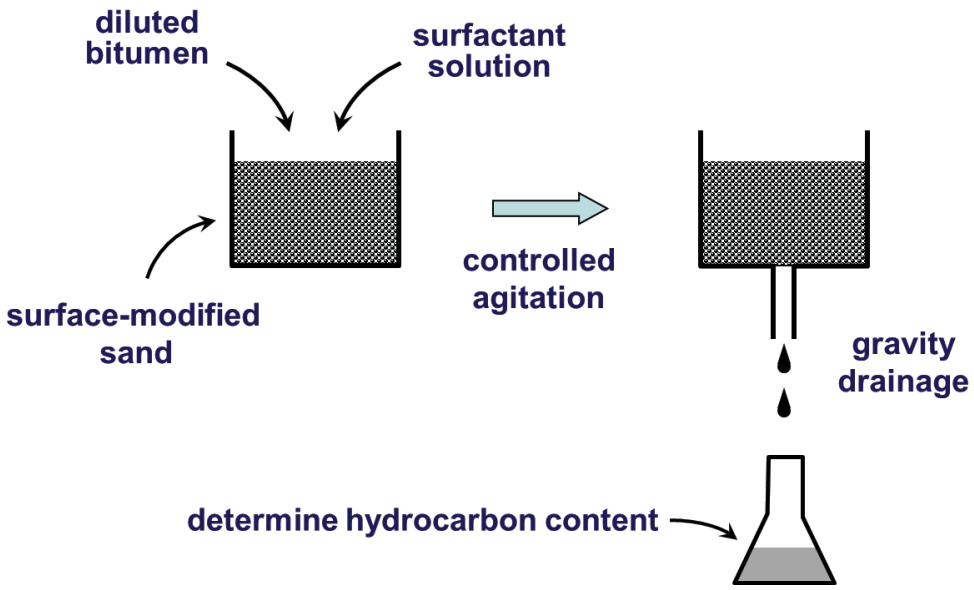

Figure 5-10: A schematic of the washing protocol. Surface-modified sand was first "contaminated" with diluted bitumen, then washed with an aqueous surfactant solution that is equal in mass to the contaminant. The amount of hydrocarbon in the drained liquid is used as a measure of the washing performance.

Figure 5-10 shows a schematic of the washing procedures. As a first step, 50.0 g of surface-treated sand was placed in a PTFE (i.e. Teflon®) bottle. The bottle was gently tapped on a hard surface until the dry sand grains were more-or-less "close-packed" (i.e. with the sand level in the bottle at its lowest). Next, the sand was "contaminated" by slowly dripping toluene-diluted bitumen (again at 10 wt% concentration) into the PTFE bottle until the sand matrix was saturated with the liquid — and before the grains were completely submerged. The amount of diluted bitumen required for this step was very repeatable: it was 8.0 g. To remediate (i.e. clean) the oil-wetted sand, 8.0 g of an aqueous surfactant solution was introduced into the PTFE bottle containing the oil/sand mixture; the concentration of SN in the aqueous solution ranged from 0 to 100 g/L (recall that the CMC is ~10 g/L). Next, the oil/water/sand mixture was agitated in one of two

ways: (a) Gentle mixing with a spatula for 2 min, at a period of about 5 s per revolution; (b) vigorous shaking on an Excella E2 platform shaker (New Brunswick Scientific) at 300 rpm for 2 min. We will refer to these two manners of mixing as the low and high shear agitations, respectively; the corresponding shear rates are estimated to be of order 1 s^{-1} and 100 s^{-1}. Following agitation, the mixture was transferred to a glass vacuum filter holder (filtration area 9.6 cm^2; Fisherbrand, Fisher Scientific) and the oil/water mixture was allowed to drain through a stainless steel screen (100 mesh) and into a collecting flask until the dripping stopped. (Note that this filtration/drainage step was carried out without any filter paper or vacuum suction.) The drained liquid is a mixture of diluted bitumen, water and surfactants in various emulsified and/or free forms. To calculate the washing efficiency, we needed to determine the amount of contaminant (i.e. diluted bitumen) contained in the drained mixture. To that end, we found it easier to instead measure the bitumen content (at 10 wt% concentration, the mass of diluted bitumen is 10× that of the bitumen); this was done as follows: The drained liquid, which typically varied between 8 to 10 mL in volume, was mixed with 200 mL of water and 200 mL of dichloromethane. This new mixture of more than 400 mL was shaken vigorously for 2 min in a separatory funnel and left to equilibrate for 24 hrs. Dichloromethane was chosen for this procedure for the following reasons: (a) it is highly miscible with bitumen and toluene, and (b) it is not a good solvent for naphthenic acids — practically all of the surfactants would partition into the aqueous phase (as verified by control tests). As such, there would be a complete phase separation of the drained liquid,

with the naphthenic acids dissolved in the top aqueous phase, and the hydrocarbon (bitumen + toluene) reporting to the bottom (dichloromethane) portion of the funnel. After 24 hrs of equilibration, the bottom liquid (toluene and bitumen dissolved in dichloromethane) was drained from the separatory funnel and transferred to a rotary evaporator to remove all solvent (dichloromethane and toluene), leaving only bitumen as the residue. (The "rotovap" was set to operate above the boiling point of toluene and was run for 2 hrs.) From the weight of the glass vial which contained the bitumen residue, the amount of bitumen in the drained liquid, m_{bit}, could be determined. Finally, we define the *washing efficiency* as

$$\frac{\text{mass of contaminant removed}}{\text{mass of original contaminant}} \times 100\%$$

where the "contaminant," which should technically be the diluted bitumen, can also be regarded as the bitumen (since the two are at a fixed ratio). Two additional comments should be made on the washing efficiency as defined: (1) It is not an absolute measure and, as such, should only be used for comparative purposes; (2) as the amount of bitumen used to contaminate the sand was 0.80 g (10% of 8.0 g), the washing efficiency is $(m_{\text{bit}}/0.80)\times 100\%$, where m_{bit} is expressed in grams.

Dynamic Light Scattering

In the course of our investigation, we encountered situations where the sizes of swollen micelles needed to be determined (see Results and Discussions). This was done with the dynamic light scattering (DLS) technique, using an ALV 5022F device at a scattering angle of 90°. The laser light scattering cell was immersed in

toluene at 23ºC. Such experiments were repeated at least three times for each sample.

Recall the two independent variables of the washing experiments (Figure 5-10) are: the sodium naphthenates concentration (0–100 g/L) and the strength of agitation (low or high shear); the dependent variable is of course the washing efficiency. Figure 5-11 shows the washing efficiency as a function of the surfactant concentration at low shear.

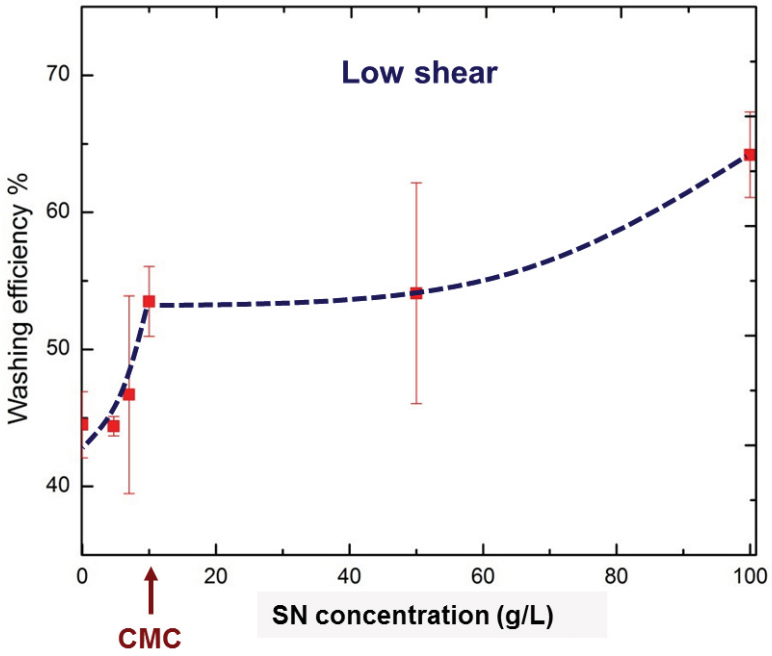

Figure 5-11: Washing efficiency as a function of sodium naphthenates concentration at low shear rate. The surfactant's critical micelle concentration (CMC) was around 10 g/L. A dashed line is included to show the functional trend; it is not based on any theoretical calculation.

As expected, the washing efficiency increased monotonically with surfactant concentration (i.e. more oil was removed as more surfactants were used). Furthermore, it is noted that the upward trend in Figure 5-11 is comprised of two distinct regimes, with the transition concentration coinciding roughly with the

CMC of the surfactant. This was most likely a consequence of the two mechanisms of emulsification, namely, *dispersion* of the oil below CMC (creating macroemulsions), and *solubilization* above CMC (creating swollen micelles). Next, the same washing experiments were repeated at high shear rate; the results are shown in Figure 5-12:

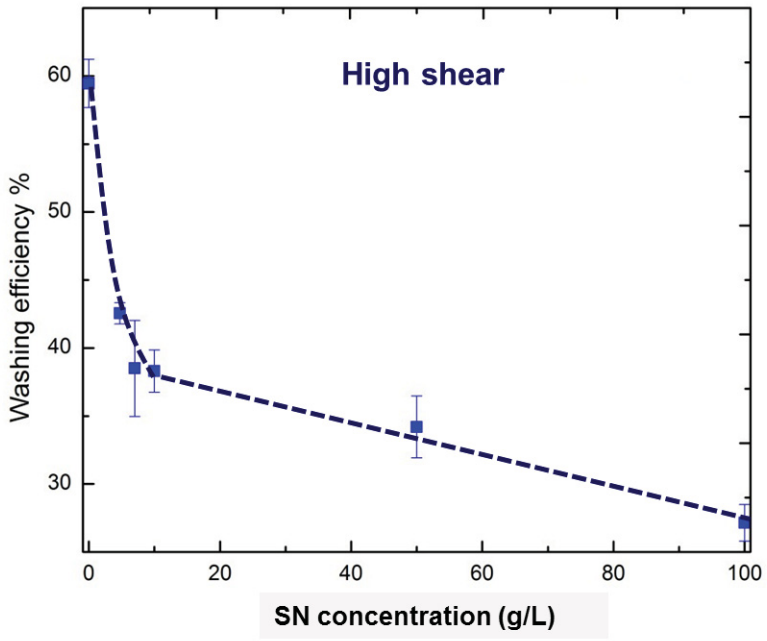

Figure 5-12: Washing efficiency as a function of surfactant concentration at high shear rate. The dashed line only illustrates the trend and is not a theoretical curve.

Surprisingly, the upward trend in Figure 5-11, which we were able to rationalize in terms of emulsification mechanisms, is now reversed. The relatively high washing efficiency at zero concentration (i.e. in the absence of surfactants) was perhaps a result of the oil being liberated and dispersed by "brute force." Once surfactants were introduced, however, the data show a precipitous drop in washing efficiency. The addition of surfactants, which was meant to

further facilitate the remediation process, proved to be counter-productive. To investigate this anomaly, we chose to focus on a simpler situation, namely, interaction between the oil phase and the aqueous phase without the involvement of sand particles.

Appearance of a third phase

We mixed 100 g of the oil phase (10 wt% diluted bitumen) with 100 g of the aqueous phase (sodium naphthenates solution at an intermediate concentration of 50 g/L) at the two shear rates described in the Experimental section. The intention of this exercise was to find out whether the oil would emulsify into the aqueous phase, or vice versa. What was observed instead was an unexpected phenomenon shown in Figure 5-13.

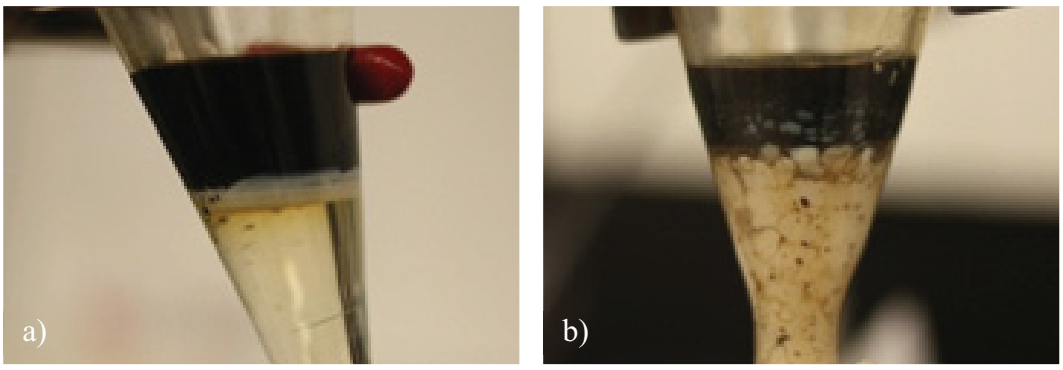

Figure 5-13: Results of mixing equals amounts of the oil phase (10 wt% diluted bitumen) and the aqueous phase (SN solution at 50 g/L) under (a) low shear, and (b) high shear. Note that the white liquid in (b) was actually quite homogeneous; what appears as "lumps" was due to streaks of black oil that were stuck to the inner wall of the vial.

At low shear, a layer of milk-like liquid was formed at the top of the aqueous phase (Fig. 5-13a). Like milk, this white liquid was completely miscible with water, but could not mix with the hydrocarbon. By contrast, with vigorous

agitation, the milk-like substance was seen to occupy the entire aqueous domain with a rather opaque white colour (Fig. 5-13b). Another important observation was as follows: even when quiescent, the "milky layer" in Figure 5-13a would spontaneously extend downward, on a time scale of ~10 hrs, while maintaining more or less the same opacity (i.e. it did not seem to dilute as its volume expanded). The growth of this milky layer could be greatly accelerated with mechanical shear, leading eventually to a final state that was similar to what is shown in Figure 5-13b (which was formed in minutes).

From the above observations, a number of deductions can be made. First, the milk-like substance had to be a water-continuous dispersion of liquid droplets or solid particles; let us suppose for now that they were liquid drops (to be justified later). We further deduce that:

1. The droplets were of order 1 μm or larger, which resulted in the emulsion's opacity.
2. The dispersed liquid must be transparent to visible light, hence the white colour of the emulsion. This eliminates the possibility of the droplets being diluted bitumen, which was a very dark liquid.
3. Based on the emulsion's position in Figure 5-13a, the dispersed liquid must have a density that was intermediate between the densities of diluted bitumen and water.
4. The dispersed liquid was not miscible with either diluted bitumen or water.

Immiscibility with oil and water implied that the dispersed substance existed as a *third phase*. Clearly, this third phase could only be made up of diluted bitumen,

water, and/or surfactants. If this material were truly a liquid, there could only be one possibility: it was a bicontinuous (BC) mixture of diluted bitumen and water, facilitated by a significant amount of surfactants which served to lower the oil-water interfacial tension and allow "random mingling" of the two inherently immiscible liquids. When the random mingling is on colloidal length scales, there can be enough entropic contribution for the mixture to become a true (i.e. thermodynamically stable) third phase that is distinct from — and immiscible with — oil and water; this is known as a bicontinuous microemulsion or "BC μE" [32, 98]. In our case, the diluted bitumen content in the BC μE must be quite low, as the third phase was essentially transparent (see Point 2 above). Another important point regarding the BC μE: if it were indeed a thermodynamic state, it should appear spontaneously under conditions which favour its formation (i.e. when the system is in the appropriate region of the phase diagram); as discussed above, this was indeed observed (recall the spontaneous growth of the milky liquid on time scale of ~10 hrs). Creation of the third phase could also be seen in "real time" when the experiment was conducted on shorter length scales.

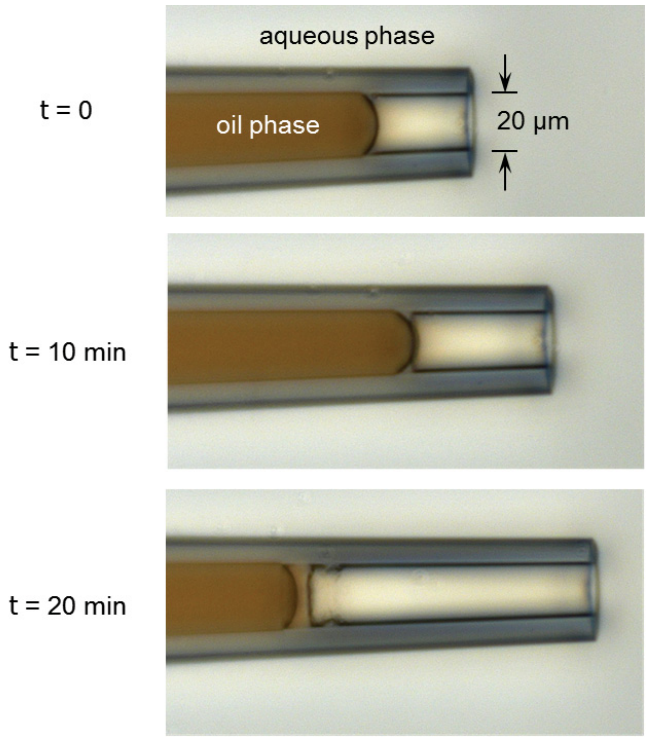

Figure 5-14: A micropipette filled with diluted bitumen was immersed in an aqueous solution of sodium naphthenates. After several minutes, a third liquid, which was immiscible with oil and water, appeared spontaneously at the oil-water interface.

Figure 5-14 shows a 20-µm glass pipette that was filled with the oil phase (10 wt% diluted bitumen), then immersed into an aqueous solution of sodium naphthenates (at 50 g/L). As seen, a third phase, which was immiscible with both oil and water, was formed spontaneously at the oil water interface after several minutes. This third phase had a slightly yellowish colour — strong evidence that it was a mix of diluted bitumen and water. Note also that the third phase conformed itself to the shape of the pipette inner wall and the leading edge of the oil, suggesting that it was fundamentally a liquid material (as opposed to rigid substances such as precipitated solid or liquid crystal). Finally, the third phase in Figure 5-14 was invisible under cross-polarized light, which indicated that it was

an isotropic liquid. All these characteristics were clear evidence that the third phase was a bicontinuous microemulsion.

Effect of the third phase on washing performance

Unlike the deductions made thus far, the following arguments are more speculative. Our first conjecture is that hydrodynamic shear can function as a *catalyst* which accelerates the formation of BC μE. Though ultimately driven by thermodynamics, the formation of BC μE can be very slow under quiescent conditions. However, mechanical agitation can greatly shorten the time for the system to reach its new equilibrium state (cf. the case from Figure 5-13a to Figure 5-13b).

We now turn to washing performance. To begin, it is noted that the BC μE is a highly surfactant-rich structure. Its formation consumes a large amount of surfactants, thus precluding the remediation function that is served by the surface active molecules. At low shear rate (Figure 5-11), formation of the BC μE was sufficiently slow that most of the surfactants were still available to emulsify the contaminant by either dispersion below the CMC, or solubilization above the CMC. (Here, "slow" implies the time scale of BC μE formation was much longer than that of the washing process.) By contrast, at high shear rate (Figure 5-12), most of the surfactants were quickly consumed in the creation of the third phase, leaving only few molecules for the emulsification of diluted bitumen. Moreover, an emulsion of the third phase (the milky liquid) may likely obstruct drainage of liberated oil from the porous sand matrix. Such a scenario is consistent with the downward trend seen in Figure 5-12.

Disappearance of the third phase

In the above discussion, the last conjecture was that dispersed droplets of BC μE (indeed, droplets of any liquid) would create additional resistance to the flow of the suspension. Such a notion is well established in colloid science: the overall rheology of an emulsion depends on factors such as the volume fraction of the dispersed phase, its drop size distribution, the viscosities of the two liquids (here, water and BC μE), their interfacial tension, etc [108]. This suggests a logical next step in our investigation: isolate the milk-like emulsion and examine its various properties — beginning with microscope images of the BC μE droplets and micromechanical tests on the individual drops (such techniques have been developed by our group for other emulsion systems [59, 109]). Unfortunately, all such efforts were futile as the milky emulsion, when isolated from the environment in which it was formed, would "disintegrate" and turn into an aqueous phase. Taking as an example the emulsion in Figure 5-13b (the milky bottom portion): when kept in the container with the diluted bitumen, it could remain stable for weeks and possibly much longer. However, when the emulsion was drained from the bottom of the vial, the milk-like dispersion turned into a slightly yellow but transparent liquid in 1–2 days. This yellowish liquid was clearly aqueous in nature, as it was miscible with water but not with a hydrocarbon such as toluene. Once again, we found the characteristic time of such a phenomenon to be much shorter on the micron scale: If observed under an optical microscope (provided the sample was retrieved and viewed quickly), droplets of the third phase, which ranged from microns to tens of microns in size,

disappeared within seconds. We believe the disappearance of the third phase can be explained by examining the relative ratios of the oil, water and surfactant components. Initially, the amounts of oil and water in the system were equal, and together they accounted for the majority of the ternary system. However, by removing the diluted bitumen, the oil fraction in the new system (which is now the milky emulsion) had suddenly dropped to almost zero. This caused a major shift of the system in phase space, as shown through a hypothetical ternary phase diagram in Figure 5-15 below.

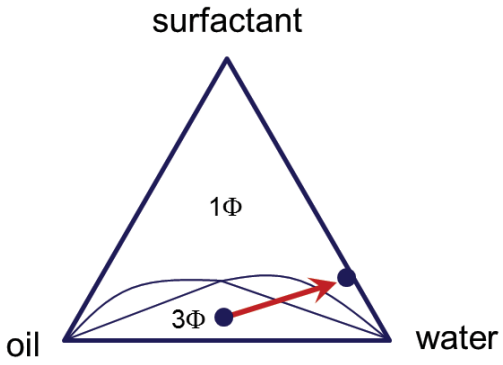

Figure 5-15: A hypothetical (but typical) ternary phase diagram of a surfactant-oil-water system. By removing the diluted bitumen (the oil), the system undergoes a major shift in phase space as shown — moving from a 3-phase (3Φ) region to a single-phase (1Φ) region of swollen micelles in water.

Figure 5-15 depicts a typical ternary phase diagram of a surfactant-oil-water system, with the boundary lines separating domains of one-, two-, and three-phase systems [22]. The arrow in the figure represents the system going from a 3-phase region (the so-called Winsor III system, in which oil, water, and a microemulsion coexist) to a single-phase region (micelles or swollen micelles suspended in water). If this explanation were true, the disappearance of the BC μE droplets would be a result of the surfactants abandoning the bicontinuous structure and

existing instead as either monomers or micelles in water. The oil (diluted bitumen) that was originally a part of the bicontinuous structure must now be solubilized by the micelles, thus giving the new aqueous liquid its yellowish colour. As the micelle sizes are on the colloidal scale, the solution appeared transparent to visible light.

We expect an aqueous solution of "disintegrated BC μE" to have the following characteristics: (a) it consists of swollen micelles solubilizing the diluted bitumen, and (b) it is saturated with surfactant monomers in solution *and* at the air-water interface. To check these, we measured the surface tension (using the Wilhelmy plate) and micelle size (using DLS) of the following two aqueous solutions:

- As a control test, we prepared a sodium naphthenates solution at 50 g/L (well above the CMC level of 10 g/L). The surface tension of this solution was 30.8 mN/m, and the micelle size was 3.1 ± 0.3 nm (i.e. the size of an "unswollen" micelle).
- The second aqueous solution was a "disintegrated BC μE" from the bottom portion Figure 5-13b (see text above the figure for its composition). The surface tension of this aqueous solution was again 30.8 mN/m, and the micelle sizes ranged from 3.6 to 48.2 nm.

With the micelle sizes in the second solution all larger than that of an unswollen micelle, and given the equality of the surface tensions, we are confident that the disappearance of the BC μE was due to the phase change as depicted in Figure 5-15.

Due to its very favourable interfacial properties (the ability to lower interfacial tension and create hydrophilic surfaces), naphthenic acids was proposed as a surfactant for cleaning oil-contaminated sand grains. However, when evaluated by actual washing experiments, the surfactant proved inadequate as a remediation agent. Specifically, with the inadvertent creation of a bicontinuous "third phase," addition of surfactants to the washing process proved counter-productive at shear rates that are representative of an actual commercial operation (Figure 5-12). On a broader picture, the ability to lower oil-water interfacial tensions has often been a primary criterion for a surfactant to be effective in soil remediation and chemical enhanced oil recovery; achievement of "ultralow" interfacial tensions and creation of microemulsions have been considered positive traits. This particular case study may offer a cautionary note to such a philosophy.

6. Summary and Recommendations

The *non-aqueous* (or solvent-based) bitumen extraction technology is studied as an alternative to the current water-based method of bitumen extraction. The current method requires withdrawal of fresh water from the Athabasca River — a practice which is the direct cause of many environmental problems [110]. The general obstacle that any non-aqueous extraction technology will encounter is the recovery of residual oil from oil-soaked sand grains; the reject sand grains must be "remediated" (i.e. cleaned) so that they can be used for subsequent land reclamation. In this research, I have investigated (a) the micro-scale interfacial phenomena that are relevant to the remediation process, and (b) the macro-scale performance of a particular surfactant (sodium naphthenates) which showed initial promise as a remediation agent.

Washing the sand grains with aqueous surfactant solutions (as a pseudo solvent) to solubilize the residual oil is a promising approach. A selected surfactant must perform two functions from a colloid science perspective (in terms of IFT and contact angle): it must (a) significantly lower the oil-water interfacial tension, which will in turn reduce the capillary forces which trap the residual oil in void spaces between the sand particles, and (b) reduce the contact angle between the oil-water interface and the solid substrate, thus enhancing 'dewetting' of hydrocarbon from the sand grain surfaces.

Non-aqueous bitumen extraction requires low to ultralow oil-water interfacial tensions to facilitate blending of the two immiscible liquids [68-70]. For such systems, it is important to note that the presence of surfactants may lead to the

inadvertent formation of microemulsion phases which can obscure IFT and contact angle measurements (sections 5.1.2 & 5.3.2). Traditional methods that are currently available can suffer from several disadvantages due to the formation of a "third phase" (a bicontinuous microemulsion). As an alternative to traditional tensiometric methods, a novel micropipette technique is developed to quantify low to ultralow IFTs and also to measure contact angles (wettability) (Sections 4.1 &4.2).

In our search for a suitable remediation agent (for good residual oil recovery), different surfactants were examined. The natural surfactants extracted from bitumen, which appeared to be essentially sodium naphthenates (SNs), was selected as a potential surfactant due to its water solubility, strong interfacial activity, and ready availability as a crude oil by-product.

Since sodium naphthenates are derived from straight-run distillates of crude oil at various fractions [85], some preliminary studies are conducted to substitute commercial sodium naphthenates with natural surfactants extracted from Athabasca bitumen (see section 5.2.2). X-ray photoelectron spectroscopy (XPS) results of natural surfactants showed the carbon–oxygen bond in carboxyl groups as an identification of sodium naphthenates. Langmuir isotherms of Athabasca natural surfactants and commercial SNs are plotted and showed the same IFT values (~ 30 mN/m) at critical micelle concentrations (CMCs); the two isotherms also exhibited almost identical interfacial areas occupied by each surfactant at saturation (~ 50 $Å^2$).

The goal of our research is to ascertain whether sodium naphthenates (SNs) have the desired interfacial properties (on the pore scale) to be a potential remediation agent. To acquire sufficiently large capillary numbers (ratio of hydrodynamic to capillary forces), the IFT is decreased from typically 20–30 mN/m (in the absence of surfactants) to values of order 1 mN/m (down to 0.6 mN/m). Also, the addition of SNs had the effect of rendering the silica surfaces hydrophilic by reducing the contact angle θ_c to values well below 90° (thus promoting liberation of oil from the solid surface). These desirable effects began to be significant as the SN concentration was increased roughly to the value of 10 mg/mL, which coincidentally is also the critical micelle concentration (see Fig. 5-7). From the micro-scale perspective, SN is shown to be a very promising agent in the remediation of oil-contaminated sand grains.

As the pore-scale interfacial properties became favourable with addition of SNs, the washing efficiencies were next investigated from a macro-scale perspective. Aqueous solutions with different surfactant concentrations were used to remove 10 wt% toluene-diluted bitumen from contaminated sand grains; the effect of agitation (under low and high shear rates) on oil remediation performance was also investigated.

Under low shear, the washing efficiency was seen to gradually increase (i.e. more oil was being washed off from contaminated sand grains) as the surfactant concentration was increased. We suggest that the underlying mechanism of washing under low shear is a combination of dispersion and solubilization. At lower surfactant concentrations (under CMC), capillary forces are reduced and the

oil is liberated from the sands and dispersed in the aqueous phase; at higher surfactant concentartions (above CMC), the formation of micelles results in solubilization of the oil phase, and hence more oil remediation and higher washing efficiencies.

In contrast, under high shear rate (30 minutes of shaking at 300 rpm), an inverse trend in washing efficiencies was seen, suggesting an entirely different mechanism of oil remediation this was in effect. Importantly, we had observed the formation of a third phase, both in jar tests and micro-scale micropipettes, which led us to understand why washing efficiencies were not favored at high shear agitations. As described earlier (Chapter 2, 4 and section 5.1), the formation of bicontinuous microemulsions (or the so-called third phase, which is neither water nor oil) at oil/water interfacial regions is the key to this new phenomenon. After applying high shear, the aqueous phase was seen to become milky, and we hypothesize that this was due to the formation of a water-continuous *macroemulsion* whose micron-sized droplets were composed of the third phase (i.e. the surfactant-rich bicontinuous microemulsions). The formation of the third phase consumed large amounts of surfactants and effectively trapped them in stable structures that were dispersed in the aqueous medium. Therefore, any additional surfactants added to the system would lead only to more thermodynamically stable microemulsions; the extra surfactants would not be available for oil remediation. Based on what we have learned from this study; we should avoid using surfactants which form the microemulsion third phase at low IFTs. Also as the third phase mostly appears at low IFTs, we can conclude that it

is not always necessary to aim for lower IFTs and small contact angles. Therefore moderate IFTs and small contact angles might work better for the choice of proper surfactant as remediation agent.

For future work, one of the focuses should be on extending the current experimental approach to a better design of the washing apparatus; the new experimental protocol should also better quantify the effect of shear rate on washing efficiency. And as part of the underlying washing mechanism, the surfactant sorption on soil should also be studied. As another task, it would be of great interest to perform a multi-parameter study with the aim of lowering the oil-water interfacial tension to more than what has been achieved in the present research (by varying pH, salinities, type of organic solvents, aromaticity of the solvents, the degree of bitumen dilution, etc). In addition, as interfacial properties and washing processes are known to be strongly temperature dependent, the effect of temperature on dynamic interfacial characteristics and washing efficiencies will also be an important study.

7. References

1. Dunbar RB. (2011). Canada's Oil Sands — A World-Scale Hydrocarbon Resource. Strategy West Inc.
2. Alberta Energy Resources Conservation Board; Alberta's Energy Reserves 2010 and Supply/Demand Outlook 2011-2020; ERCB ST98-2011.
3. Woynillowicz, D., Severson-Baker, C. & Raynolds, M. (2005). "Oil Sands Fever: The Environmental Implications of Canada's Oil Sands Rush"; The Pembina Institute.
4. Richardson, J.F., Harker, J.H. & Backhurst, J.R. (2002). Coulson and Richardson's Chemical Engineering, Volume 2, Fifth Edition: Particle Technology and Separation Processes; Butterworth Heinemann, Oxford.
5. Sparks, B.D. & Meadus, F.W. (1979). "A Combined Solvent Extraction and Agglomeration Technique for the Recovery of Bitumen from Tar Sands"; Energy Processing Canada, 55-61.
6. Sparks, B.D. & Meadus, F.W. (1981). "A Study of Some Factors Affecting Solvent Losses in the Solvent Extraction-Spherical Agglomeration of Oil Sands"; Fuel Processing Technology, 4: 251-264.
7. Meadus FW, Chevrier PJ, Sparks B.D. (1982). "Solvent extraction of Athabasca oil-sand in a rotating mill-1. Dissolution of bitumen"; Fuel Processing Technology, 6: 277-287.
8. Meadus FW, Bassaw BP, Sparks B.D. (1982). "Solvent extraction of Athabasca oil-sand in a rotating mill-2. Solids-liquid separation and bitumen quality"; Fuel Processing Technology, 6: 289-300.
9. Sparks, B.D., Meadus, F.W. & Hoefele, E.O. (1988). "Solvent Extraction Spherical Agglomeration of Oil Sands"; US Patent 4,719,008.
10. Rosenbloom, W.J. (1975). "Recovery of Oil from Tar Sand by an Improved Extraction Process"; US Patent 3,875,046.
11. Benson, A.M. (1969). "Filtration of Solvent-Water Extracted Tar Sand"; US Patent 3,459,653.

12. Savage, W.E. & Cheney, H.A. (1971). "Process of Extracting Tar from Tar Sand"; US Patent 3,553,099.
13. Hsieh, C.R. & Clifford, R.K. (1987). "Solvent Extraction Process for Recovering Bitumen from Tar Sand"; US Patent 4,676,889.
14. Johnson, C.B. (1999). "Thin Layer Solvent Extraction"; US Patent 5,911,541.
15. Karnofsky, G.B. (1984). "Process for Solvent Extraction of Bitumen from Oil Sand"; US Patent 4,448,667.
16. Brand, J.D., Oyler, J.F. & Zavada, R. (1987). "Circular Solvent Extractor"; US Patent 4,683,029.
17. Adeyinka, S. (Imperial Oil Ltd.), private communication.
18. Pillai, V, Kanicky, J.R. & Shah, D.O. (1999). "Applications of Microemulsions in Enhanced Oil Recovery"; in Handbook of Microemulsion Science and Technology (P. Kumar & K.L. Mittal, editors), Marcel Dekker, New York; pp. 743-754.
19. Wasan, D. & Payatakes, A. (1982). Interfacial Phenomena in Enhanced Oil Recovery; American Institute of Chemical Engineers Symposium Series, New York.
20. Jones DM, Watson JS, Meredith W, Chen M, Bennett B. (2001). "Determination of Naphthenic Acids in Crude Oils Using Non-aqueous Ion Exchange Solid-phase Extraction"; Anal Chem, 73: 703-7.
21. Tomczyk NA, Winans RE, Shinn JH, Robinson RC. (2001). "On the Nature and Origin of Acidic Species in Petroleum. 1. Detailed acid type distribution in a California crude oil"; Energy and Fuels, 15: 1498-1504.
22. Taupin, C., Dvolaitzky, M. and Ober, R. (1984). "Structure of microemulsions: role of the interfacial flexibility"; J. Il Nuovo Cimento D, Vol. 3, N. 1: 62-74.
23. Kellay, H., Binks, B.P., Hendriim, Y., Lee, L.T. and Meunier, J. (1994). "Properties of Surfactant Monolayers in Relation to Microemulsion Phase Behaviour"; Advances in Colloid and Interface Science, 49: 85 -112.

24. Lee, L.T., Langevin, D., Wong, K., Abillon, O. (1990). "Microemulsions: experimental aspects"; J. Phys. 2 SA333-SA338.

25. Abillon, O., Lee, L.T., Langevin, D. and Wong, K. (1991). "Microemulsions: Structures, Surfactant Layer Properties and Wetting Transitions"; Physica A North-Holland 172: 209-218.

26. Kellay, H., Hendrikx, Y., Meunier, J., Binks, B.P. and Lee, L.T. J. de Physique (France) II, in press.

27. Helfrich, W. (1973). "Elastic Properties of Lipid Bilayers: Theory and Possible Experiments"; Zeitschrift für Naturforschung 28c 693-703.

28. Safran, S.A. (1994) Statistical Thermodynamics of Surfaces, Interfaces, and Membranes, Perseus Publishing.

29. Kegel, W.K., Overbeek, J.T.G. & Lekkerkerker, H.N.W. (1999). "Thermodynamics of Microemulsions I"; in Handbook of Microemulsion Science and Technology (P. Kumar & K.L. Mittal, editors), Marcel Dekker, New York; pp. 13-44.

30. Huse, D.A. & Leibler, S. (1991). "Are Sponge Phases of Membranes Experimental Gauge-Higgs Systems"; Phys. Rev. Letters, 66: 437-440.

31. Scriven, L.E. (1976). "Equilibrium Bicontinuous Structure"; Nature, 263: 123-125.

32. de Gennes, P.G. & Taupin, C. (1982). "Microemulsions and the Flexibility of Oil/Water Interfaces"; J. Phys. Chem. 86: 2294-2304.

33. Adamson, A. W. (1990). Physical Chemistry of Surfaces, 5th ed., New York: John Wiley & Sons.

34. Alexander, A. E. and Hayter, J. B. (1971). Determination of surface and interfacial tension, in A. Weissberger and B. W. Rossiter (eds.), Physical Methods of Chemistry, Part V, 4th ed., New York: John Wiley & Sons.

35. Couper, A. (1993). Surface tension and its measurement, in B. W. Rossiter and R. C. Baetzold (eds.), Physical Methods of Chemistry, Vol. 9A, 2nd ed., New York: John Wiley & Sons.

36. Padday, J. F. (1969). Surface tension. II. The measurement of surface tension, in E. Matijevic (ed.), Surface and Colloid Science, Vol. 1, New York: John Wiley & Sons.

37. Drelich, J., Fang, Ch. and White, C. L. (2002). "Measurement of Interfacial Tension in Fluid–Fluid Systems" in Encyclopedia of Surface and Colloid Science, Marcel Dekker, New York, p. 3152.

38. Harkins, W.D. and Jordan, H.F. (1930). "A method for determination of surface and interfacial tension from the maximum pull on a ring"; J. Am. Chem. Soc. 52: 1751–1772.

39. Sugden, S. (1922). "The determination of surface tension from the maximum pressure in bubbles"; J. Chem. Soc. 121: 858–866.

40. Rehbinder, P.A. (1924). "Dependence of surface activity and surface tension of solutions upon temperature and concentration."; Z. Phys. Chem. 111: 447–464.

41. Adamson, A.W. & Gast, A.P. (1997). Physical Chemistry of Surfaces, 6th Ed.; John Wiley & Sons, Inc.: New York.

42. Lord Rayleigh, OM.; F.R.S. (1916). "On the theory of the capillary tube"; Proc. R. Soc. London, Ser. A, 92: 184–195.

43. Tate, T. (1864). "On the magnitude of a drop of liquid formed under different circumstance"; Phil. Mag. 27: 176–180.

44. Harkins, W.D. & Brown, F.E. (1919). "The determination of surface tension (free surface energy), and the weight of falling drops: the surface tension of water and benzene by the capillary height method."; J. Am. Chem. Soc. 41: 499–525.

45. Ambwani, D. S. and Fort, Jr. T. (1979). Pendant drop technique for measuring liquid boundary tensions, in R. J. Good and R. R. Stromberg (eds.), Surface and Colloid Science, Vol. 11, New York: Plenum Press.

46. Lin, S., McKeigue, K. and Maldarelli, C. (1990). "Diffusion-controlled surfactant adsorption studied by pendant drop digitization"; AIChE J., 36: 1785-1795.

47. Kwok, D. Y., Vollhardt, D., Miller, R., Li, D. and Neumann, A. W. (1994). "Axisymmetric drop shape analysis as a film balance"; Colloids Surf., A, 88: 51-58.

48. Schoel, W. M., Schurch, S. and Goerke, J. (1994). "The captive bubble method for the evaluation of pulmonary surfactant: surface tension, area, and volume calculations"; Biochim. Biophys. Acta, 1200: 281-290.

49. Drelich, J. (1993). "The Role of Wetting Phenomena in the Hot Water Process for Bitumen Recovery from Tar Sand."; Ph.D. Dissertation, The University of Utah: Salt Lake City, Utah, USA.

50. Rudin, J. & Wasan, D.T. (1992). "Mechanisms for lowering of interfacial tension in alkali/acidic oil systems"; Colloids Surf. 68: 81–94.

51. Dukhin, S.S., Kretzschmar, G. & Miller, R. (1995). "Dynamics of Adsorption at Liquid Interfaces: Theory, Experiment, Application"; Elsevier: Amsterdam.

52. Rosen, M.J. (1976). "Surfactants and Interfacial Phenomena"; Wiley-Interscience: New York.

53. Dynamic Properties of Interfaces and Association Structures (1996); Pollai, V., Shah, D.O., Eds.; ACS Press: Champaign, Illinois.

54. Lucassen, J. (1979). "The shape of an oil droplet suspended in an aqueous solution with density gradient ☆: A new method for measuring low interfacial tensions"; Journal of Colloid and Interface Science, 70: 355-365.

55. Chatenay, D., Langevin, D., Meunier, J., Dourbon, D., Lalanne, P., Bellocq, A.M. (1982). J Dispersion Sci Technol 3:245.

56. Langevin, D. (1985). In: Physics of Amphiphiles: Micelles, Vesicles and Microemulsions, XC Corso, Soc Ital di Fisica, Bologna, p 181.

57. Evans, E.; Skalak, R. (1980). "Mechanics and Thermodynamics of Biomembranes"; CRC Press, Inc.: Boca Raton, Florida.

58. Evans, E.; Needham, D. (1987). "Physical properties of surfactant bilayer membranes: thermal transitions, elasticity, rigidity, cohesion, and colloidal interactions."; J. Phys. Chem., 91: 4219–4228.

59. Moran, K.; Yeung, A.; Masliyah, J. (1999). "Measuring interfacial tensions of micrometer-sized droplets: a novel micromechanical technique"; Langmuir, 15: 8497–8504.

60. Slattery, J. C. and Chen, J. (1978). "Alternative solution for spinning drop interfacial tensiometer"; J. Colloid Interface Sci., 64: 371-373.

61. Vonnegut, B. (1942). "Rotating bubble method for the determination of surface and interfacial tensions"; Rev. Sci. Instr., 13: 6–16.

62. Princen, H.M.; Zia, I.Y.Z.; Mason, S.G. (1967). "Measurement of interfacial tension from the shape of a rotating drop"; J. Colloid Interface Sci., 23: 99–107.

63. Nagarajan, N., Webb, W.W., Widom, B. (1982). J. Chem. Phys, 77:5771.

64. CAZABAT, A.M., LANGEVIN, D., MEUNIER, J., POUCHELON, A., (1979). Proceedings of 3rd International Conference on Surface and Colloid Science, Stockholm.

65. Earnshaw, J.C., McGivern, R.C. (1987). J Phys D, Appl Phys, 20:82.

66. LANGEVIN, D., MEUNIER, J., (1977). Photon correlation spectroscopy and velocirnetry, Plenum Press.

67. Yeung, A., Dabros, T., Masliyah, J., (1998). "Does equilibrium interfacial tension depend on method of measurement?"; J. Colloid Interface Sci., 208: 241–247.

68. Fanun, M. (2009). Microemulsions: Properties and Applications; CRC Press Taylor & Francis Group: Florida.

69. Kumar, P.; Mittal, K. L. (1999). Handbook of Microemulsion Science and Technology; Marcel Dekker: New York.

70. Shah, D. O. (1998). In Micelles, Microemulsions, and Monolayers Science and Technology; Marcel Dekker: New York; Chapter 1.

71. Seeto, Y., Puig, J. E., Scriven, L. E., Davis, H. T. (1983). J. Colloid Interface Sci., 96: 360-372.

72. Sottmann, T., Strey, R. (1997). J. Chem. Phys., 106: 8606-8615.

73. Torza, S. (1975). Rev. Scientific Instruments, 46: 778-783.

74. Aveyard, R., Binks, B.P., Clark, S., Mead, J. (1986). J. Chem. Soc., Faraday Trans. 1, 82: 125-142.

75. Aveyard, R., Binks, B.P., Mead, J. (1987). J. Chem. Soc., Faraday Trans. 1, 83(8): 2347-2357.

76. Aveyard, R., Binks, B.P., Mead, J. Clint, J.H. (1988). J. Chem. Soc., Faraday Trans. 1, 84(3): 675-686.

77. Wielebinski, D., Findenegg, G. H. (1988). J. Progress in Colloid Polymer Sci., 77: 100–108.

78. Langevin, D. (1986). Colloids Surfaces, 21: 313-322.

79. Evans, E., Rawicz, W. (1990). Phys. Rev. Lett., 64: 2094-2097.

80. Hunter, R.J. (1986). Foundations of Colloid Science, Volume I. New York: Oxford University Press.

81. Chau, T.T. (2009). "A Review of Techniques for Measurement of Contact Angles and Their Applicability on Mineral Surfaces."; Minerals Eng, 22:213-219.

82. Ghosh, O., Miller, C. A. (1987). J. Phys. Chem., 91: 4528-4535.

83. Hunter, R. J. (1989). Foundations of Colloid Science, 2nd ed.; Oxford University Press: New York; Chapter 5.

84. Scott, A.C., MacKinnon, M.D., Fedorak, P.M. (2005). "Naphthenic Acids in Athabasca Oil Sands Tailings Waters Are Less Biodegradable than Commercial Naphthenic Acids."; Environ Sci Technol, 39: 8388-94.

85. Brient, J.A., Wessner, P.J., Doyle, M.N. (1995). Naphthenic acids. In: Encyclopedia of Chemical Technology. 4th ed. Kroschwitz JI Ed.; JohnWiley&Sons: NewYork; Vol.16, 1017-1029.

86. Chandra, M.S., Zacharia, J., Horvath-Szabo, G. (2011). "Impact of Pre-equilibrium on the Assessment Methodology of Interfacial Tension Measured between Aqueous and Heavy Oil Phases."; Energy and Fuels, 25: 2542-2550.

87. Seifert, W.K., Teeter, R.M. (1969). "Preparative Thin-layer Chromatography and High-resolution Mass Spectrometry of Crude Oil Carboxylic Acids."; Anal Chem, 41: 786-95.

88. Clemente, J.S., Prasad, N.G.N, Fedorak, P.M. (2003). "A Statistical Comparison of Naphthenic Acids Characterized by Gas Chromatography-Mass Spectrometry."; Chemosphere, 50: 1265-74.

89. Clemente, J.S. (2004). The Characterization, Analyses and Biodegradation of Naphthenic Acids [M.Sc. Thesis]. Edmonton (AB): University of Alberta.

90. Herman, D.C., Fedorak, P.M., MacKinnon, M.D., Costerton, J.W. (1994). Can J Microbiol, 40: 467.

91. Afshar, S., Yeung, A. (2011). "Considerations When Determining Low Interfacial Tensions."; J Colloid Interface Sci, 364: 276-278.

92. Moran, K., Yeung, A., Masliyah, J. (2000). "Factors Affecting the Aeration of Small Bitumen Droplets."; Canadian J Chem Eng, 78: 625-634.

93. Grant, J., Dyer, S., Woynillowicz, D. (2008). Fact or fiction: Oil sands reclamation. The Pembina Institute.

94. Wu, J., Dabros, T. (2012). "Process for solvent extraction of bitumen from oil sand."; Energy & Fuels, 26(2): 1002-8.

95. Ang, C.C., Abdul, A.S. (1991). "Aqueous surfactant washing of residual oil contamination from sandy soil."; Ground Water Monitoring & Remediation, 11(2): 121-7.

96. Mulligan, C.N., Yong, R.N., Gibbs, B.F. (2001). "Surfactant-enhanced remediation of contaminated soil: A review."; Engineering Geology, 60(1-4): 371-80.

97. Sheng, J.J. (2011). Modern chemical enhanced oil recovery theory and practice. New York: Elsevier.

98. Sjöblom, J., Lindberg, R., Friberg, S.E. (1996). "Microemulsions - phase equilibria characterization, structures, applications and chemical reactions."; Advances in Colloid and Interface Science, 65125-287.

99. Deshpande, S., Shiau, B.J., Wade, D., Sabatini, D.A., Harwell, J.H. (1999). "Surfactant selection for enhancing ex situ soil washing."; Water Research, 33(2): 351-60.

100. Abdul, A.S., Gibson, T.L., Rai, D.N. (1990). "Selection of surfactants for the removal of petroleum products from shallow sandy aquifers."; Ground Water, 28(6): 920-6.

101. Afshar, S., Mirmontazeri, L., Yeung, A. (2014). "Potential use of naphthenic acids in soil remediation: Examination of pore-scale interfacial properties."; Fuel, 116: 395-398.

102. Horvath-Szabo, G., Masliyah, J.H., Czarnecki, J. (2001). "Phase behavior of sodium naphthenates, toluene, and water."; Journal of Colloid and Interface Science, 242(1): 247-54.

103. Cyr, T.D., Strausz, O.P. (1983). "The structures of tricyclic terpenoid carboxylic acids and their parent alkanes in the alberta oil sands."; Journal of the Chemical Society, Chemical Communications, (18).

104. Cyr, T.D., Strausz, O.P. (1984). "Bound carboxylic acids in the Alberta oil sands."; Organic Geochemistry, 7(2): 127-40.

105. Yang, X., Czarnecki, J. (2005). "Tracing sodium naphthenate in asphaltenes precipitated from Athabasca bitumen."; Energy & Fuels, 19(6): 2455-9.

106. Jin, Y., Liu, W., Liu, Q., Yeung, A. (2011). "Aggregation of silica particles in non-aqueous media."; Fuel, 90(8): 2592-7.

107. Liu, W., Jin, Y., Tan, X., Yeung, A. (2011). "Altering the wettability of bitumen-treated glass surfaces with ionic surfactants."; Fuel, 90(9): 2858-62.

108. Tadros, T.F. (1994). "Fundamental principles of emulsion rheology and their applications."; Colloids and Surfaces A: Physicochemical and Engineering Aspects, 91: 39-55.

109. Yeung, A., Dabros, T., Masliyah, J., Czarnecki, J. (2000). "Micropipette: A new technique in emulsion research."; Colloids and Surfaces A: Physicochemical and Engineering Aspects, 174(1-2): 169-81.

110. Fischer, L. & Lemphers, N. (2011). "Keystone XL in context: oilsands and environmental management; Two decades of ineffective policies have left their mark on the Canadian landscape"; The Pembina Institute.